

Short-term spatial and temporal patterns of  
glacio-fluvial sedimentation at Feegletscher,  
Swiss Alps

William Dackus

submitted to the University of Hertfordshire in partial  
fulfilment of the requirements of the degree of MSc by  
Research

October 2020

## Abstract

Analysis of short-term spatial and temporal patterns of glacio-fluvial sedimentation associated with recent glacier retreat at Feegletscher, Swiss Alps, was undertaken. Data was collected through glacial imagery, ablation, meteorological, and proglacial channel monitoring to understand how sediment transport in a glaciated catchment with two geomorphologically contrasting proglacial zones functions during, and is responding to, recent glacier retreat. The research was performed during the 2019 ablation season on the Feegletscher Süd and Feegletscher Nord, Switzerland, whose proglacial streams are situated in geomorphologically contrasting proglacial zones. To the best of this investigation's knowledge, this is the first study to identify short-term intra-basin spatial and temporal patterns of glacio-fluvial sedimentation of two geomorphologically contrasting proglacial zones. The Feegletscher Nord's upper proglacial area is characterised by a narrow gorge and a waterfall that leads into a braided proglacial source of unstable, unconsolidated fine glacio-fluvial sediment deposits, and the lower proglacial area displayed consolidated morainic sediment deposits and reworked paraglacial debris. The Feegletscher Süd's upper proglacial area is characterised by a clean bedrock forefield with minimal quantities of glacio-fluvial sediment deposits, followed by a proglacial channel that is constrained by incised lateral moraines. Examples of data analysis techniques that were used are the cross correlation of meteorological and proglacial channel data to determine links between all variables, and hysteresis plots of suspended sediment concentration-discharge to indicate glacio-fluvial dynamics.

This research showed that there was variability in fluvio-glacial sedimentation between the multiple monitoring stations along the Feegletscher Nord's proglacial stream, and between the Feegletscher Nord's and Süd's proglacial stream. Both clockwise and anti-clockwise hysteresis was observed at all monitoring sites. The Feegletscher Süd showed an overall clockwise hysteresis, the upper monitoring site on the Feegletscher Nord showed anti-clockwise hysteresis, and the lower monitoring site on the Feegletscher Nord showed equal amounts of clockwise and anti-clockwise. The variability in hysteresis between the monitoring stations is attributed to sediment exhaustion, and the overall availability and

stability of fine grained sediment within each proglacial area, which is controlled by variations in sedimentary and geomorphological characteristics.

The differences in glacio-fluvial sedimentation at Feegletscher demonstrate that even within a relatively small glaciated catchment a range of spatial and temporal patterns exist, and a major control on determining these patterns is the location and quantity of the monitoring stations within the proglacial forefield. The additional complexity of comparing geomorphologically contrasting proglacial zones showed the importance of considering the geomorphological history of the proglacial zone when identifying the location and quantity of monitoring stations. The short-term spatial and temporal patterns of glacio-fluvial sedimentation and variability between each monitoring station demonstrated that long-term fully integrated studies are required to get a full understanding of glacio-fluvial sedimentation. A fully integrated catchment-wide study that integrated meteorological inputs to the catchment, as well as inflow, through-flow, and outflow of glacier meltwater and sediment would enable the ability to fully extrapolate suspended sediment concentrations and fluxes, sediment transportation mechanism, and to acquire a full understanding of the impacts caused by future glacier retreat.

## Table of Contents

Abstract.....	i
1 Introduction.....	1
2 Review .....	3
2.1 Glacial thermal regime .....	3
2.2 Albedo.....	4
2.3 Glacial Hydrology.....	5
2.3.1 Hydrological Network Morphology.....	6
2.3.2 Water Movement in Glacier Drainage Network .....	8
2.3.3 Drainage Network Dynamics.....	10
2.3.4 Glacier Runoff.....	12
2.4 Sediment Transport and Release .....	16
2.4.1 Mechanisms of Sediment Transport .....	18
2.4.2 Proglacial Sediment Mobilisation .....	23
3 Research aims and objectives.....	26
4 Field site.....	27
4.1 The Alps .....	27
4.1.1 Geological and glacial history.....	27
4.1.2 Contemporary climate .....	31
4.1.3 Future climate .....	31
4.2 The Feegletscher.....	32
4.2.1 Form and mass balance.....	32
4.2.2 Glacier hydrology .....	36
4.2.3 Geomorphology and geology.....	37
5 Data collection.....	42

5.1	Method .....	42
5.1.1	Proglacial channel Monitoring .....	42
5.1.1.1	Discharge .....	42
5.1.1.2	Suspended Sediment Concentration .....	45
5.1.2	Meteorological Data .....	47
5.1.3	Ablation Monitoring .....	48
5.1.4	Glacial Proglacial Imagery .....	50
6	Data Series .....	50
6.1	Meteorology .....	50
6.1.1	Air Temperature .....	50
6.1.2	Rainfall .....	53
6.1.3	Lapse Rate .....	53
6.2	Glacier Ablation .....	55
6.2.1	Melt Rate .....	55
6.2.2	Drone RGB Imagery .....	55
6.3	Proglacial Stream Data .....	60
6.3.1	Discharge .....	60
6.3.2	Water Temperature .....	62
6.3.3	Suspended Sediment Concentration .....	63
6.3.4	Suspended Sediment Flux .....	66
6.4	Suspended Sediment Dynamics .....	70
6.5	Statistical Analysis .....	92
6.5.1	Cross Correlation .....	92
6.5.1.1	Diurnal Discharge - Suspended Sediment Concentration .....	96
7	Discussion .....	100
7.1	Hydrology .....	100

7.2	Proglacial Suspended Sediment .....	102
7.3	Future Deglaciation .....	110
7.4	Future Research.....	111
8	Conclusion .....	113
	Reference List.....	114
	Appendix .....	138

Figure 1	- Idealised cross-section of a temperate alpine glacier demonstrating the hydrological components (Fountain and Walder, 1998).....	6
Figure 2	- Schematic diagrams of an idealised subglacial linked cavity network (Fountain and Walder, 1998) .....	12
Figure 3	- Discharge versus SSC at intraday scale during the late ablation season of a temperate valley glacier (Perolo <i>et al.</i> , 2018). .....	19
Figure 4	- Characteristics of diurnal hysteresis between the detrended, log discharge (logQdt), and SSC (logSSCdt) series. (A-C) at the Arctic systems (Hodson & Ferguson, 1999) .....	23
Figure 5	- Simplified geological map of the western European Alps (modified from Schmid <i>et al.</i> , 2004 by Vernon, 2008).....	29
Figure 6	- Relief map of the European Alps with the location of the Saaser Valley/study site marked (modified from Fitzsimons & Veit, 2001) .....	30
Figure 7	- Photo of Feegletscher from 12 <sup>th</sup> September 2019 (Oberli, 2019).....	33
Figure 8	- Location map of Feegletscher within Switzerland.....	34
Figure 9	- Photograph showing meltwater flowing from Feegletscher Nord into a bedrock ridge and down through a waterfall into a small braided proglacial area (2019).....	37
Figure 10	- Photograph of the lateral moraine that is located on the northern side of Feegletscher Nord's valley (2019).....	39
Figure 11	- Photograph of Feegletscher Nord's braided proglacial area and moraine slopes (2019).....	40
Figure 12	- (A) Deposition of supraglacial rock avalanche debris at the Feegletscher Nord in 1974 (photograph by Michael Hambrey); (B) Feegletscher Nord in 1985 as it advanced over	

blocks from the Guglen rock avalanche (photograph by Benedikt Schnyder); (C) Feegletscher Nord in 2010 viewed from a similar position; (D) morphology of the glacially reworked rock avalanche debris (Cook, Porter & Bendall, 2013).....	41
Figure 13 - Location map of sampling sites on the Feegletscher and the proglacial area of the Feegletscher.....	43
Figure 14 - Discharge calibration of the Upper North River site on the Feegletscher Nord's proglacial stream. ....	44
Figure 15 - Discharge calibration of the Lower North River site on the Feegletscher Nord's proglacial stream. ....	44
Figure 16 - Discharge calibration of the South River site on the Feegletscher Süd's proglacial stream. ....	45
Figure 17 - Suspended sediment concentration (SSC) calibration of the Upper North River site on the Feegletscher Nord's proglacial stream. ....	46
Figure 18 - Suspended sediment concentration (SSC) calibration of the Lower North River site on the Feegletscher Nord's proglacial stream. ....	46
Figure 19 - Suspended sediment concentration (SSC) calibration of the South River site on the Feegletscher Süd's proglacial stream. ....	47
Figure 20 - Tinytag data logger with a temperature probe that is located at the Upper North River site in the proglacial area of the Feegletscher Nord.....	48
Figure 21 - Photograph showing ablation stake and Tinytag sensor located at the Ablation site on the Feegletscher Nord.....	49
Figure 22 - Air temperature record at the Ablation Site on the Feegletscher Nord (DOY 191 - 201); Upper North River Site (DOY 193 - 201) and Lower North River site (DOY 190 - 210) of the Feegletscher Nord's proglacial stream and rainfall data recorded at the Lower North River Site in the proglacial area of the Feegletscher Nord (DOY 190 - 210) .....	51
Figure 23 - Air temperature recorded at Lower North River site in the proglacial area of the Feegletscher Nord (DOY 190 - 250) .....	52
Figure 24 - Lapse Rate data for Lower North River Site-UN River Site (DOY 193 - 201); Lower North River Site-Ablation Site (DOY 191 - 200); Upper North River Site-Ablation Site (DOY 193 - 200) .....	54
Figure 25 - Average daily temperature at the Ablation Site and recorded surface melt on the Feegletscher Nord during DOY 191 - 201. ....	55

Figure 26 - DOY 193 drone imagery of the albedo site on the Feegletscher. ....	57
Figure 27 - DOY 199 drone imagery of the albedo site on the Feegletscher .....	58
Figure 28 - DOY 200 drone imagery of the albedo site on the Feegletscher. ....	59
Figure 29 - Calibrated discharge for the Upper North River site (DOY 195 - 199) and Lower North River site of the Feegletscher Nord's proglacial stream (DOY 190 - 210) and the South River site of the Feegletscher Süd's proglacial stream (DOY 191 - 236). ....	61
Figure 30 - Calibrated discharge record at the Upper North River site (DOY 195 - 199) and Lower North River site (DOY 190 - 210) of the Feegletscher Nord's proglacial stream; the South River site of the Feegletscher Süd's proglacial stream (191 - 210) and rainfall data recorded at the Lower North River Site (DOY 190 -210). ....	62
Figure 31 - Water temperature recorded at the South River site of the Feegletscher Süd's proglacial stream (DOY 195 - 251). ....	63
Figure 32 - Calibrated suspended sediment concentration (SSC) for the Upper North River site during DOY 195 - 199 (Feegletscher Nord, 2019). ....	65
Figure 33 - Calibrated suspended sediment concentration (SSC) for the Lower North River site location during DOY 190 - 209 (Feegletscher Nord, 2019). ....	65
Figure 34 - Calibrated suspended sediment concentration (SSC) for the South River site location during DOY 191 - 236 (Feegletscher Süd, 2019) .....	66
Figure 36 - Suspended Sediment Flux recorded at the Lower North River site location during DOY 190 - 209 (Feegletscher Nord, 2019). ....	68
Figure 35 - Suspended Sediment Flux for the Upper North River site location during DOY 195 - 199 (Feegletscher Nord, 2019). ....	68
Figure 38 - Suspended Sediment Flux recorded at the Upper North River Site (DOY 195 -199); Lower North River site (DOY 190 - 209); South River (DOY 191 - 209).....	69
Figure 37 - Suspended Sediment Flux for the South River site location during DOY 191 - 236 (Feegletscher Süd, 2019). ....	69
Figure 39 - Simple line graphs between smoothed discharge and suspended sediment concentration (SSC) series recorded at the Upper North River site for each of the selected hydrological day sub-periods (DOY 195 - 198). ....	72
Figure 40 - Simple line graph between smoothed discharge and suspended sediment concentration (SSC) series recorded at the Upper North River site for each of the selected hydrological day sub-period of DOY 199.. ....	73

Figure 41 - Simple line graphs between smoothed discharge and suspended sediment concentration (SSC) series recorded at the Lower North River site for each of the selected hydrological day sub-periods (DOY 190 - 193). .....	79
Figure 42 - Simple line graphs between smoothed discharge and suspended sediment concentration (SSC) series recorded at the Lower North River site for each of the selected hydrological day sub-periods (DOY 194 - 197). .....	80
Figure 43 - Simple line graphs between smoothed discharge and suspended sediment concentration (SSC) series recorded at the Lower North River site for each of the selected hydrological day sub-periods (DOY 198 - 201).. .....	81
Figure 44 - Simple line graphs between smoothed discharge and suspended sediment concentration (SSC) series recorded at the Lower North River site for each of the selected hydrological day sub-periods (DOY 202 - 205). .....	82
Figure 45 - Simple line graphs between smoothed discharge and suspended sediment concentration (SSC) series recorded at the Lower North River site for each of the selected hydrological day sub-periods (DOY 206 - 207). .....	83
Figure 46 - Breakdowns of selected simple line graphs between smoothed discharge and suspended sediment concentration (SSC) series recorded at the Lower North River site. Blue represents the beginning section and orange represents the end section of the sub-periods up to the breakdowns found in Figure 45 (DOY 202-203).....	83
Figure 47 - Breakdowns of selected simple line graphs between smoothed discharge and suspended sediment concentration (SSC) series recorded at the Lower North River site. Blue represents the beginning section and orange represents the end section of the sub-periods up to the breakdowns found in Figures 45 and 46 (DOY 204-207). .....	84
Figure 48 - Breakdowns of selected simple line graphs between smoothed discharge and suspended sediment concentration (SSC) series recorded at the Lower North River site (DOY 202-205) .....	85
Figure 49 - Breakdowns of selected simple line graphs between smoothed discharge and suspended sediment concentration (SSC) series recorded at the Lower North River site (DOY 206-207).....	86
Figure 50 - Simple line graphs between smoothed discharge and suspended sediment concentration (SSC) series recorded at the South River site for each of the selected hydrological day sub-periods (DOY 191 - 194). .....	87

Figure 51 - Simple line graphs between smoothed discharge and suspended sediment concentration (SSC) series recorded at the South River site for each of the selected hydrological day sub-periods (DOY 195 - 198). .....	88
Figure 52 - Simple line graphs between smoothed discharge and suspended sediment concentration (SSC) series recorded at the South River site for each of the selected hydrological day sub-periods (DOY 199 - 202) .....	89
Figure 53 - Simple line graphs between smoothed discharge and suspended sediment concentration (SSC) series recorded at the South River site for each of the selected hydrological day sub-periods (DOY 203 - 206) .....	90
Figure 54 - Simple line graphs between smoothed discharge and suspended sediment concentration (SSC) series recorded at the South River site for each of the selected hydrological day sub-periods (DOY 207 - 210) .....	91
Table 1 - Rainfall recorded at the Lower North River site in the proglacial area of the Feegletscher Nord during DOY 190 - 210 .....	53
Table 2 - Results of cross-correlation analysis performed on the discharge, SSC, water temperature, and air temperature.....	95
Table 3 - Cross correlation analysis results for the Lower North River (DOY 190 - 208), Upper North River (DPY 195 - 199), and South River (191 - 210).....	99
Table 4 - Cross correlation analysis results for sub-period breakdowns (Figure 45, 46, 47).100	
Appendix A - Detailed overview of hysteresis loops for the Upper North River Site.....	138
Appendix B - Detailed overview of hysteresis loops for the Lower North River site. ....	139
Appendix C - Detailed overview of hysteresis loops for the South River site. ....	141

## 1 Introduction

Glacial erosion rates are estimated at  $0.01 \text{ mm yr}^{-1}$  in polar regions,  $1 \text{ mm yr}^{-1}$  for small temperate glaciers, and  $10\text{-}100 \text{ mm yr}^{-1}$  for large, rapidly flowing temperate glaciers (Hallett *et al.*, 1996). Various studies have shown that for warm-based glaciers, erosional mechanisms and sediment flux are primarily controlled by the subglacial drainage network (Østem, 1975; Collins, 1979; Hallett *et al.*, 1996; Delaney *et al.*, 2018b). The majority of this research has taken place in the alpine environment, and found major links between glacier meltwater discharge and suspended sediment concentration (SSC) over different temporal scales (Fenn, 1989; Delaney *et al.*, 2018b; Guillon *et al.*, 2018). The development and morphology of the subglacial drainage network can particularly impact and modify the relationship between glacier meltwater discharge and SSC (Souchez & Lorrain, 1987; Swift *et al.*, 2002, 2005a; Tananaev, 2015; Delaney *et al.*, 2018b). This is mainly because the subglacial drainage system is a major factor on the availability of material for mobilisation and the rate of glacio-fluvial sediment removal (e.g. Hubbard *et al.*, 1995; Swift *et al.*, 2005a; Delaney *et al.*, 2018b). Past knowledge surrounding mechanisms of glacio-fluvial sediment transport is questioned by more modern studies that challenge the appropriateness of using proglacial data of meltwater discharge and SSC to assess the functioning and morphology of the subglacial network (e.g. Gulley *et al.*, 2012a). This is because studies that do not represent the whole basin may produce uncertainties in the overall inflow, through-flow, and outflow of meltwater discharge and suspended sediment flux/concentration. Surface melt levels are a key driver of subsequent delivery of meltwaters to englacial and subglacial zones and ultimately to the proglacial zone and delivery of water/sediment to that area. Forecast changes to glacier surface melt under a changing climate that is resulting in progressive deglaciation will potentially have implications for the close linkages between basin-scale surface melt rates and the resultant delivery of sediment and meltwater delivery and fluxes to englacial and subglacial environments.

Progressive deglaciation results in the exposure of surfaces that may be vulnerable to rapid erosion through the operation of subaerial processes (Church & Ryder, 1972; Ballantyne, 2002a, 2002b). Exposure of such environments can cause an acceleration of geomorphological processes associated with sediment transport, entrainment, and re-

working, which can cause enhanced sediment flux and yield. Newly deglaciated areas, such as proglacial forefields, can store and discharge debris which consequently impacts the overall transportation and concentration of suspended sediment (Warburton, 1990; Bača, 2008; Carrivick *et al.*, 2013; Leggat *et al.*, 2015). Climate change is predicted to continue and exacerbate current progressive deglaciation which has become dominant since the 20<sup>th</sup> Century, and has the capacity to give rise to enhanced levels of geomorphological activity (e.g. Farinotti *et al.*, 2009; McGuire, 2010; Carrivick *et al.*, 2013), and it is hypothesised that this may have considerable impacts on the overall sediment production within glaciated basins (Ballantyne, 2002a; Porter *et al.*, 2010; Lane *et al.*, 2017). This may potentially have an effect on the pattern of sediment transfer of proglacial and ice-marginal sediments (Lukas *et al.*, 2005; Carrivick *et al.*, 2013). A wealth of studies have been performed on the impacts of the increased geomorphological activity, and show that slope-ice surface interactions that control sediment transport are complex (e.g. Schrott *et al.*, 2003; Otto *et al.*, 2009; Uhlmann *et al.*, 2013; Carrivick and Heckmann, 2017). However, they lack detailed assessment as to how enhanced delivery of sediments and changes in meltwater production rates will combine to alter basin scale sediment fluxes, and there are few studies that attempt to quantify these fluxes.

Progressive deglaciation may initially increase glacier meltwater discharge during the ablation season of an alpine catchment causing a so-called 'deglaciation discharge dividend' (Collin, 2008), but over a larger temporal scale, glacier meltwater discharge will considerably reduce because of an overall loss in ice mass and levels of meltwater discharge will consequently decline (Alcamo *et al.*, 2007; Collins, 2008; Kaser *et al.*, 2010) with resultant modifications to SSC and total sediment fluxes within and from glacial catchments (Swift *et al.*, 2005b; Lane *et al.*, 2017). However, the detailed nature of relationships between meltwater discharge and sediment fluxes in proglacial zones remains incompletely understood due to the complexity of proglacial areas in that they can operate as a sediment source and a sediment sink during different periods of the melt season (Misset *et al.*, 2019).

Enhanced knowledge is needed on how sediment transport dynamics and changes in meltwater production rates will combine to alter basin scale sediment fluxes. It is necessary to understand how recent glacier retreat is currently influencing, and will further alter, sediment transport in glacier networks, therefore, it is key to analyse temporal and spatial

patterns of sedimentation to see how the overall input; temporary storage; and discharge of such debris is influenced. To do this effectively, integrated, multi-annual catchment wide research is an appropriate approach to offers a means of assessing in detail linkages between surface energy inputs and consequent melt rates, meltwater production, and glacio-fluvial transport of sediment.

## 2 Review

### 2.1 Glacial thermal regime

A control of a range of glacial processes is the thermal regime of the ice, i.e. temperate (warm-based), polar (cold-based), or polythermal (Benn & Evans, 2010; Menzies & Meer, 2017). These glacial processes all have an impact on many mechanisms and processes, such as meltwater flowpaths and discharge, sediment production and transport, chemical denudation, and the solute composition of subglacial meltwaters (Benn & Evans, 2010). The heat balance will control the thermal regime at the subglacial bed interface, which is shown by the following equation:

$$\Delta H_B = H_A + H_S + H_F + H_G \quad (1)$$

where  $H_B$  represents the heat balance,  $H_A$  represents the heat transfer between the atmosphere and ice or snow,  $H_S$  is the heat from the temperature of amassing snowfall,  $H_F$  is the heat produced by frictional pressure contrasting ice deformation and flow, and  $H_G$  represents geothermal heat (Aschwanden, 2016). Temperate glaciers are made up of warm ice that is at or near to the pressure melting point, which means that the pressure created by the overlying ice produces enough downwards pressure to produce melting of the basal ice and may be significant enough to enable glacier motion (Hubbard & Nienow, 1997). Temperate glaciers have both water and ice, and an interstitial liquid content that can reach an approximate maximum value by volume of 9%, which is important for the flow of glaciers (Pettersson *et al.*, 2004). Temperate glaciers are also characterised by crevasses and moulins, which are caused due to high rates of glacier motion and glacier ice deformation. Both crevasses and moulins are forms of large-scale permeability and allow meltwater to drain through englacial and subglacial flowpaths (Fountain, Jacobel, Schlichting & Jansson, 2005). These temperate glaciers are generally located in mid-latitude alpine regions. Cold-based glaciers, in contrast, are made up of ice that is below its melting point, and therefore

they are frozen to the basal bed surface (Bennett & Glasser, 1996). Cold-based glaciers have no meltwater at the ice-bed boundary (Hodgkins, Tranter & Dowdeswell, 1997) and minor interstitial water (Irvine-Fynn *et al.*, 2011). Cold-based glaciers are generally located in Arctic or Antarctic conditions and typically have lower rates of glacier velocity and ice deformation when compared to temperate glaciers (Hodgkins *et al.*, 1997).

Polythermal glaciers are characterised by having a perennial concurrence of both cold and warm ice with an inner temperate region that is enclosed by a cold-based margin (Blatter and Hutter, 1991; Brown, Tranter, Hodson & Gurnell, 1996; Fowler and Larson, 1978). Polythermal glaciers are frequent in areas with prolonged below-freezing winter air temperatures where near-surface air temperature gradients cause net conduction of heat away from the glacier (e.g. Blatter and Hunter, 1991). Polythermal and many temperate glaciers can exhibit the formation of superimposed ice from meltwater, which infiltrates the snowpack and then freezes causing a reduction in ice permeability (Irvine-Fynn *et al.*, 2011). Polythermal glaciers and many temperate glaciers have well-developed supraglacial drainage but temperate glaciers have well developed basal drainage systems, and this is critical when it comes to the sediment flux of a temperate glacier which is majorly controlled by meltwater inflow, through-flow, and outflow (Hodson & Ferguson, 1999; Hodgkins *et al.*, 2003). Polythermal systems can also have high sediment fluxes despite a lack of widespread basal drainage (Hodson & Ferguson, 1999). There are still problems with these classifications due to temporal and spatial variability in the thermal regime and it is obvious that different thermal regimes have different characteristics that control meltwater flowpaths (e.g. Fountain & Walder, 1998; Pettersson *et al.*, 2004; Fountain *et al.*, 2005).

## 2.2 Albedo

The surface albedo of a glacier impacts the glacier's overall energy balance and dictates annual meltwater production and mechanics, and subsequent sediment production and evacuation (Perovich *et al.*, 2002). The definition of surface albedo is the proportion of reflected solar radiation at the land surface to the total incoming solar radiation over the whole solar spectrum and can be used as an indicator for the surface melt of a glacier (Dickinson, 1983). Surface albedo is a key physical factor affecting the Earth's climate (Kiehl *et al.*, 1996), and quantifying changes in the energy transfer between land surface and atmosphere allows for more accurate and precise climate models to be generated (Warren

*et al.*, 1980; Shuai *et al.*, 2011). The largest energy source for glacier melt is the absorption of shortwave radiation; this is true under most atmospheric conditions (Male & Granger, 1981; Chy'lek *et al.*, 1983; Paterson, 2000; Neshyba *et al.*, 2003; Pedersen *et al.*, 2005). Shortwave radiation absorption varies depending on incident radiation absorption and surface albedo (Stroeve *et al.*, 1997; Klok *et al.*, 2003; Warren *et al.*, 1982). Both of these factors are temporally variable and it is important to consider the variability of snow and ice albedo in space and time if used for input surface energy models (Stroeve *et al.*, 1997; Klok *et al.*, 2003; Zuo & Oerlemans, 1996). There are strong links between snow and ice albedos on local climate, surface energy balance, and melt rates (Cess *et al.*, 1991; Klok *et al.*, 2004). There is a lack of direct surface data of snow and ice albedo and often the data is discontinuous and/or contains error from a lack of instrumentation monitoring (van den Broeke *et al.*, 2004). Albedo measurements can be obtained from satellites in which data is more spatially continuous compared to other forms of data sets, but the albedo measurements depend on clear skies to reduce error (Stroeve *et al.*, 1997; Klok *et al.*, 2003). Satellite albedo data collected for complex terrains is more prone to error compared to simple terrain. The use of commercially available UAVs offers a potential temporal solution for small scale studies to monitor albedo and potentially link to larger-scale basin melt and discharge (Fugazza, 2019), and it is important to fully understand how glacial hydrology impacts and is impacted by these factors.

### 2.3 Glacial Hydrology

At the beginning of the ablation season, the subglacial drainage of a temperate alpine glacier is characterised by having a distributed network with water film flow (Weertman, 1964), porewater movement through permeable subglacial sediment (Boulton & Hindmarsh, 1987), and linked cavities. As the ablation season becomes well developed subglacial drainage for a temperate alpine glacier is characterised by discrete channels such as identified by Röthlisberger (1972) and Nye (1976). A Röthlisberger channel is a channel that is melted up into the basal ice (Röthlisberger, 1972) and a Nye channel is a channel that is carved down into the subglacial bedrock (Nye, 1976). In major subglacial drainage systems, meltwater transports large amounts of suspended sediment and as the ablation season advances, the drainage network evolves in a headward direction (Nienow, Sharp & Willis, 1998), however, these drainage networks are partially theoretical and depend on the

seasonal evolution of the temperate glaciers drainage network. Therefore, this means that glacial hydrology can vary greatly spatially and temporally, and given that subglacial drainage systems transfer large amounts of sediment it is clear that the hydrological system morphology that enables that transfer requires a detailed examination to truly understand the relationship between meltwater flux and sediment transfer.

### 2.3.1 Hydrological Network Morphology

During the summer months, solar radiation to the surface of a temperate glacier is at its highest and generates large amounts of snow- and ice-derived melt (Hock, 2005). Englacial and supraglacial drainage route meltwater from the glacial snow and ice to a subglacial drainage system (Figure 1) (Hock, 2005). Points of weakness in a glacier, such as moulins and crevasses, act as a point of access for surface water to be transported. Such glacial features could be present from previous years or develop over the present ablation period (Fountain *et al.*, 2005). Meltwater can also be stored and/ or transported englacially before it ends up at the bed of a glacier where the meltwater will either flow and progress through the subglacial drainage system or become subglacially stored. Meltwater within the glacier hydrological system is therefore comprised of water from the surface melt, stored subglacial and englacial water, and melt produced at the basal ice to the subglacial surface boundary and through ice deformation and associated friction.

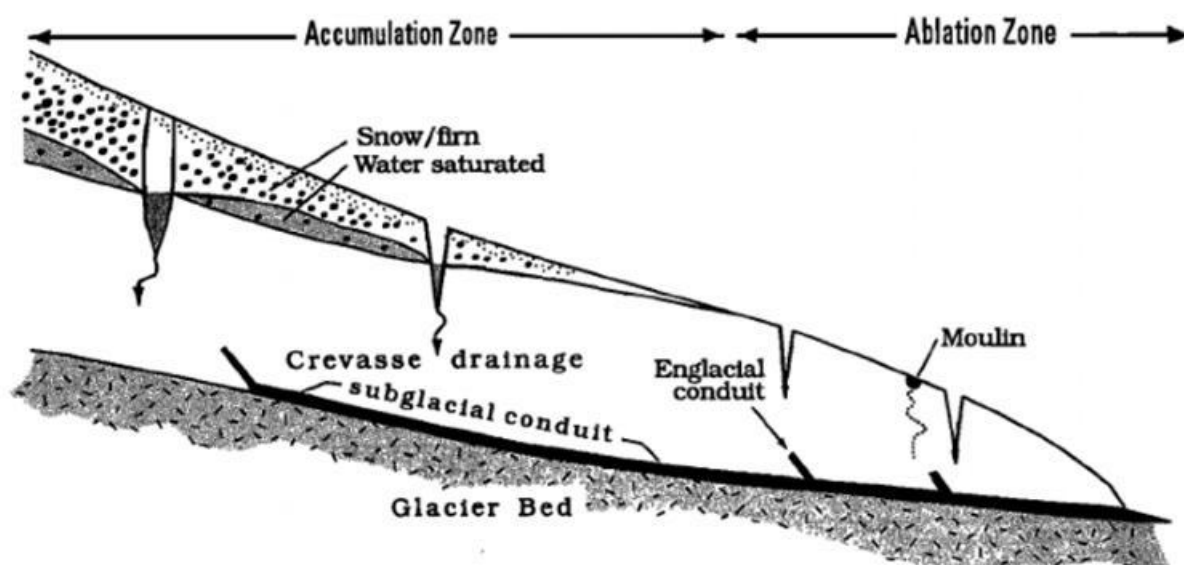


Figure 1 - Idealised cross-section of a temperate alpine glacier demonstrating the hydrological components. In the accumulation zone where snow/ firn is present water permeates downwards through the snow/ firn

to the water-saturated layer and then from the saturated layer through ice fractures to the subglacial drainage system. In the ablation zone, meltwater flows on the surface of the glacier into crevasses and moulins to the subglacial drainage system (Fountain and Walder, 1998).

Glaciers transport water through supraglacial, englacial, and subglacial drainage systems. Alpine glaciers' subglacial drainage networks can be hydraulically inefficient during the 'winter' accumulation season and show a positive correlation between water pressure and discharge. Hydraulically inefficient, spatially distributed drainage networks can be present over a high percentage of the area of the glacier subsurface. These hydraulically resistive flowpaths may comprise of a spatially distributed network of cavities and smaller 'links' known as a linked cavity network where water pressure enables the cavities and conduits to progress into a more hydraulically efficient flowpath (Kamb, 1987). During winter, cavities can be separated from the main drainage network leading to the potential for sediment and water to be subglacially stored (Kamb, 1987). Distributed braided canal networks are formed under glaciers, which are underlain by soft, deformable sediments (Walder & Fowler, 1994). These braided canal networks are characterised by broad, shallow pathways located through or over soft sediment located at the glacier-bed boundary (Clark & Walder, 1994; Walder & Fowler, 1994). Where temperate ice overlays hard bedrock, the ice-bed boundary may be characterised by a film of water (Hallet, 1979; Lappégard *et al.*, 2006). This water film is typically only multiple millimetres in depth but might cover a high percentage of a glacier bed (Schoof, 2004; Lappégard *et al.*, 2006). A water film is limited in its ability to transport water and studies have shown that such films only transfer water produced by local basal melting (Hallet, 1979; Lappégard *et al.*, 2006). Basal melting will occur if the ice is at the pressure-melting point, and more energy is produced by geothermal and ice-bed frictional forces than is conducted away from the ice. It is believed that the primary function of the subglacial water film is to transfer water from areas of pressure melting to areas of regelation (Hallet, 1979). Excess water in the water film can enter channels or other drainage links, and water films can gain water from drainage links at times of high discharge (Sharp *et al.*, 1989; Hubbard & Sharp, 1993).

The subglacial drainage network of a temperate glacier develops over the summer ablation season from a spatially distributed hydraulically inefficient system into a spatially discrete and hydraulically efficient system, which is characterised by a negative correlation between

water pressure and meltwater discharge (Fountain & Walder, 1998; Nienow *et al.*, 1998; Hoffman & Price, 2014; Gimbert *et al.*, 2016). Subglacial drainage network morphology varies spatially and temporally, and many studies have found that the morphology of subglacial drainage networks constantly evolves (Hubbard & Nienow, 1997; Swift *et al.*, 2005a; Bartholomew *et al.*, 2010; Meierbachtol *et al.*, 2013; Hoffman & Price, 2014; Gimbert *et al.*, 2016; Andrews *et al.*, 2018). Hydraulically efficient drainage networks are characterised by channelised systems that can be situated through the ice, bedrock, or sediment, such as those identified by Röthlisberger (Röthlisberger, 1972) and Nye (Nye, 1976). In comparison to R-channel, N-channels are much more spatially stable and permanent but less common parts of the subglacial drainage network (Souchez & Lorrain, 1987) because processes such as ice creep, deformation, and headward ice movement can close up or block R-channels (Hooke *et al.*, 1990). Both R- and N-channels can have a larger hydraulic roughness in comparison to supraglacial or englacial drainage, however, flow velocities are much higher. R- and N-channels have been shown to have flow velocities of 0.2-0.8 ms<sup>-1</sup> compared to distributed systems, such as linked cavity networks, of 0.025 ms<sup>-1</sup> to 0.4 ms<sup>-1</sup> (Kamb, 1987; Nienow *et al.*, 1998).

### 2.3.2 Water Movement in Glacier Drainage Network

The hydraulic efficiency of the drainage system is regulated by its hydraulic potential and its resistance to flow (Hubbard & Nienow, 1997). The cross-section of a channel or conduit is determined by ice deformation and turbulent frictional heating. The hydraulic potential of water at atmospheric pressure in the supraglacial zone is dependent on the water's mass and elevation (Benn & Evan, 2010). However, for water flowing through a glacier englacially or subglacially, water can be exposed to changes in pressure and elevation (Benn & Evan, 2010). The elevation and pressure components of hydraulic potential can be expressed as:

$$\phi = \rho_w g z + P_w \quad (2)$$

where  $\phi$  is hydraulic potential,  $\rho_w$  is water density,  $g$  is gravitational acceleration,  $z$  is elevation, and  $P_w$  is water pressure (Benn & Evan, 2010). Hydraulic potential in a subglacial channel or conduit is described by:

$$\phi = \phi_o + \phi_e + P_w \quad (3)$$

where  $\phi$  is the hydraulic potential,  $\phi_0$  is a constant depending on the morphology of the conduit,  $\phi_e$  is the potential due to elevation, and  $P_w$  is water pressure (Shreve, 1972; Flowers & Clarke, 2000). The hydraulic pressure for water-filled conduits in steady-state conditions is directly affected by water flow, which produces melt from turbulent frictional heating, and ice deformation from the water-ice overburden pressure gradient (Shreve, 1972). The pressure gradient created means that water-filled conduits and channels do not always transfer water and sediment in the direction of the basal gradient and can flow against or perpendicular to subglacial bed gradients (Hubbard & Nienow, 1997). Hydraulic pressure is significantly higher in distributed systems compared to channelised systems, which are often at atmospheric pressure because they grow at a faster rate than they contract (Hooke, 1984; Röthlisberger & Lang, 1987).

The hydraulic pressure of channels and conduits can be smaller than the ice over-burden pressure in bordering ice because the frictional melting within a channel or conduit causes a decrease in water pressure (Shreve, 1972). As pathway diameters increase, so does the difference in hydraulic pressure and ice over-burden pressure (Shreve, 1972). Larger channels and conduits are subjected to lower hydraulic pressure (Shreve, 1972). Shreve (1972) described how this means that the resultant pressure gradient means that larger diameter channels can capture more water than smaller channels and leads to the evolution of branched drainage systems. Conversely, Sharp *et al.* (1993) explained that subglacial drainage channel and conduit expansion and contraction will vary with fluctuations in meltwater discharge, ice depth, glacier surface gradient, ice-bed movement velocity, and the substrate morphology, and thus the environment described by Shreve is rarely experienced. Structural and rheological controls and characteristics of glacier ice are suggested to have a high effect on the overall architecture of meltwater drainage features, and local hydraulic potential (Fountain *et al.*, 2005; Gulley *et al.*, 2009). The drainage system composition is affected by the inconsistency in subglacial geomorphology and glacial morphology, leading to drainage structures that vary temporally and spatially, and consequently, both discrete and distributed drainage networks can exist in the subglacial environment (Hubbard *et al.*, 1995).

### 2.3.3 Drainage Network Dynamics

Over time drainage systems evolve and seasonal evolution of temperate glacier drainage systems is commonly observed with numerous examples being reported in the literature (e.g. Collins, 1979; Swift *et al.*, 2002, 2005a; Liu *et al.*, 2018). Research performed at Haut Glacier D'Arolla, Switzerland shows a major variation in the seasonal evolution of the drainage network structure (Nienow *et al.*, 1998). The research found that a hydraulically inefficient distributed drainage system progresses into a hydraulically efficient system that is characterised by channels and extends glacier wide (Nienow *et al.*, 1998). As the ablation season progresses, glacier runoff increases which cause the distributed drainage system to advance into a channelised network, which in comparison is hydraulically efficient. The headward evolution of the hydraulically efficient system reconnects separated sources of stored water and sediment (Nienow *et al.*, 1998).

Water-linked cavities can open up at the glacier-bed boundary when basal water pressure surpasses the local ice pressure. This condition often occurs on the downglacier side of basal landforms, where ice pressure at right angles to the bed is minimal. Linked cavities can be formed on the downglacier side of step cavities which is described as a basal landform that has a sudden step in its form (Kamb, 1987). Another form of linked cavities are wave cavities, where the glacier bed surface changes much more gently (Kamb, 1987). The two basic cavity geometries are effectively formed by the same means.

Water-linked cavities are predicted to be made up of lee-side cavities which are connected by narrow orifices (Figure 2). Water flow velocities will be low, as transit is restricted by the orifices, and water is temporarily stored in disconnected cavities. Water-linked cavities are not always connected in a continuous transport link all of the time, and the cavity network fluctuates with water storage, as cavities expand and contract in diameter and the quantity of orifices varies temporally (Kamb; 1987; Sharp *et al.*, 1989).

The theory that subglacial water could flow through systems of linked cavities was first developed by Lliboutry (1979) and was advanced further by Kamb (1987). Kamb (1987) described that distributed interconnected cavities can collapse into a channelised network if water pressure within the cavities deviates significantly above the steady-state pressure. Pressure deviation could cause the formation of pathways between cavities and the overall

form of the pathways is impacted by glacier surface slope and substrate sediment strength. Linked cavity systems begin to reduce in size after the ablation season has occurred and stay like this until the beginning of the next ablation season. This occurs because there is a decrease in ice deformation and frictional melt, leading to the closure of cavities.

Various dye tracer investigations have examined the evolution of a hydraulically inefficient drainage system into an efficient drainage network (e.g. Li *et al.*, 2018). Transfer velocity of dye, which is injected into supraglacial water pathways, is measured, and velocity increases and a reduction in dye dispersal may indicate drainage system evolution from a hydraulically inefficient distributed to a hydraulically efficient discrete network (Nienow *et al.*, 1998; Li *et al.*, 2018). This shift in the drainage network is strongly impacted by the amount of supraglacial water created and links to the relationship between the headward growth of the discrete network and the speed of retreat of the transient snowline (Nienow *et al.*, 1998). Both Nienow *et al.* (1998) and Swift *et al.* (2005a) demonstrate that glacier ablation and subglacial hydrological mechanisms are linked, and this can be seen throughout an ablation season as hydrographs become more peaked. Gulley *et al.* (2012b) determined that the distribution of moulins and crevasses across a glacier surface is a key variable controlling the distribution of subglacial channels and conduits, however, the work performed by Gulley *et al.* (2012b) was mostly performed on polythermal systems. The highly variable location of such features means that subglacial channel expansion can be episodic in nature which can impact both meltwater discharge and SSC (Fountain and Walder, 1998; Gulley *et al.*, 2012b). The speed at which seasonal channelisation takes place can be impacted by heavy rainfall. Studies have shown that heavy rainfall causes high discharges which increase the rate of channel formation (Nienow *et al.*, 1998). However, the development of channel networks can be slowed by the presence of firn, which allows for slower infiltration of meltwater to the basal system (Miller *et al.*, 2020). A large, distributed amount of firn would be needed for it to significantly hinder the generation of channels (Nienow *et al.*, 1998). During progressive deglaciation, more conduits and channels remain open during winter because there will be a reduction in ice-overburden pressure and therefore a resultant reduction in creep-closure (Flowers, 2008). Conduit and channel expansion and contraction can vary dependent on meltwater flux, ice thickness, ice surface gradient, bed gradient and geomorphology, and ice-bed sliding velocities (Flowers, 2008).

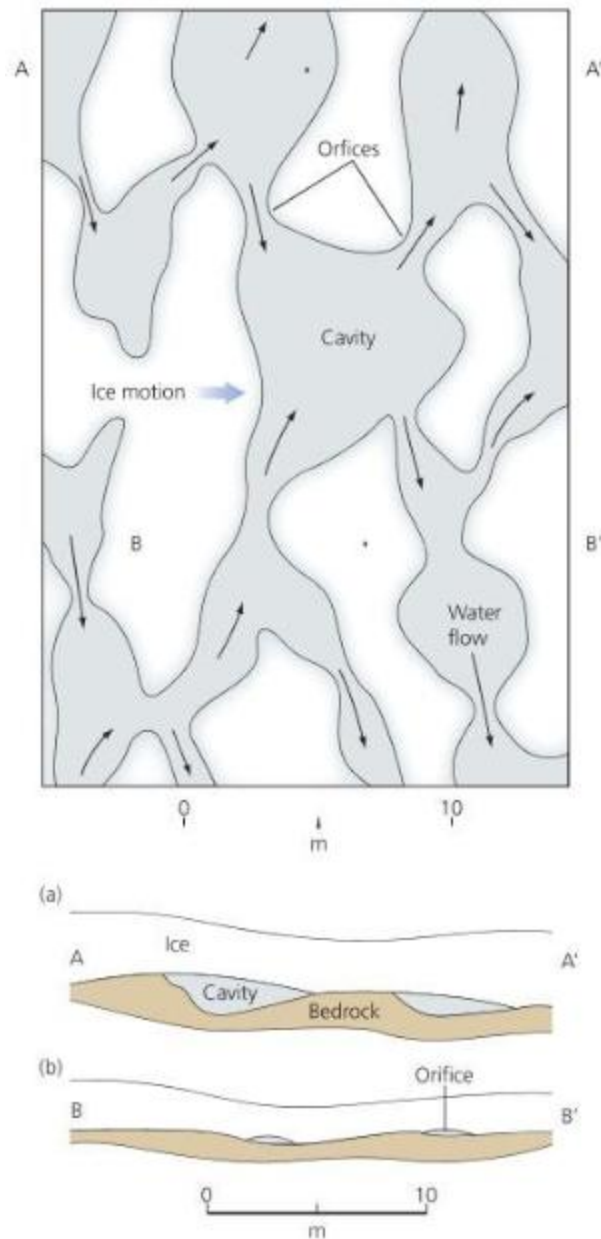


Figure 2 - Schematic diagrams of an idealised subglacial linked cavity network. (a) plan view and (b) cross-sections through cavities (A-A') and orifices (B-B'). (Fountain and Walder, 1998, after Kamb, 1987). White sections are areas of ice-bed contact; blue sections are areas of ice-rock separation. Black arrows demonstrate the direction of meltwater flow within the subglacial cavities and the blue arrow demonstrates the ice motion. Orifices represent the most constricted part of the subglacial cavity network and are the areas where the most energy is lost.

### 2.3.4 Glacier Runoff

Glaciers can store and release water on varying temporal scales, and therefore, glaciers have a significant impact on the amount and timing of water runoff in a catchment, which can in turn directly impact factors such as sediment flux. The discharge of proglacial rivers

reacts to various factors, such as rainfall, snow, and ice melt, the release of water stored in the glacier, non-glacial groundwater flow, and weather systems. The discharge of proglacial rivers experiences daily and annual cycle fluctuations depending on the quantity of water received from each source.

Glacier discharge into proglacial rivers is driven at its simplest form by diurnal temperature cycles. Rising and falling discharge is superimposed onto the melt season base flow. The base flow of a proglacial stream can be generated from the following variables: subglacial meltwater; water released from storage in snow, firn, or subglacial and englacial cavities; and groundwater sources (Röthlisberger and Lang, 1987). These variables only differ by small amounts in diurnal scales but can differ significantly when studied over monthly or yearly scales. A lag is seen between daily discharge peaks and the time of maximum melting. The proportion of diurnal minimum to maximum water transfer will lessen with greater catchment and glacier volume. In alpine environments, the lag is usually only approximately 1 to 2 hours (e.g. Collins, 1979; Fountain & Walder, 1998), however, the lag depends on the status of the drainage network and the total distance the meltwater has to transfer before it is discharged from the glacier (Hock & Hooke, 1993). Glaciers that have extensive snow cover and have inefficient subglacial drainage networks have longer lag times in comparison to glaciers with firn-free surfaces and efficient, well evolved subglacial channels and conduits (Röthlisberger and Lang, 1987; Jansson *et al.*, 2003). Lag times should reduce throughout the ablation period as hydraulically efficient channelised subglacial drainage systems develop (e.g. Swift *et al.*, 2002; Beaund *et al.*, 2018; Nanni *et al.*, 2020). Various studies have used the shape and magnitude of proglacial river hydrographs to examine the glacier drainage system morphology and functioning (e.g. Brown *et al.*, 1996; Collins; 1998). Flowers & Clarke (2002), Flowers (2008), and Covington *et al.* (2012) all show that the exact influence of surface meltwater inputs and the stage of development of the subglacial drainage network is still disputed. Covington *et al.* (2012) suggest that the subglacial hydrological process could have a smaller influence in determining hydrographs when conduit subglacial drainage networks exist because such systems have a shortage of stored water and flow constraints. The main determinant of proglacial river hydrographs is argued to be caused by discharge contributions from glacier surface meltwater, and therefore,

proglacial river hydrographs may dominantly reflect the degree of supraglacial melt and meltwater contributions to the subglacial hydrological network (Covington *et al.*, 2012).

The storage of water in reservoirs, such as supraglacial channels and pools, the active layer of supraglacial ice, englacial stores and conduits, and subglacial cavities and conduits can modify runoff regimes (Jansson *et al.*, 2003). Over an ablation season, the temporal scale upon which storage and discharge of such reservoirs can vary greatly (Jansson *et al.*, 2003; Bartholomew *et al.*, 2010; Colgan *et al.*, 2011). Storage of water can be hard to interpret without observational proof, and reservoirs have subsequently been conceptualised (Hannah & Gurnell, 2001).

The climatic regime (e.g. timing and quantity of precipitation and maximum temperature) of a glacierised catchment greatly contributes to the seasonal runoff. Environments that experience a precipitation maxima in winter and a temperature maxima in summer witness glacier meltwater as the major proglacial river variable for runoff in the summertime instead of other factors such as rainfall (e.g. European Alps). This will cause a shift in the discharge peak in relation to the precipitation maximum. The European Alps can experience both solid and liquid precipitation which can add to mass storage and glacier runoff. The European Alps is mainly subjected to solid precipitation at elevations of 3500-4000 m a.s.l. (Röthlisberger and Lang, 1987). Conversely in the European Alps, 0°C isotherms can occur above 4500m, which is well above the elevation of most glaciers located there, and this means that ablation, precipitation, and runoff have a complex link (Collins, 1998). This all means that alpine glaciers rarely receive a single state of precipitation that covers the entire surface of the glacier's elevation range. Glaciers in the European Alps are likely to be subjected to large discharge events during mid-summer if exposed to large amounts of liquid precipitation and extreme glacier surface melt rates (Röthlisberger and Lang, 1987). The shift in discharge peak in relation to precipitation maxima described above will occur to a greater effect in low-latitude mountain regions (e.g. Cordillera Blanca, Peru). Such regions have a more obvious wet season and dry season and during the latter, glacier runoff is an important source of water for approximately half of the year (Juen *et al.*, 2007). Conversely, in regions such as the Himalayas, where the precipitation maxima are experienced during summer and the minima are experienced during the winter, the glaciers do still have a significant impact on the runoff cycle, and proglacial river discharge follows the seasonal

pattern of glacier melt but runoff characteristics are highly influenced by monsoonal activity (e.g. Hasnain, 1996; Hasnain, 1999; Hasnain & Thayyen, 1999).

The start of a glacier melt season of a warm-based system is usually characterised by a spring event (sudden flood), which is usually activated by heavy rainfall and/or high surface melt rates (Röthlisberger and Lang, 1987; Anderson *et al.*, 1999; Flowers and Clarke, 2000; Mair *et al.*, 2003). Water is transported to the bed and overwhelms the inefficient winter subglacial drainage network which often causes large amounts of water and sediment to be discharged from the glacier. After the spring event has taken place, the glacier continues to experience the evolution of its supraglacial, englacial, and subglacial drainage networks, and this establishes the melt season diurnal cycles in discharge (Mair *et al.*, 2003). These obvious diurnal cycles start to break down as discharge declines in late summer and quantities of englacial and subglacial water and snow in the ablation zone have reduced (Mair *et al.*, 2003). Glacier runoff dwindles and discharge becomes low during the autumn and winter seasons (Flowers and Clarke, 2000).

Flood events do not only occur at the beginning of the melt season but can occur at any time due to climatic events (e.g. precipitation events, periods of higher than average temperature), variations in morphology, and outbursts from supraglacial lakes (Björnsson *et al.*, 2003; Mair *et al.*, 2003). High air temperature, high solar radiation levels, or increased turbulent heat flux in warm, windy weather can cause periods of rapid glacier surface melting (Benn & Evans, 2010). During such phases, an increase in baseflow is often observed in proglacial hydrographs, as more water is discharged from snow and firn aquifers. The proglacial river may experience more significant diurnal variations that reflect quickflow from areas of bare ice surfaces (Haritashya *et al.*, 2006). Quickflow signifies the most quickly responding hydrological processes and components of a catchment (Thomas & Goudie, 2000). At temperate glaciers, the largest discharges caused by weather are due to rainfall during summer and autumn storms, which both add directly to catchment runoff and contribute to enhanced melting of snow and ice (Haritashya *et al.*, 2006).

Overall, the meltwater discharge of a glacier can be impacted by various factors, such as morphology and development of the drainage network dynamics (Kamb; 1987; Sharp *et al.*, 1989; Swift *et al.*, 2005a), climatic regime (Röthlisberger & Lang, 1987; Collins, 1989), and

the storage and discharge of meltwater aquifers (Jansson *et al.*, 2003). Meltwater generated at the ice surface will ultimately enter the glacier hydrological system, where it has the opportunity to entrain sediments, particularly where extensive subglacial drainage exists. While meltwater is in a subglacial drainage system it has access to a substrate of sediment or bedrock, which can be eroded and mobilised, therefore the rate at which sediment is transferred through a glacierised basin is significantly influenced by the capacity of subglacial meltwater to transport basal sediment, the mechanisms that the basal sediment is accessed and entrained, and the erodibility of the underlying substrate (Hodgkins *et al.*, 2003).

#### 2.4 Sediment Transport and Release

In glacierised basins erosion rates, as indicated by, for example, sediment concentration and sediment load, have been extensively studied (e.g. Hodson & Ferguson, 1999; Bogen & Bønsnes, 2003; Hodgkins *et al.*, 2003; Gao *et al.*, 2013; Delaney *et al.*, 2018b; Lane *et al.*, 2017). Various studies have calculated total sediment yield, which is controlled by the glaciological characteristics, substratum characteristics, topographic variables, temporal and climatic variables in a catchment (Evans, 1997). Bogen & Bønsnes (2003) described that the total sediment yield of a glacier is not merely controlled by its latitude and altitude and that within a glacial grouping (alpine and Arctic) variations in total sediment yield are evident. These internal variations in total sediment yield are because of the overall dynamics of glacial mechanisms and the thermal regime of the glacier (e.g. Knudsen *et al.*, 2007).

In a glaciated catchment, sediment is derived from subaerial, subglacial, and proglacial sources. Sediment is then transported through glacier networks by a combination of ice flow, supraglacial, englacial, subglacial, and proglacial mechanisms (Fenn, 1987), and the majority of debris is usually transported by flowing water (Kirkbride, 1995; Alley *et al.*, 1997; Delaney *et al.*, 2018b). These mechanisms act on various temporal and spatial scales, thus, leading to complicated patterns and relationships between sediment transportation and fluvial inputs (Kirkbride, 1995; Alley *et al.*, 1997; Delaney *et al.*, 2018b). The sediment balance equation simply explains this with phases of erosion, transport, and sedimentation and can be described as a balance equation:

$$\Delta S_s = G_p + F_p + W_p - G_t - F_t - M_t \quad (4)$$

where  $S_s$  expresses the quantity of sediment stored in the catchment, the terms  $G$ ,  $F$ ,  $W$ , and  $M$  represent glacial, fluvial, weathering, and mass movement mechanisms with  $p$  representing sediment creation and  $t$  representing sediment transfer (Fenn, 1987). These methods of sediment creation and transfer may result in sediment at the base of the glacier which can become entrained and mobilised by meltwater (e.g. Rempel, 2008).

There are five major categories of sediment production in glacial environments: fluvial erosion, chemical weathering, physical weathering, abrasion, and plucking/quarrying (Boulton, 1982; Fenn, 1987). Fluvial erosion is described as the erosion of materials by the action of flowing water (as sheet-wash or channelised flow), chemical weathering is the decomposition of minerals into ionic constituents, and these mechanisms operate concurrently, and often interdependently (Fenn, 1987). The erosional mechanism of abrasion is the wear of the subglacial surface achieved when the force exerted by particles dragged across the bed during basal sliding exceeds the indentation hardness and fracture toughness of the bed (Riley, 1982), and plucking/ quarrying is block removal in association with failure along physical discontinuities when adhesion between ice and block exceeds adhesion between the block and parent material (Fenn, 1987). Lastly, the erosional mechanism of physical weathering can be described as the mechanical breakdown of rock into finer sized material via the application of gravitational, expansion, or hydraulic forces (Fenn, 1987).

Debris input to glaciers can be present at the interface between valley walls and the ice surface, but for most temperate alpine glaciers the majority of sediment input occurs at the bed (Benn & Evans, 2010). Ice-bed sediment interactions have been well documented from studying recently deglaciated surfaces and through direct subglacial research (e.g. Hambrey *et al.*, 1999; Evans *et al.*, 2006). Glaciers have beds that can be composed of both bedrock and sediment (e.g. Iverson *et al.*, 1995; King *et al.*, 2008). Research shows that bed loading at the ice-bed interface of a glacier will cause the deposition of a layer of basal till, which is usually less than 10 cm in depth (Souchez & Lorrain, 1987). Gulley *et al.* (2012a) found that the bed of an Arctic glacier was characterised by large boulders on a bed of sorted sediments and walls of fine-grained till. The characteristics of subglacial tills, such as

sedimentological, rheological, and strength, are dependent on the geology of the glacierised catchment, the erosive mechanisms present, and the efficiency of such mechanisms (Haldorsen, 1981; Evans *et al.*, 2006; Cofaigh *et al.*, 2007; Lovell *et al.*, 2015). This means that the makeup of glacier beds can vary greatly spatially and temporally, and given that subglacial sediments beneath temperate glaciers contribute to the majority of sediment flux into the proglacial rivers it is clear that the mechanisms that enable that flux require a detailed examination to aid understanding of the relationships between meltwater flux and sediment transfer.

#### **2.4.1 Mechanisms of Sediment Transport**

Most sediment inputs to a glacier typically concentrate at the bed or within a few metres of it, and therefore, the dominant form of sediment transport for a temperate glacier is subglacially (Swift *et al.*, 2005b; Benn and Evans, 2010). The area of concentrated material at the bed or margin of a glacier consists of the basal tractive zone and the suspension zone (Boulton and Eyles., 1979). The basal tractive zone is the area directly in contact with the bed itself, and the suspension zone is the area close to but not in contact with the subglacial bed (Boulton and Eyles., 1979). The basal tractive zone can have a thickness of one clast if the bed is hard bedrock. The tractive zone can be much thicker when the substrate is composed of till and unlithified sediments. Rapid shear forces occur between the basal tractive zone sediment and basal ice. The sediment transport rates are directly proportional to the strain rate and thickness of the basal tractive zone, and inversely proportional to sediment porosity (Benn and Evans, 2010). Early studies found high rates of debris transfer due to the fast deforming layers of sediment (e.g. Boulton., 1979, 1987; Alley *et al.*, 1987; Hooke and Elverhøi, 1996). Alley (2000) observed that shallower shear forces occurred between the basal ice and tractive zone, with reduced strain speeds at increased depth. When melting or freezing occurs sediment can be transferred between the suspension zone and the tractive zone (Benn and Evans., 2010). Rates of debris transfer in the basal tractive zone are dependent on the thickness and concentration of the basal sediment, basal sliding velocities, and strain rates within the glacier (Boulton., 1979, 1987; Alley *et al.*, 1987; Hooke and Elverhøi, 1996; Alley, 2000).

Glacial drainage systems can transfer large quantities of sediment through glaciers, and the subglacial drainage system is the main source of sediment transfer within the catchment of

a temperate, debris-free glacier (Gurnell, 1987, 1996; Bogen, 1996; Hodson *et al.*, 1997; Buoncristiani and Campy, 2001; Swift *et al.*, 2002, 2005).

The rates of sediment transfer within a glacial stream or river are impacted by the availability of sediment and the characteristics of meltwater flow. During flood events, SSC in proglacial streams usually peak before discharge does, and sediment concentrations are usually lower during the falling limb of a hydrograph compared to the rising limb (Gurnell, 1982). This difference in SSC for the same give discharge shows the fast rates of till evacuation from the subglacial environment and the consequential exhaustion in sediment availability (Gurnell, 1982). Proglacial streams are observed to experience pulses in SSC that are not apparently driven by energy inputs at the ice surface are caused by the collapse of a flowpath wall or development of the subglacial fluvial drainage network structure. Seasonal fluctuations in SSC are also evident (Swift *et al.*, 2002). During winter, concentrations of suspended sediment are low at approximately a few milligrams per litre, but during spring and summer, concentrations increase to approximately a few decigrams per litre (e.g. Bača, 2008). These patterns follow that of discharge, however late in the melt season, patterns in SSC divert from discharge and this reflects exhaustion in the availability of fine-grained sediment (Figure 3) (e.g. Bača, 2008; Perolo *et al.*, 2018).

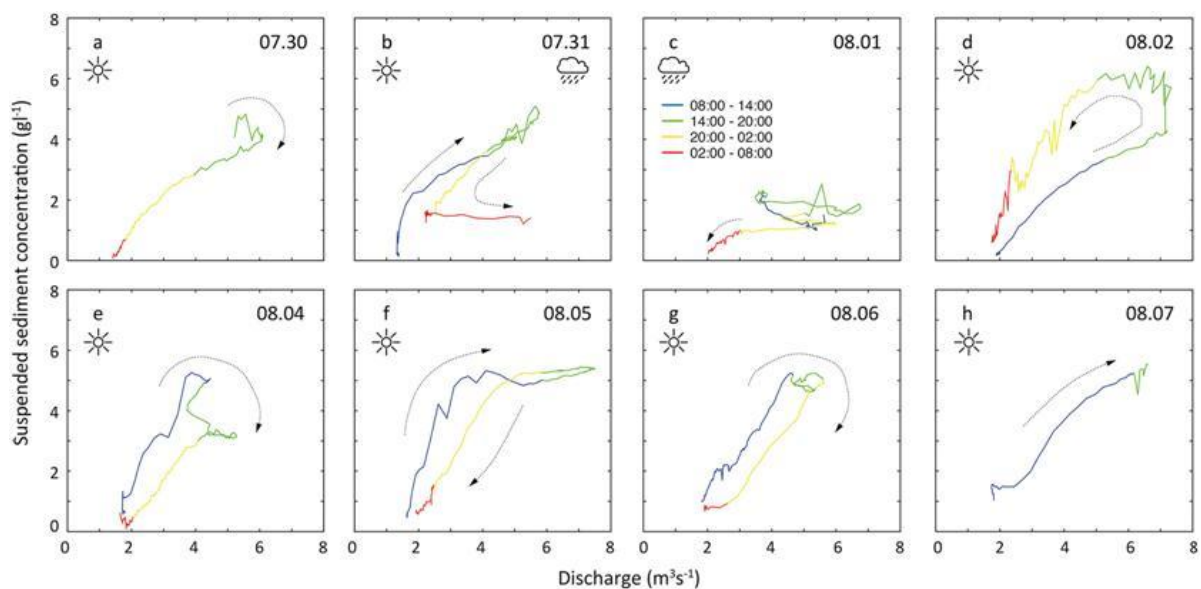


**Figure 3 - Discharge versus SSC at intraday scale during the late ablation season of a temperate valley glacier (Haut Glacier d'Arolla, Switzerland). Clockwise hysteresis loops suggest the flushing of finer material and limitation during the day (Perolo *et al.*, 2018).**

Particle size and quantity of transported sediment increases as bedload driving factors increase. Fluvial bedload is defined as the grains of sediment that are moved close to the bed of a stream or river, in continuous or discontinuous contact with the bed (Allen, 1982, 1985; Haas *et al.*, 2011). The fluvial bedload of a stream can be minor amounts of silt for low flow, to large loads of all grain sizes, through to large, heavy boulders for extreme flood events. Research completed at the proglacial river of Lyngsdalselva, Norway, found that bedload transfer was much larger during discharges of  $10 \text{ m}^3\text{s}^{-1}$  compared to  $5 - 8 \text{ m}^3\text{s}^{-1}$  (Ashworth and Ferguson, 1986). Therefore, this reflects that proglacial streams can transport large volumes of sediment due to their characteristically high discharge, however, it is important to remember that high discharges do not always reflect high sediment flux due to the potential for transient sediment exhaustion patterns (Pearce *et al.*, 2003). A 1969 study on the proglacial stream of Nigardsbreen, Norway, concluded that during a month-long period in summer, bedload transport comprised approximately 400 tonnes of sediment (Østem, 1975). Gurnell (1987) researched various temperate glaciers and reported that fluvial bedload transfer accounted for approximately 30 to 60 per cent of overall sediment load, and a study completed by Østem and Olsen (1987) found that fluvial bedload transfer was approximately 10 to 20 per cent of the total sediment load, with 80 to 90 per cent being transferred as suspended load. The obvious difference in sediment transfer reflects that transfer conditions can differ significantly between glaciers and glacial environments.

Glacial sediment removal is greatly impacted by the higher availability of meltwater throughout the ablation period; the build up of sediment at the basal ice-bed interface over winter; higher surface runoff causing increased basal ice-bed separation and higher basal sliding; subglacial flowpath variability and the development of a channelised subglacial drainage system (Swift *et al.*, 2002, 2006; Iverson *et al.*, 2019). Distributed drainage networks often cover large proportions of the basal substrate, but are characterised by slow flow rates and the limited size of transport pathways which restrict sediment transfer within the subglacial network (Alley *et al.*, 1997). A limit on sediment transfer will cause more sediment to be retained subglacially, which may lead to the build-up of a thick sediment layer at the ice-bed interface and a reduction in bedrock erosion. Conversely, channelised drainage networks generally cover lower proportions of the basal area compared to

distributed drainage networks, but have much faster flow rates which enable rapid removal of subglacial debris from conduits and cavities.

Research performed on the proglacial stream of the temperate alpine glacier Haut Glacier d'Arolla showed that suspended sediment flux (SSF) increased steeply in a non-linear relationship with discharge (Swift *et al.*, 2002, 2005a). The relationships found were much greater than would be expected from theoretical discharge capacity calculations (Swift *et al.*, 2002, 2005a). An increase in proglacial discharge of 7.5 times led to an increase in suspended sediment of 12.5 times. This non-linear relationship shows the development of the glacial drainage network from late winter and spring to the summer ablation season, where a hydraulically inefficient distributed network evolves into a hydraulically efficient, high-flow channelised network. High fluctuations in the diurnal discharge lead to enhanced quantities of water exchange between channels and/or conduits and the bed, thus establishing efficient sediment removal. Therefore it is clear that during winter and spring, suspended sediment evacuation from distributed drainage networks will be low and sediment will primarily be stored underneath glaciers (Swift *et al.*, 2002; Swift, 2006). As subglacial drainage systems evolve during the melt season, the retained sediment will be evacuated (Swift *et al.*, 2002a; Swift, 2006). During periods where large quantities of meltwater are rapidly produced, sediment will be easily transferred from underneath a glacier to glacier margins and down the valley by proglacial streams.

Research on SSC and discharge has revealed that sediment transfer is constrained less by discharge than sediment availability (e.g. Haritashya *et al.*, 2006; Geilhausen *et al.*, 2013; Mao and Carrillo, 2016, Lane *et al.*, 2017). During the ablation season, diurnal patterns of sediment removal by subglacial drainage networks are often characterised by maximum values in discharge occurring with the lowest concentrations of suspended sediment at the same moment in time (Swift *et al.*, 2005a). This reflects the rapid diurnal exhaustion of glacial sediment by subglacial drainage networks, recurring independently of the diurnal fluctuations in discharge. The link between suspended sediment transport and meltwater output does not only show the entrainment and transfer by discharge but its reliance on sediment availability. Therefore, predicting SSC from discharge can be difficult. Relationships between SSC and discharge have been used in the past to predict discharge and SSC with the utilisation of suspended sediment rating curves (e.g. Gurnell, 1987; Fenn,

1989), and they are produced by linear regression analysis of discharge and SSC values (Gurnell, 1987; Fenn, 1989). Sediment rating curves are often characterised by significant quantities of scattering and a strong linear correlation is often unusual (Gurnell & Fenn, 1984; Fenn, 1989). Haritashya *et al.* (2006) showed that relationships between SSC and proglacial discharge are especially complex at short hourly temporal scales. Different temporal scales may produce sediment rating curves that vary in form and correlation (e.g. Fenn *et al.*, 1985). However, suspended sediment rating curves are now discredited for predicting discharge because the glacio-fluvial sedimentary system is more complex than the generalised relationship between discharge and SSC. The complexity of the correlation between discharge and SSC is reflected through the transient exhaustion in sediment supply often observed in temperate alpine systems and reflected in hysteresis relationships, evident when SSC is plotted against meltwater discharge on a diurnal timescale (Figure 3 and 4). Hysteresis between SSC and discharge is produced by a lag in time to peak between the two variables when measured over the same diurnal scale (Hodson & Ferguson, 1999; Tananaev, 2015; Zuecco *et al.*, 2016; Guillon *et al.*, 2018; Hamshaw *et al.*, 2018). Typically, diurnal values in SSC peak before discharge, as daily availability of sediment available to be entrained reaches zero. Taking a typical daily melt cycle, in the early morning proglacial discharge begins to rise and, as it does so, sediments that have accumulated at subglacial channel margins, for example, are available for entrainment by basal meltwaters and so sediment load rises in tandem with discharge. However, as the day progresses, and discharge rises, a point is reached whereby the majority of available basal sediment has been entrained and flushed from the basal drainage network, with the result that sediment flux starts to drop, even though discharge may be still rising. As discharge falls overnight and towards the morning, sediment availability at subglacial channel margins progressively increases to be available for entrainment and flushing from the system as discharge rises again the following morning (Richards & Moore, 2003). Therefore, this relationship shows that even with large meltwater discharges, there is an exhaustion in sediment supply at different temporal extents (e.g. Richards & Moore, 2003; Riihimaki, 2005; Guillon *et al.*, 2018). Records of discharge of a glacial river are useful in approximating the availability of sediment for transfer, and the exhaustion of sediment is a factor that influences scattering.

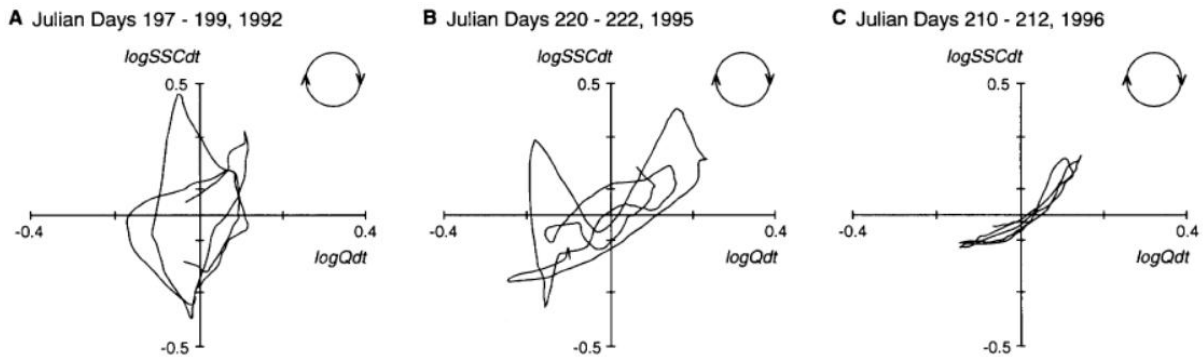


**Figure 4 - Characteristics of diurnal hysteresis between the detrended, log discharge ( $\log Q_{dt}$ ), and SSC ( $\log SSC_{dt}$ ) series. (A-C) Simple line graphs for three consecutive days of high diurnal discharge variability at the Arctic systems of Austre Brøggerbreen, Finsterwalderbreen, and Erdmannbreen respectively (the open circles show the direction of the hysteresis between the two variables (Hodson & Ferguson, 1999).**

Sediment exhaustion has been studied through various statistical models of SSC, which allow for approximations to be made about the availability of sediment (e.g. Hodson & Ferguson, 1999; Fausto *et al.*, 2012; Joshi *et al.*, 2016). Statistical models of SSC are mostly directed towards temporal fluctuations, especially fluctuations caused by factors unrelated to proglacial discharge. The statistical models also try to understand meltwater routing, sediment availability, and supply. To determine the factors driving these variables models use discharge based predictor factors that relate to changes in sediment (e.g. Irvine-Fynn *et al.*, 2005a; Swift *et al.*, 2005b; Stott & Mount, 2007; Fausto *et al.*, 2012; Joshi *et al.*, 2016). The complex glacio-fluvial sedimentary system that is reflected through transient exhaustion in sediment supply demonstrates the importance of an understanding of how sediment transfer is modified within the glacier forefield.

#### **2.4.2 Proglacial Sediment Mobilisation**

Proglacial areas have seen much investigation and are seen as high energy locations which are major sources of glaciogenic material which is available for reworking (e.g. Carrivick *et al.*, 2013; Geilhausen *et al.*, 2013; Mao and Carrillo, 2016; Carrivick and Heckmann, 2017; Delaney *et al.*, 2018b; Guillon *et al.*, 2018). Proglacial investigations show that there are temporal and spatial disparities within SSC records that are caused by processes of non-glacial origins (Gurnell, 1982; Gurnell & Warburton, 1990; Gurnell *et al.*, 1992; Guillon *et al.*, 2018). Short-term capture and excavation of debris in proglacial streams have the potential to impart significant impacts on SSC fluctuations (Guillon *et al.*, 2018). Arctic and alpine

studies have revealed that proglacial areas are of major importance as a source and sink of debris transferred by a proglacial stream (e.g. Hodgkins *et al.*, 2003; Misset *et al.*, 2019). Various studies have determined that levels of non-glacial sediment flux increase with distance from the glacial terminus (Gurnell & Warburton, 1990; Gurnell *et al.*, 1992, Orwin & Smart, 2004a) because as the distance from the glacial terminus increases so does the extent of available sediment sources that can be exploited by a combination of subaerial or fluvial reworking (Hammer and Smith., 1983). For example, research completed on the proglacial zone of the Small River Glacier, Canada, found that approximately 80 per cent of the overall suspended sediment yield was sourced from the proglacial river compared to the subglacial area (Orwin and Smart., 2004a). A study performed on Hilda Glacier, Alberta, Canada, found that proglacial channel stream supplied 47 per cent of total suspended sediment yield (Hammer and Smith., 1983), however, the Arctic catchments may not be fully representative of the alpine environment. Proglacial channels within the Arctic and alpine environments act as a source and a sink of sediment during an ablation season (Hodgkins *et al.*, 2003; Misset *et al.*, 2019), and Maizels (1979) and Hodgkins *et al.* (2003) reported that this is also true over successive ablation seasons as the runoff system of glaciated Arctic catchments controls adjustments in sediment storage. Hodgkins *et al.* (2003) reported that at Finsterwalderbreen, Svalbard, discrete glacial meltwater discharge events were linked to enhanced sediment removal from the glacial and proglacial area. Glacial landforms in the Arctic and alpine forefields act as temporary supplies of glaciogenic debris, which can become entrained by a proglacial stream and other glacio-fluvial processes (Lønne & Lyså, 2005). Comparisons can be seen between alpine and Arctic proglacial systems, and this is reflected in the fact that both environments can act as sources and stores for sediment (e.g. Hodgkins *et al.*, 2003; Jansson *et al.*, 2003; Schrott *et al.*, 2003; Orwin & Smart, 2004a; Otto *et al.*, 2009).

In the proglacial area, the youngest and most recently exposed sediment is the most vulnerable to mechanisms of transfer and erosion, such as rainfall, glacio-fluvial processes, and transportation by debris flow (Ballantyne, 2002a, 2002b; Misset *et al.*, 2019). As the exposure time increases for such a paraglacial surface, rates of sediment transport are reduced due to exhaustion of readily transferred fine-grained particles (Church & Ryder, 1972; Gurnell *et al.*, 2000; Ballantyne, 2002a). Church and Ryder (1972) applied the term

paraglacial to both 'nonglacial processes that are directly conditioned by glaciation' (pp3059) and the period 'during which paraglacial processes occur' (pp3059). In 2002, Ballantyne described paraglacial as 'non-glacial earth-surface processes, sediment accumulations, landforms, land-systems and landscapes that are directly conditioned by glaciation and deglaciation'. However, Slaymaker (2009) suggested that this description was too broad and that it should be restricted to geomorphic transition, or adjustment, to non-glacial conditions. Greater exposure time leads to the possibility of sediment stabilisation caused by the growth of vegetation, which will further reduce the mobilisation of sediment (Gurnell *et al.*, 2000; Orwin & Smart, 2004b). The importance of geomorphological processes in the transfer of newly exposed glaciogenic sediments is demonstrated as sediment mobilisation is dominated by fluvial processes as the distance from the glacier terminus increases (Carrivick *et al.*, 2013). Deglaciation and subsequent aging of exposed terrain reflect the significance of the transition of the area from glacial mechanisms of sediment mobilisation and conditioning to fluvial mechanisms (Church & Ryder, 1972).

Paraglacial activity can add complexity to the glacio-fluvial environment by interconnecting ice-marginal slope and glacio-fluvial mechanisms (Etzelmüller *et al.*, 2000; Porter *et al.*, 2010). Research performed at Austre Brøggerbreen, Svalbard, found that stochastic outputs in SSC were linked to ice-marginal and valley-side sediment sources (Porter *et al.*, 2010) rather than as might usually be the case in a temperate alpine system, entrainment, and flushing from the subglacial drainage network. Porter *et al.* (2010) concluded that this was caused by debris flows produced by the melting of ice-marginal slope units. Debris flows can deposit sediment in various locations, such as the glacier surface, where the sediment can be input into the glacio-fluvial system through meltwater pathways, such as moulins. Therefore, ice-marginal deposition into the glacial system can impact the total suspended sediment flux recorded in the proglacial stream, however, the interpretations of the morphology and functioning of subglacial drainage systems based on interpretations of meltwater discharge and SSC time series need to be treated with caution. Stochastic pulses in sediment in a temperate glacier system may be misinterpreted as linking to the drainage network evolution instead of, for example, ice-marginal inputs. The availability of sediment stores/ sources is likely to be enhanced as deglaciation progresses due to climate warming, meaning that the significance of ice-marginal inputs has the potential to further increase.

The ever-changing glacial environment is further increasing the difficulty in interpreting researched variables, such as suspended sediment. Deglaciation has the means to introduce the need for the development and evolution of arctic and alpine models of glacio-fluvial sediment transport to incorporate ice-marginal mechanisms, and such development would lead to enhanced complications in defining sediment transfer rates and factors.

### **3 Research aims and objectives**

Knowledge surrounding the dynamics of glacio-fluvial sedimentation has commonly been provided by spatial measurements based on a single proglacial stream or multiple proglacial streams with the same geomorphological characteristics (e.g. Orwin and Smart, 2004). No study has reported any attempt to perform an intra-basin study of sediment dynamics on proglacial rivers with contrasting geomorphology, and this is surprising considering the high sediment loads of alpine glacial environments and the forecasted changes to future climate change in these locations. This project attempts to fill this gap with the aim of identifying the fluvio-glacial characteristics of two contrasting alpine proglacial rivers and to evaluate short-term spatial and temporal patterns of sedimentation associated with the recent glacier retreat of the Feegletscher, Swiss Alps.

To achieve this aim the following objectives should be met:

1. Installation of proglacial hydrological, monitoring stations on bedrock, and separate, sediment-dominated proglacial stream to quantify sediment fluxes and dynamics through the forefield.
2. Analyse data primarily using cross correlation of meteorological and proglacial channel data to determine the strength of relationships between all variables, and hysteresis plots of SSC-discharge to indicate glacio-fluvial dynamics.
3. Use objectives 1 and 2 to assess how rapid, recent glacier retreat is impacting the sediment dynamics of the proglacial streams that are characterised by contrasting geomorphological settings.

Sediment mobilisation within the proglacial area is not limited to fine sediment, but throughout this study, the focus is upon fine sediment and not coarse material because coarse material is usually harder to measure and is less well understood (Lane et al., 2017).

## 4 Field site

### 4.1 The Alps

#### 4.1.1 Geological and glacial history

An alpidic orogenesis occurred during the Upper Eocene and Oligocene when the African and European Plates converged in N-S direction forming the European Alps, a collision mountain belt (Schmid *et al.*, 1996; Fitzsimons & Veit, 2001) (Figures 5 and 6). During this time the Penninic Ocean disappeared and the European Alps began to be lifted above sea level with the main uplift occurring during the Miocene/Pliocene (30 million years BP) (Fitzsimons & Veit, 2001). Within the European Alps mountain system, the Swiss Alps form the divide between the French and Italian Alps (which are orientated North-South) and the Austrian Alps, which are orientated East-West (Figure 5). The inner districts of the Alps consist of large numbers of thrust sheets composed of crystalline, ophiolitic rocks, and Mesozoic sediments (Kühni & Pfiffner, 2001) (Figure 5). One of the main areas of elevation is the middle section of the European Alps, where there are numerous granite mountains, which reach altitudes above 4000 m (Kühni & Pfiffner, 2001). These granite peaks are orientated in an ENE-WSW direction and stretch for approximately 200 km. (Kühni & Pfiffner, 2001). The main section of the Alps is approximately 950 km in length (France to Austria). At their longest north-south magnitude, the European Alps is 300 km in width (Austria to Italy). The northern and southern Swiss Alps are divided by two large valleys; the Rhone and Rhine rivers are located in these two longitudinal valleys. The Saaser Valley, Switzerland is the field location for this research and is situated in the southern division of the Alps (Figure 6).

Ivy-Ochs *et al.* (2008) describe the glacial change in the European Alps from the late Pleistocene to the Little Ice Age. 12 – 10.5 ka before present (BP) displayed glacier expansion because of the c. 1300 year long Younger Dryas that is shown by moraine construction. During this period, climate conditions became increasingly dry and temperatures increased which resulted in widespread glacier retreat by 10.5 ka BP (Ivy-Ochs *et al.*, 2008). From c. 10.5 - 3.3 ka BP, there was a climatic shift towards a warmer and drier environment, which caused further glacial retreat (Ivy-Ochs *et al.*, 2008) with the exception of minor glacier advancements at c. 4.3–3.6 ka BP (Joerin *et al.*, 2006). This culminated in

the Little Ice Age (c. 1350 - 1850 AD) where glaciers reached their maximal extent during the Holocene (Grove, 2004; Ivy-Ochs *et al.*, 2008). Between 1850 and 1900, glaciers have undergone minor advance and retreat phases until the 20<sup>th</sup> Century where extensive, widespread, retreat has become dominant.

From c. 1850, glacier vertical and lateral retreat in the Swiss Alps has been greatly documented (Bauder, Funk & Huss, 2007; Farinotti, Huss, Bauder & Funk, 2009). There were two stages of glacier re-advance in the 1920s and 1980s (Haeberli & Beniston, 1998). In 1999 the Swiss Alps were estimated to have an ice volume of c. 74 km<sup>3</sup>, while between 1999 and 2008 there was a total loss of c. 8.8 km<sup>3</sup> (Farinotti *et al.*, 2009). In 2009, there were 5345 glaciers in the whole of the European Alps (Farinotti *et al.*, 2009). The majority of the 5345 glaciers are estimated to be below 0.5 km<sup>2</sup> in size and only c. 50 of the glaciers have an area greater than c. 8.5 km<sup>2</sup> (Zemp, Haeberli, Hoelzle & Paul, 2006).

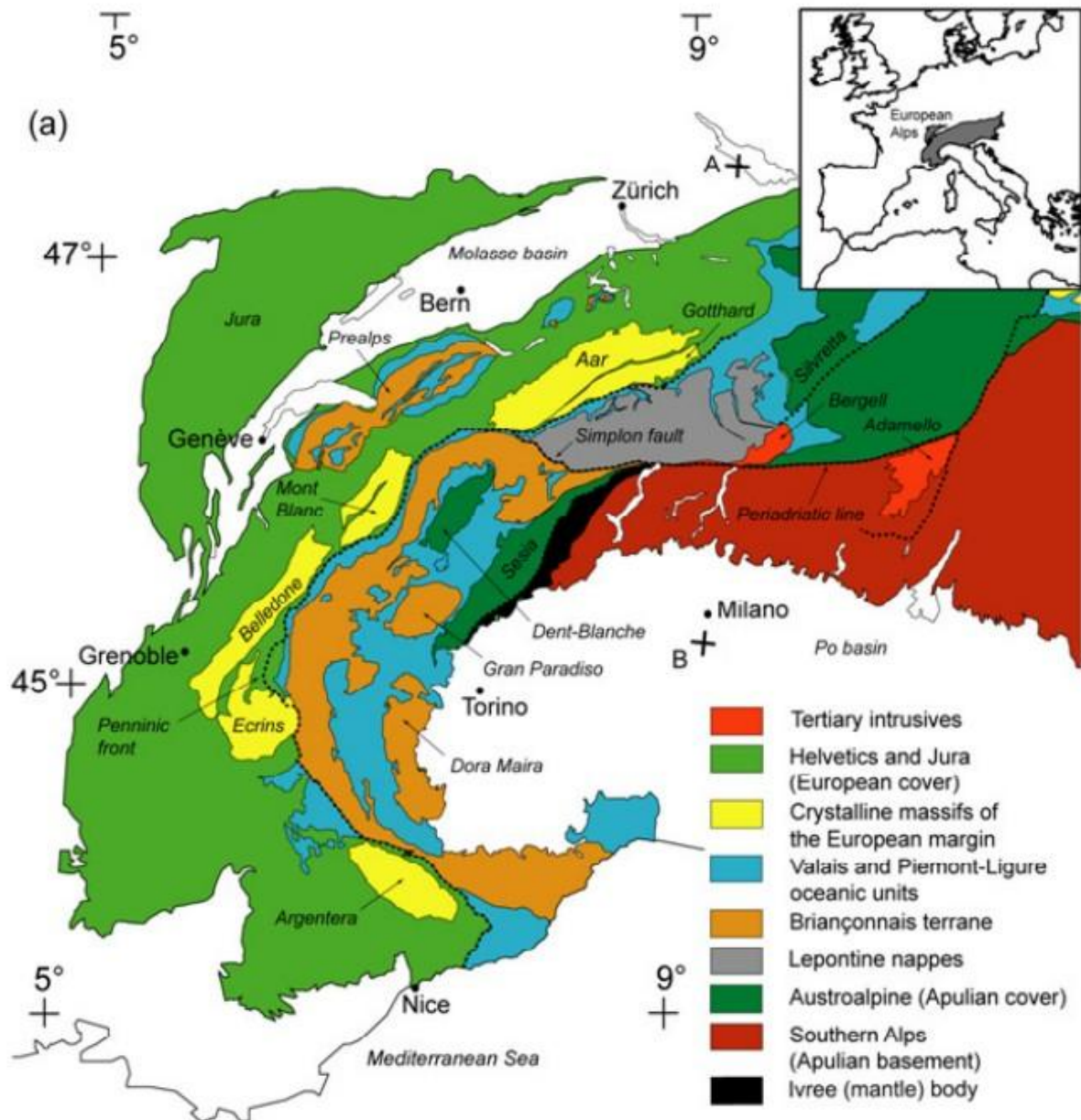


Figure 5 - Simplified geological map of the western European Alps (modified from Schmid et al., 2004 by Vernon, 2008)

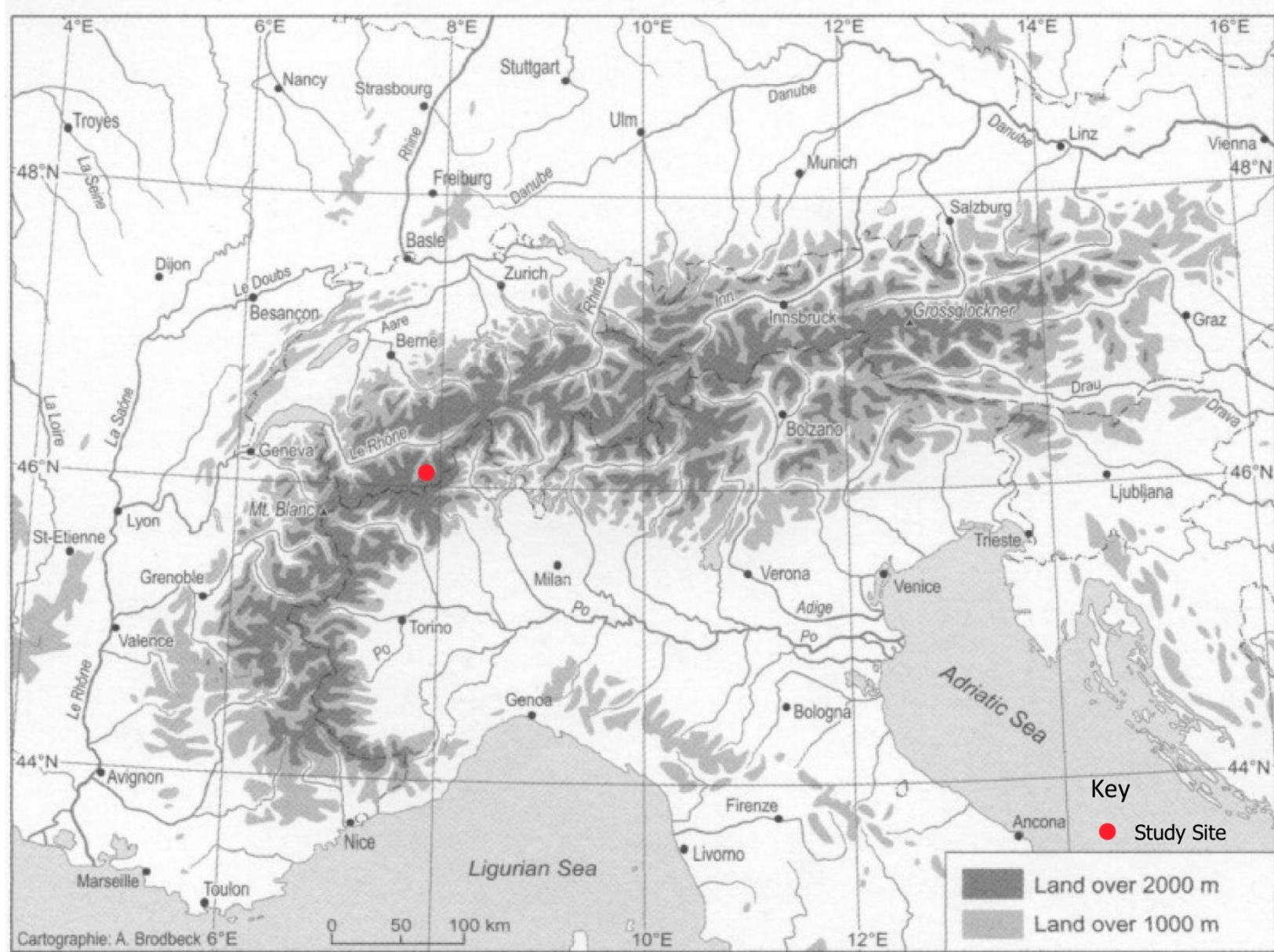


Figure 6 - Relief map of the European Alps with the location of the Saaser Valley/study site marked (modified from Fitzsimons & Veit, 2001)

#### 4.1.2 Contemporary climate

The Atlantic Ocean greatly influences the climate of Switzerland (FOMCMS, 2018). Prevailing westerly air masses are a critical source of moisture in the Alps and low-pressure networks in the Mediterranean are a critical source of long-lasting cold and wet environments (FOMCMS, 2018). The northern and southern ranges operate as topographic boundary and an obstacle which cause the inner alpine valleys to be drier compared to surrounding areas (FOMCMS, 2018)(Figure 6). The Feegletscher is situated in one of these valleys, and therefore, experiences the relatively dry, alpine climate of the Valais (Sold, Huss, Machguth, Joerg, Vieli, Linsbauer *et al.*, 2016). Examination of MeteoSwiss meteorological records for the Saaser district shows a mean monthly rainfall of 46.4 mm, while the mean May-September precipitation is greater at 51.9mm (2007-2017 data), and the district receives an estimated 800-1200 mm of annual precipitation (Swiss Meteorological Survey, Zürich). Winter precipitation primarily falls as snow above an altitude of approximately 1300 m above sea level. Snowfall is unlikely to occur in the low-lying areas of northern, western, and the extreme south of Switzerland (FOMCMS, 2018). The average May-September temperature for Valais is 18.3 °C, with an average annual temperature of c.+1.5°C (Swiss Meteorological Survey, Zürich). The average May-September temperature for Saas-Fee is 8.76 °C (1829m a.s.l), with a mean annual temperature of approximately +2.7°C (1829m a.s.l) (Swiss Meteorological Survey, Zürich) Farinotti (2010) produced the environmental lapse rate from multiple MeteoSwiss stations at elevations spanning from 272 to 3570 m above sea level and, estimated Valais to have an environmental lapse rate of  $-5.6 \times 10^{-3} \text{ } ^\circ\text{C m}^{-1}$  or  $0.56 \text{ } ^\circ\text{C } 100\text{m}^{-1}$ .

#### 4.1.3 Future climate

According to CH2018 (2018), seasonal temperatures in alpine regions of Switzerland will increase over the whole extent of the 21<sup>st</sup> century with a larger rise in summer. By 2085, average seasonal temperatures are expected to increase by c. 3.2-4.6 °C over Switzerland's alpine regions (CH2018, 2018). Precipitation during the summer months is projected to decrease by the end of the 21<sup>st</sup> century, with impacts most obvious in western Switzerland (CH2018, 2018). Climate scenario projections for 2085 show that there will be an average decrease in summer precipitation of 13% in eastern alpine regions and 20% in western alpine regions of Switzerland (CH2018, 2018). In contrast, precipitation in winter is

projected by CH2018 (2018) to increase by the end of the 21<sup>st</sup> century. Eastern alpine regions of Switzerland are expected to see this change the most (CH2018, 2018). The extent of 21<sup>st</sup> century precipitation changes is highly dependent on emission scenarios (CH2018, 2018).

## 4.2 The Feegletscher

### 4.2.1 Form and mass balance

The study was located on the forefield of the Feegletscher Nord, Süd, and the Feegletscher Nord glacier. The Feegletscher is located in the Saaser Valley, Switzerland (46° 06' N., 7° 54' E) (Figures 6 and 8). The Feegletscher is a small ice-field outlet glacier that is less than 10 km<sup>2</sup> and spans an altitude of over 4000 m a.s.l to c. 2650 m a.s.l. The Feegletscher is directly fed from two main snow accumulation areas, which are located on the east side of the Alphubel (c. 4206m a.s.l) and the north-east side of Allalinhorn (c. 4027 m a.s.l). The Feegletscher is divided into two separate glacier tongues; the northern lobe (Feegletscher Nord) and the southern lobe (Feegletscher Süd) with the Langflüh ridge separating the two lobes, and both glacier lobes are oriented and flow in a north-east direction. (Figures 7, 8, and 13). The total volume of both lobes is unknown as no ground penetrating radar or similar bathymetric type survey has been undertaken.



Figure 7 - Photo of Feegletscher from 12<sup>th</sup> September 2019 (Oberli, 2019). The rock ridge running from top centre to bottom right indicates the approximate position of the divide between the north and south lobes.

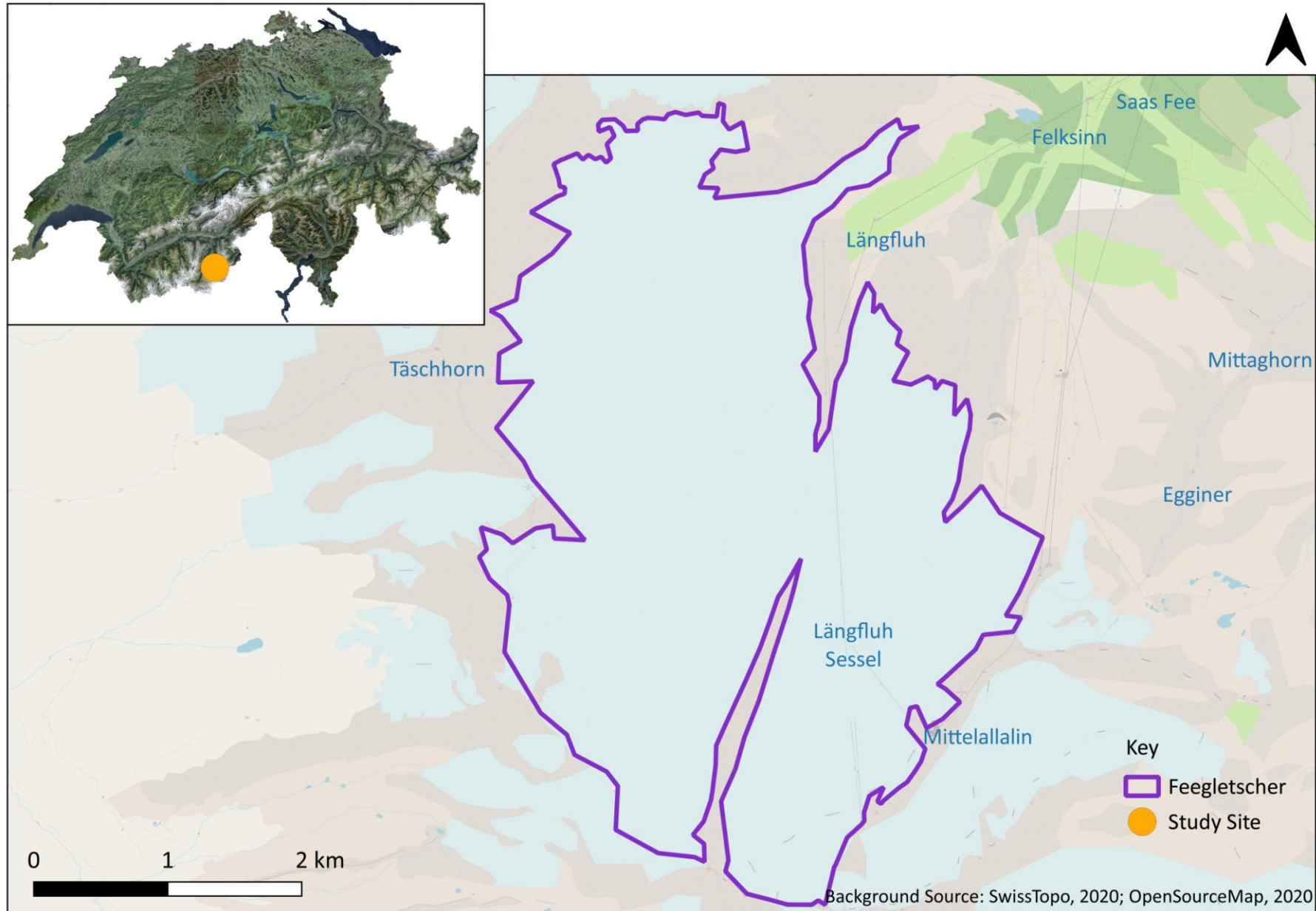


Figure 8 - Location map of Feegletscher within Switzerland. The rough overall ice cover extent of the Feegletscher is marked by the purple line and has been determined by the OSM (2020) base map presented.

The Feegletscher Süd snout is defined by a largely crevassed icefall in the lower reaches and has an uneven terminus of approximately 2.5 km in width. The upper sections of the Feegletscher Nord are heavily crevassed, but the lower section of the glacier is constrained by steep topography closer to the terminus. The terminal area of the Feegletscher Nord now seems to be almost completely separated from the main ice field, bearing all the characteristics of stagnant ice. Surface debris cover increases on lower sections of the glacier, especially on the stagnant section of the Nord lobe (Whalley, 1979). Assessment of a high-resolution DEM (swissALTI3D by SwissTopo, 2009) shows the glacier length to be 4.87 km across an elevation range of 2024 m. Glacier area was calculated from geocorrected satellite imagery as 7.56 km<sup>2</sup> and the mean glacier surface slope angle is steep at 29.1° (Smart, 2015). Ground-penetrating radar surveys of Feegletscher Süd have been performed and show that it has a maximum ice thickness of 67-72 m over the elevation range of 2900-3460 m a.s.l. (Urbini & Baskaradas, 2010). No such surveys have been carried out on the Feegletscher Nord.

Data regarding the change in Feegletscher's length has been collected since 1883 and shows a general trend of glacial retreat, with short periods of glacial advance. Deglaciation occurred by c. 9 ka BP, but the location was frequently reclaimed by ice during the Holocene (e.g. Röthlisberger and Schneebeli, 1979; Röthlisberger *et al.*, 1980). From 1923 Feegletscher Nord had been retreating at an annual rate of between 2 and 60 m (SAS/VAW, 2009). Then like many other alpine glaciers, Feegletscher advanced during the 1970 and 1980s due to climate cooling during the 1950s to 1970s (e.g. Beniston *et al.*, 1994). Feegletscher advanced at a yearly velocity of 6 to 97 m to a maximum position in 1988 (SAS/VAW, 2009, Cook *et al.*, 2013). The 1988 maximum position is shown in the proglacial area by an end moraine which is located towards the up-valley end of the LIA moraine (Cook *et al.*, 2013). Since attaining the 1988 maximum position, the North lobe has retreated by c. 800 m to its current position (as of July 2019) which is evident from the exposed bedrock formerly covered by glacier ice (Figures 9, 10, and 11). The recession during this period was comparable to the recession of the glacier between 1923 and 1956, with sustained retreat until 1997 at a rate of 5 to 55 m a<sup>-1</sup>. From 1997 to 1998 and 2000 to 2001 the glacier experienced a rapid retreat of 111 m and 209 m respectively (SAS/VAW, 2009). By 2008,

Feegletscher Nord had lowered c. 90 m (Curry *et al.*, 2009) and retreated c. 1100 m from its 1818 AD Little Ice Age (LIA) maximum position (Bircher, 1982, SAS/VAW, 2014).

#### 4.2.2 Glacier hydrology

There has been a lack of published hydrological data on the Feegletscher, although hydrological and hydrochemical analysis of the Fee catchment was conducted by Collins (1979) and hydrological analysis was also conducted by Smart (2015). Collins (1979) found that between 1966 and 1972 the total annual runoff was c.  $37\text{-}54 \times 10^6 \text{ m}^3$  with 88.7 % of annual runoff taking place between the summer months of May to September and 50% occurring between July and August. During the month of September, Feegletscher was hypothesised to englacially and/or subglacially store a total of six percent of overall annual runoff (Collins, 1979).

Contemporary hydrological studies indicated that Feegletscher Nord transports surface meltwater rapidly through the glacial and hydrological network to the proglacial area with lag times between peak melt to peak discharge ranging from +252 minutes to a lag of -40 minutes (Smart, 2015). In common with other alpine systems, this short time to peak is likely due to a combination of features that may include the highly crevassed surface that facilitates ready access to englacial drainage systems, and the steep topography, which likely enables a steep glacier bed which is known to facilitate the development of efficient subglacial drainage conditions (e.g. Flowers, 2008).

Hydrological studies suggest that Feegletscher adjusts rapidly to inputs of meltwater at the beginning of the ablation season (e.g. Collins, 1979). Meltwater transportation is restricted in early summer by the drainage network, but later in the ablation season conduit systems have developed and are effective at transporting meltwater (Collins, 1979). The effectiveness of the drainage system during the ablation season is reflected by short lag times between surface air temperature and meltwater discharge (Smart, 2015). Ground-penetrating radar surveys conducted on Feegletscher Süd revealed the presence of superficial and subsuperficial meltwater conduits (Urbini & Baskaradas, 2010; Urbini, 2012, pers comms). These conduits were located between c. 5 to 15 m beneath the glacier surface at sites where the maximum ice depth was between 20 to 30 m (Urbini & Baskaradas, 2010; Urbini, 2012, pers comms). No spring flood or outburst events of subglacial stored water

have been reported or recorded to have occurred for Feegletscher Nord (Schnyder, 2012, pers. comm.). Meltwater discharges from the Feegletscher Nord at a single channel to a bedrock ridge and down through a waterfall then into a small braided proglacial zone (Figure 9) before joining larger proglacial channels that finally join into the Feevispa River that flows towards the Rhone valley.



Figure 9 - Photograph showing meltwater flowing from Feegletscher Nord into a bedrock ridge and down through a waterfall into a small braided proglacial area (2019).

#### 4.2.3 Geomorphology and geology

Due to post-LIA retreat, steep glaciogenic deposits made up of a stacked, multi-crested, lateral moraine have been uncovered on the northern side of the glacial forefield (Curry *et al.*, 2009). The northern area of the proglacial zone of Feegletscher Nord is bordered by an c. 60 to 120 m high, c. 700 m long LIA moraine that is oriented in an east-west direction and the exposed glaciogenic material has been reworked into gullies and cones (Curry *et al.*, 2009) (Figures 10, 11, and 12). The volume of the northern moraine is much larger than that of the southern moraine, meaning that the glacier forefield is asymmetrical in cross-section

(Curry *et al.*, 2009). Therefore, the northern moraine has the potential to yield higher sediment supplies, however, it is well cemented and therefore the cementation may limit the ability to yield sediments (Curry *et al.*, 2009). There are large quantities of ground-level sediments exposed by retreat and input from valley sides up-valley of the northern moraine. Heavy rainfall and snowmelt cause debris flows and translational sliding which rework the glacial sediment (Curry *et al.*, 2006). The moraine is situated below the discontinuous permafrost limit (c. 2350 to 2650 m) and it extends from an altitude of c. 2060 m a.s.l. to c. 1940 m a.s.l (Curry *et al.*, 2009), and therefore, sediment is more readily accessible for transfer compared to areas that are above the discontinuous permafrost limit. The AD 1818 ice maximum is visible on the moraine at c. 2020 m a.s.l and is shown by a distinct step and N-E orientated ridge. Up-valley from the AD 1818 ice limit, the moraine's proximal slopes reach over 100 m in height, however, the down-valley slope height does not exceed 70 m. The steepness of the proximal slope of the lateral moraine varies from the most recently deglaciated sections (up-valley) to the oldest deglaciated sections (down-valley). Recently deglaciated sections have a steepness of c. 80°, compared to the oldest sections that show a steepness of c. 50° (Curry *et al.*, 2009). The proximal slopes have minimal vegetation cover and are generally unstable when compared to the largely vegetated distal slopes. The distal slopes have a gradient of c. 33° (Curry *et al.*, 2009).

The lateral moraine found at Feegletscher Nord is morphologically similar to many others that have been studied within the European Alps (e.g. Curry *et al.*, 2006). Moraine slopes are a dynamic environment and at the Feegletscher Nord moraine slope adjustment occurred within c. 80 years (Curry *et al.*, 2006). During that progressive slope stabilisation happened with gullies, arêtes, and debris cones being levelled and replaced with vegetated cones and debris aprons, levees, and lobes (Curry *et al.*, 2006).

The forefield of Feegletscher Nord is characterised by several ephemeral braided proglacial rivers, generally dominated by two larger rivers during the peak melt season. The geomorphology of the glacial forefield is influenced by the surrounding slopes (Figures 9, 10, and 11) and frequent small rockfalls from the steep northern bedrock walls provide material to the forefield. During 1954 a large rock avalanche (referred to locally as the Guglen rock avalanche) took place, involving some c.  $1 \times 10^6 \text{ m}^3$  of rock (Ruppen *et al.*, 1988). Most of the rockfall landed down-valley of the glacier however, some sediment was deposited on the

surface of the Feegletscher Nord (Whalley and Krinsley, 1974). Large amounts of the rock from the Guglen event were reworked by the glacier as it advanced and only a small section was left unaffected (Figures 11, 12A, and 12D) (Whalley and Krinsley, 1974). Large angular boulders (< 6.5 m in diameter) of mica-schist can be found in the unmodified sections of the rock avalanche material (Cook *et al.*, 2013).

The lithology of the valley is mostly made up of Palaeozoic mica-schist, especially in the northern part of the catchment where Feegletscher Nord is situated (Bearth, 1968; Cook *et al.*, 2013). Bedrock outcrops located on the southern side of the valley are Mesozoic metasedimentary rocks, mainly quartzite (Cook *et al.*, 2013). The southern area of the catchment is underlain by ophiolite containing serpentinite, amphibolite, and albite-schist.



Figure 10 - Photograph of the 60-120 m high, c. 700 m long lateral moraine is located on the northern side of Feegletscher Nord's valley (2019).



Figure 11 - Photograph of Feegletscher Nord's braided proglacial area and steep moraine slopes (2019).

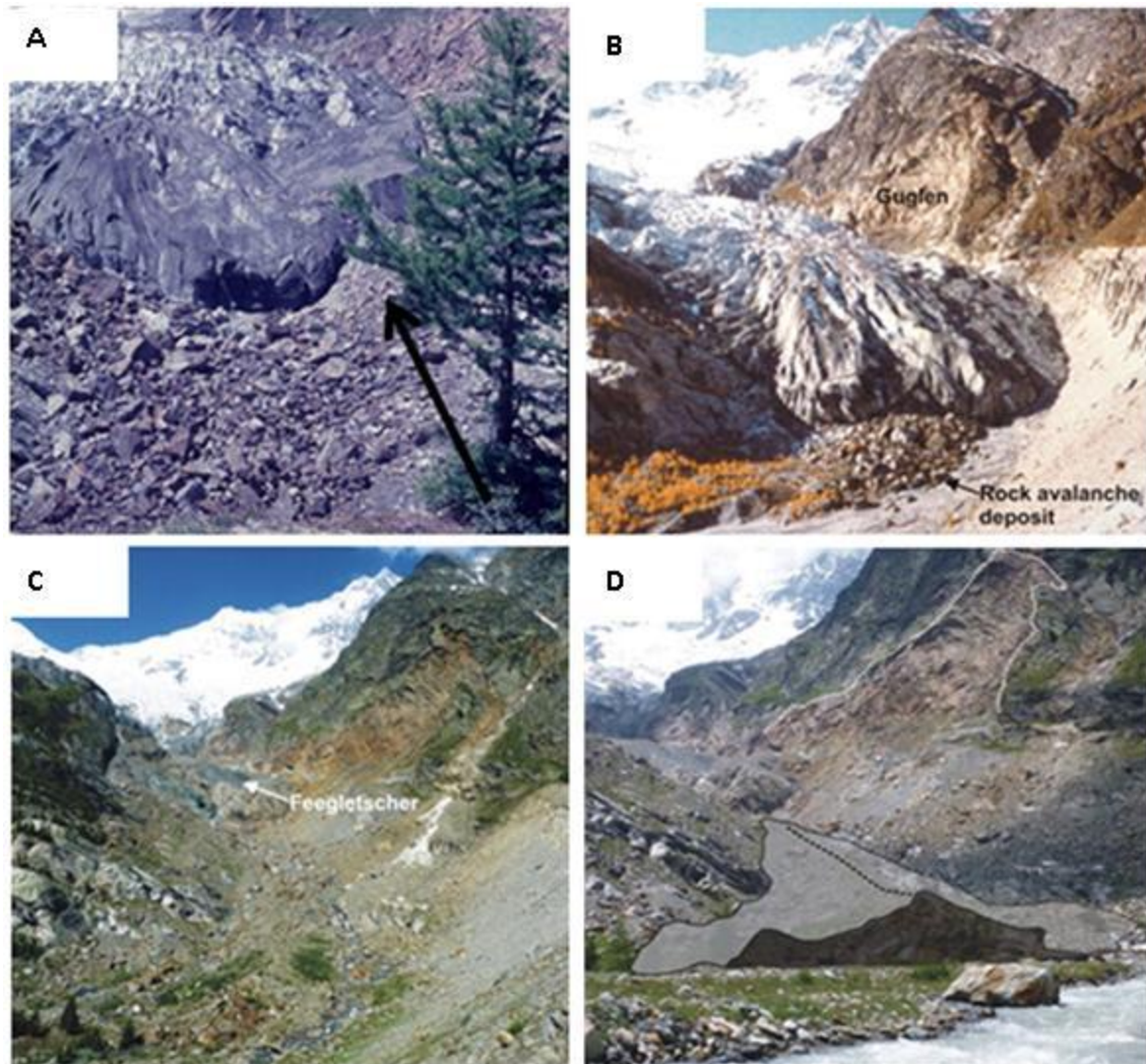


Figure 12 - (A) Deposition of supraglacial rock avalanche debris at the Feegletscher Nord in 1974, marked by black arrow (photograph by Michael Hambrey); (B) Feegletscher Nord in 1985 as it advanced over blocks from the Guglen rock avalanche, viewed approximately from the east-facing west (photograph by Benedikt Schnyder); (C) Feegletscher Nord in 2010 viewed from a similar position; (D) morphology of the glacially reworked rock avalanche debris (dark-shaded area depicts unaltered rock avalanche debris; grey-shaded area depicts reworked rock avalanche debris; black dotted line shows the crest of lower valley hummocky zone; white-dotted line shows Guglen rock avalanche scar (Cook, Porter & Bendall, 2013).

## 5 Data collection

### 5.1 Method

#### 5.1.1 Proglacial channel Monitoring

Proglacial stream monitoring was performed during June-July 2019, DOY 190-251. A series of Campbell CR1000 data logger gauging stations were set up in three locations; two on the Feegletscher Nord's proglacial stream and one on the Feegletscher Süd's proglacial stream (Figure 13). The data loggers were set up to scan data at five second intervals and record average data every 2 minutes. After DOY 202, the sampling interval was changed to every 4 minutes for the data logger located on the Feegletscher Süd proglacial stream, and this was to preserve battery life and increase the data recording period. All gauging stations were set up to monitor steam stage and turbidity and the gauging sites were situated in locations with stable channel cross-sections that were possible to access regularly. Due to the logistics of having multiple monitoring stations across Feegletscher's catchment monitoring time periods and overall samples collected differed slightly between sites.

##### 5.1.1.1 Discharge

The proglacial stream stage was recorded using a Druck PDCR pressure sensor at all three proglacial gauging stations. Salt dilution gaugings were performed at all sites during an array of proglacial stream conditions to determine a stage to discharge relationship (e.g. Orwin & Smart, 2004a). Salt dilutions were conducted using 0.5 kg of salt dissolved into c. 10 L of stream water and added upstream of a submerged electrical conductivity (EC) probe (Hanna HI 8733 probe) with an accuracy of  $\pm 2$  %. Electrical conductivity was measured at five second intervals for the duration of the passage of the salt wave. A rating curve was derived and used to generate discharge from the time series of stage data for each station (Figures 14, 15, 16).

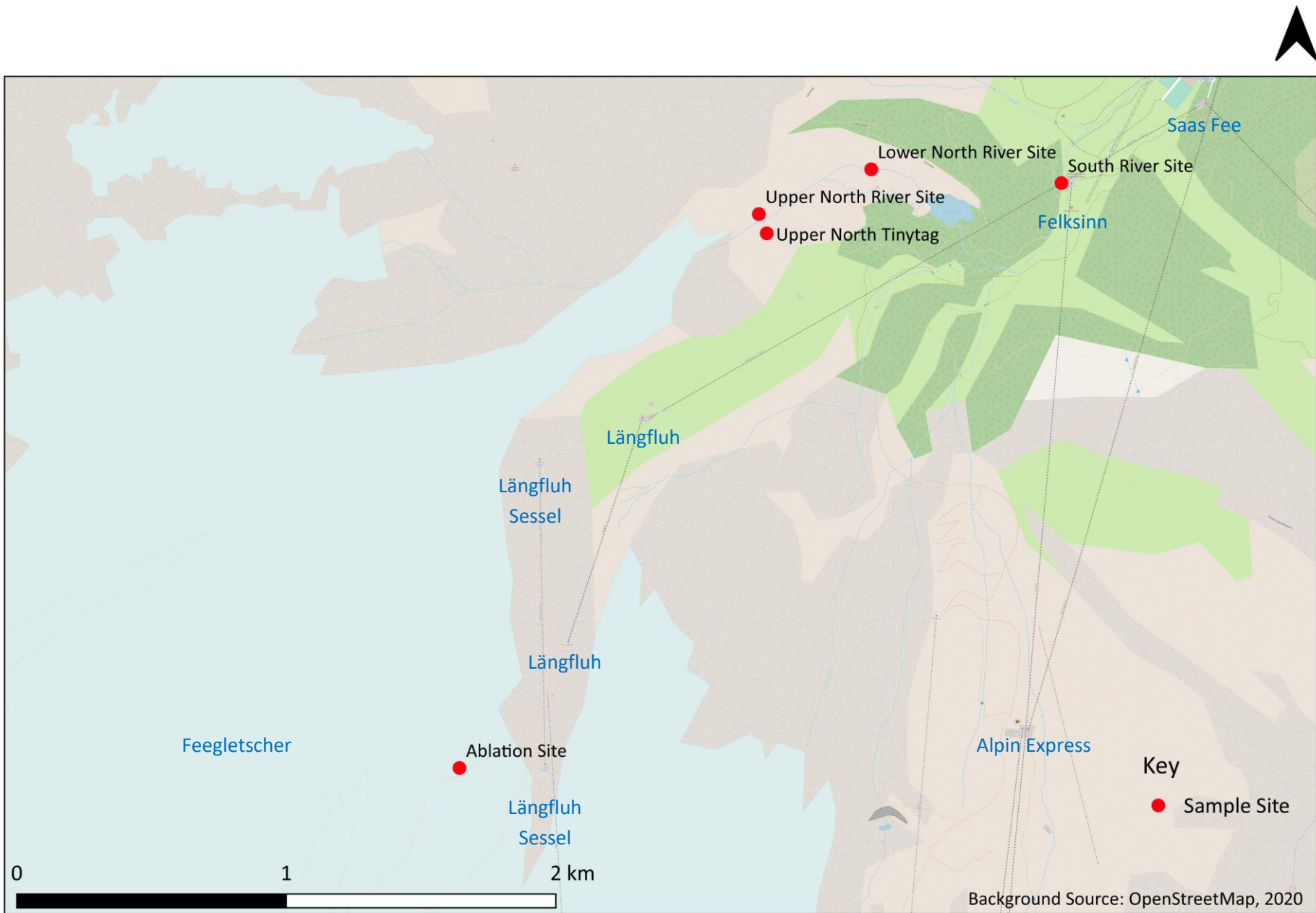


Figure 13 - Location map of sampling sites on the Feegletscher and the proglacial area of the Feegletscher

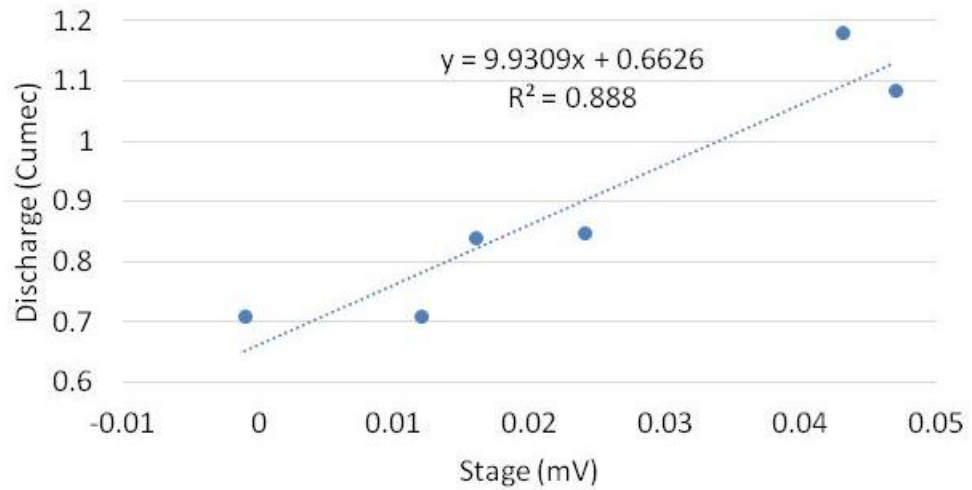


Figure 14 - Discharge calibration of the Upper North River site on the Feegetscher Nord's proglacial stream.

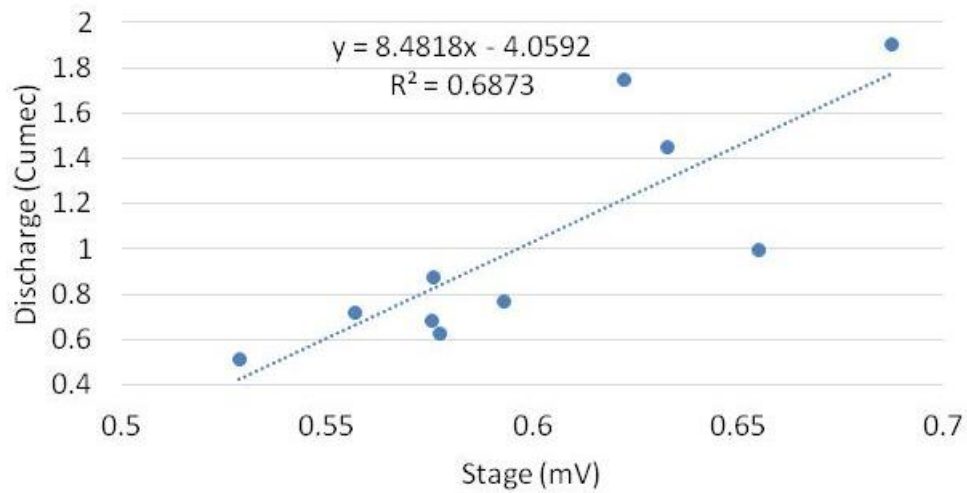


Figure 15 - Discharge calibration of the Lower North River site on the Feegetscher Nord's proglacial stream.

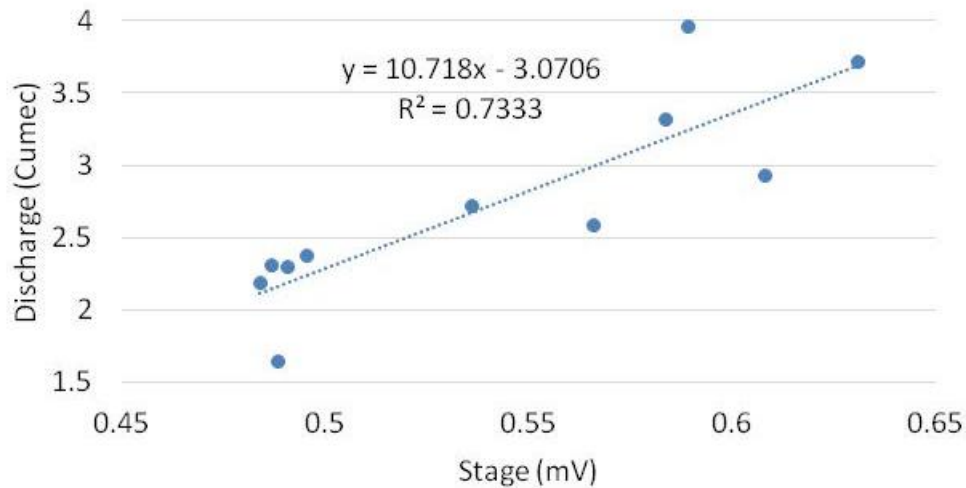


Figure 16 - Discharge calibration of the South River site on the Feegletscher Süd's proglacial stream.

#### 5.1.1.2 Suspended Sediment Concentration

Turbidity was monitored at all three gauging stations by using infra-red Partech IR15C turbidity sensors. SSC was determined gravimetrically (e.g. Collins 1990; 1995). 200 ml samples of meltwater were manually extracted from each proglacial stream site at an array of proglacial stream conditions and vacuum filtered using pre-weighed Whatman Grade no. 3 filter papers (6  $\mu\text{m}$  particle retention). The pre-weighed filter papers were weighed using an analytical balance with an accuracy of  $\pm 0.00195$  g. The filter papers were then oven-dried at 105 °C for 60 minutes, allowed to cool, and reweighed. SSC was then calculated in  $\text{g l}^{-1}$ . The SSC samples allow the turbidity values to be calibrated when a rating curve is applied to each time-series of turbidity against SSC values (Figure 17, 18, 19). This technique and the relationship between turbidity and SSC are well reviewed in the glaciological research literature (e.g. Hodson & Ferguson, 1999; Swift *et al.*, 2005a).

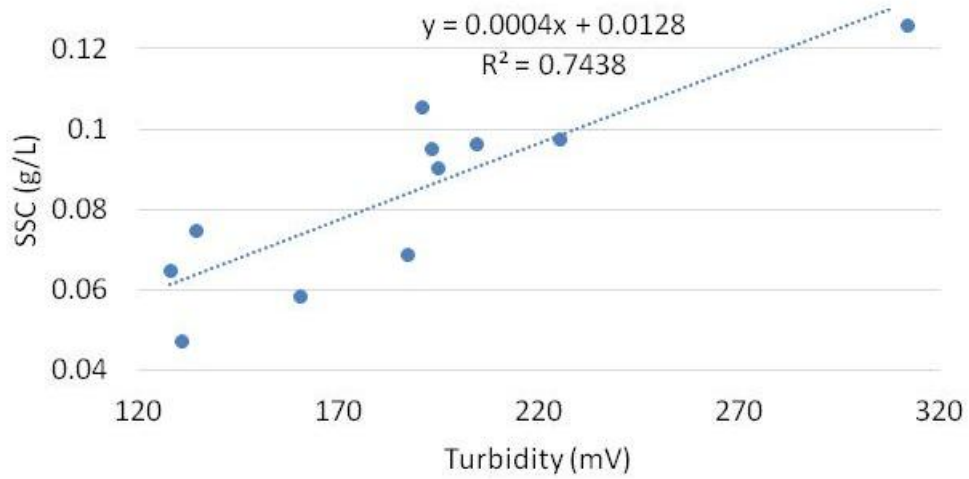


Figure 17 - Suspended sediment concentration (SSC) calibration of the Upper North River site on the Feegletscher Nord's proglacial stream.

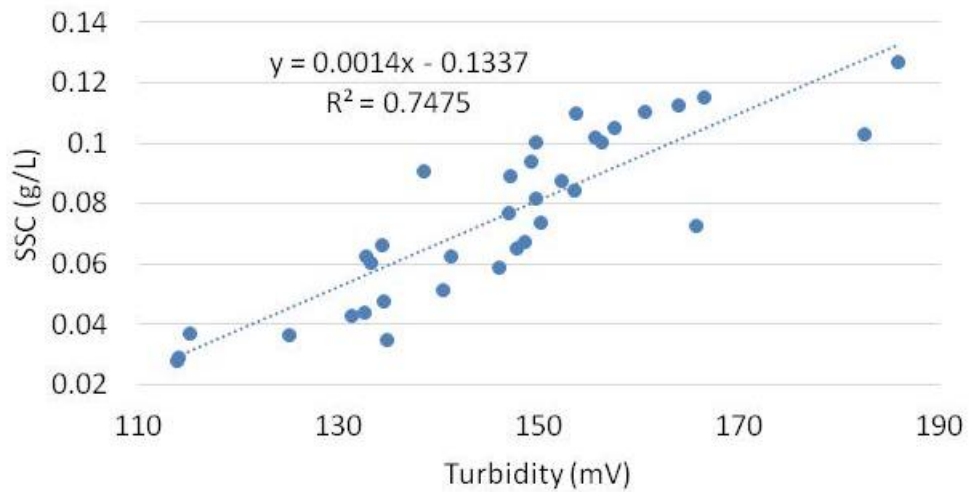
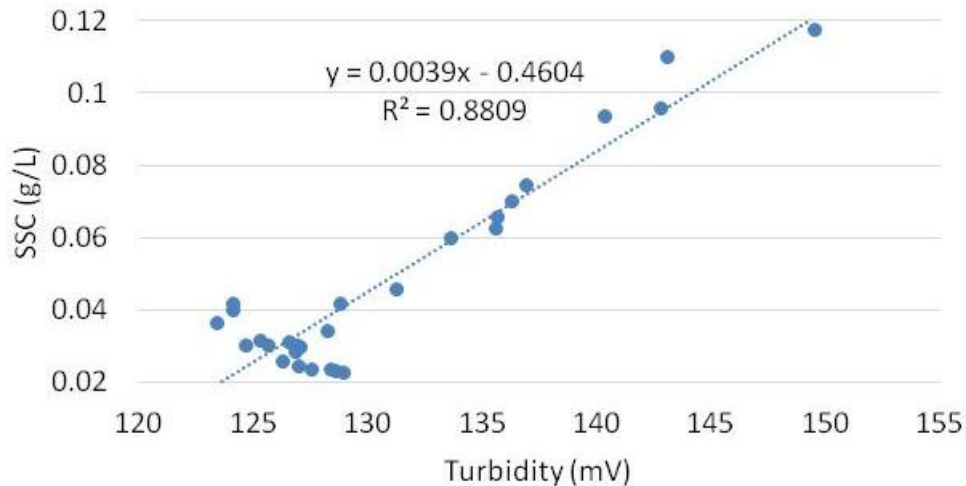


Figure 18 - Suspended sediment concentration (SSC) calibration of the Lower North River site on the Feegletscher Nord's proglacial stream.



**Figure 19 - Suspended sediment concentration (SSC) calibration of the South River site on the Feegletscher Süd's proglacial stream.**

### 5.1.2 Meteorological Data

Meteorological data were collected during June-July 2019 to help inform the interpretation of discharge and SSC data sets. Two air temperature stations were installed in the proglacial zone of the Feegletscher Nord and one station was set up on the Feegletscher itself (Figure 13 - Lower North River Site, Upper North Tinytag, and Ablation site). These stations were comprised of a Tinytag TGP-4020 data logger with a thermoelectric temperature probe surrounded by a radiation shield to eliminate any direct impact from radiation and to ensure adequate air flow around the probe (Figure 20 and 21). The Tinytag data loggers were set to measure air temperature every two seconds and store the averaged temperature data every two minutes. The accuracy of the temperature probe is stated as  $\pm 0.02$  °C. Due to logistical issues, the meteorological data were collected over different time periods. Air temperature data were collected during DOY 191-200 for the Feegletscher, DOY 193-201 for the upper Feegletscher Nord proglacial river site, and during DOY 190-251 for the lower Feegletscher Nord proglacial river site (Figure 13). Time periods and overall samples collected differed slightly between sites because of the logistics of having multiple monitoring stations across Feegletscher's catchment. Rainfall data were situated at the lower Feegletscher Nord proglacial river site during DOY 190-210. The loggers collected data over an elevation range of 1935-2939m asl. Data was recorded by a Campbell Scientific tipping bucket rain gauge ARG100 wired to a Campbell Scientific CR10x data logger, set to scan every 10 seconds and output averaged data every two minutes. Qualitative observations of general weather

conditions and cloud cover were noted every two hours for DOY 190-210 to aid subsequent interpretation of data sets.



Figure 20 - Tinytag TGP-4020 data loggers with thermoelectric temperature probes surrounded by a radiation shield that is located at the Upper North Tinytag site in the proglacial area of the Feegletscher Nord.

### 5.1.3 Ablation Monitoring

An ablation stake was set up on the Feegletscher Nord at an elevation of approximately 2939 m a.s.l. (Figure 13) and it remained in place from DOY 191 to DOY 200. Multiple stakes would have given a better spatial and temporal representation of whole glacier surface ablation processes, however, this was not logistically possible and so the installed ablation stake was intended only to give an approximate estimation of ice surface ablation. The ablation stake was drilled vertically into the ice to a depth of 0.5 metres. The upper part of the glacier is used for skiing and snow is transferred daily from the accumulation zone downslope to maintain the ski routes. The location for the ablation stake avoided these sections of the glacier to reduce ablation result errors. The ablation stake was monitored daily where possible. Data collection was performed using a tape measure and measurements were taken to within  $\pm 0.01$  m. A flat surface was used as a guide for the glacier surface because of the uneven ice surface and because the area around the base of the ablation stake conducts more heat and therefore has the potential to cause increased melt around the stake base (Hubbard & Glasser, 2005; Rutter *et al.*, 2011).



Figure 21 - Photograph showing ablation stake and Tinytag sensor with a radiation shield located at the Ablation site on the Feegletscher Nord.

#### 5.1.4 Glacial Proglacial Imagery

RGB imagery was collected through repeat drone flights and similar techniques as Gindraux *et al.* (2017), and Jouvét *et al.* (2017) were used. The RGB camera was configured to capture images at a frequency of one every second over a set flight plan. However, this was later amended to a two second capture rate through spaced removal of images from the flight set. This was necessitated by the high density of images and subsequent overlap of land coverage, which led to several issues when attempting to mosaic the images in Pix4d photogrammetry software. The images were then reviewed and data captured below an altitude of 100m were removed as these covered non-relevant phases of the flight, such as the drone taking off and landing. It also meant that the images that were left were all captured at a consistent angle, and were, therefore, easier to work with. Pix4D was used to stitch the images together and create an orthomosaic; the output composite generated via the stitching of individual images linked through mutual georeference points.

## 6 Data Series

### 6.1 Meteorology

#### 6.1.1 Air Temperature

The air temperature recorded at the Upper North; Lower North; and Ablation site all showed diurnal cycles (Figure 22, 23). The Upper North site demonstrated a slightly increasing temperature trend during the period of measurement (DOY 193 - 201) with DOY 196 failing to follow the increasing temperature trend (Figure 22). The Upper North site recorded a mean air temperature of 11.52 °C (DOY 193 - 201) with a maximum air temperature of 19.63 °C (DOY 198), and a minimum air temperature of 2.74 °C (DOY 196) (Figure 22). During the first week of measurement (DOY 193 - 196), the mean air temperature recorded at the Upper North site was 10.29 °C, and the mean increased by 2.22 °C to 12.51 °C in the second week (DOY 197 - 201). The air temperature recorded at the Lower North site had an overall increasing temperature during the Ablation and Upper North site periods of measurement (DOY 191 - 201), however, the total period of measurement at the Lower North site showed a reducing temperature (DOY 190 - 251) (Figure 22, 23). The Lower North site recorded a mean air temperature of 12.89 °C during DOY 190 - 251 with a maximum air temperature of 26.6 °C (DOY 206) and a minimum air

temperature of 3.75 °C (DOY 196). During the first week of recording air temperature (DOY 190 - 196), the lower north site experienced a mean of 11.32 °C. The mean air temperature during week 2 (DOY 197 - 203) was 13.54 °C, which is an increase of 2.22 °C compared to DOY 190 -197. DOY 204 - 210 demonstrated another increase in the mean air temperature. An increase of 1.13 °C was experienced, giving the Lower North site a mean air temperature of 14.67 °C. Lastly, the Ablation site showed a small positive trend (DOY 191 - 201) (Figure 22). The Ablation site recorded a mean air temperature of 3.49 °C (DOY 191 - 201), a maximum air temperature of 7.55 °C (DOY 197), and a minimum air temperature of -2.08 °C (196). During the first week of air temperature measurement, the Ablation site recorded an average of 3.10 °C (DOY 191 - 196). The mean air temperature during week 2 increased by 1.03 °C to give a mean of 4.13 °C (DOY 197 - 200).

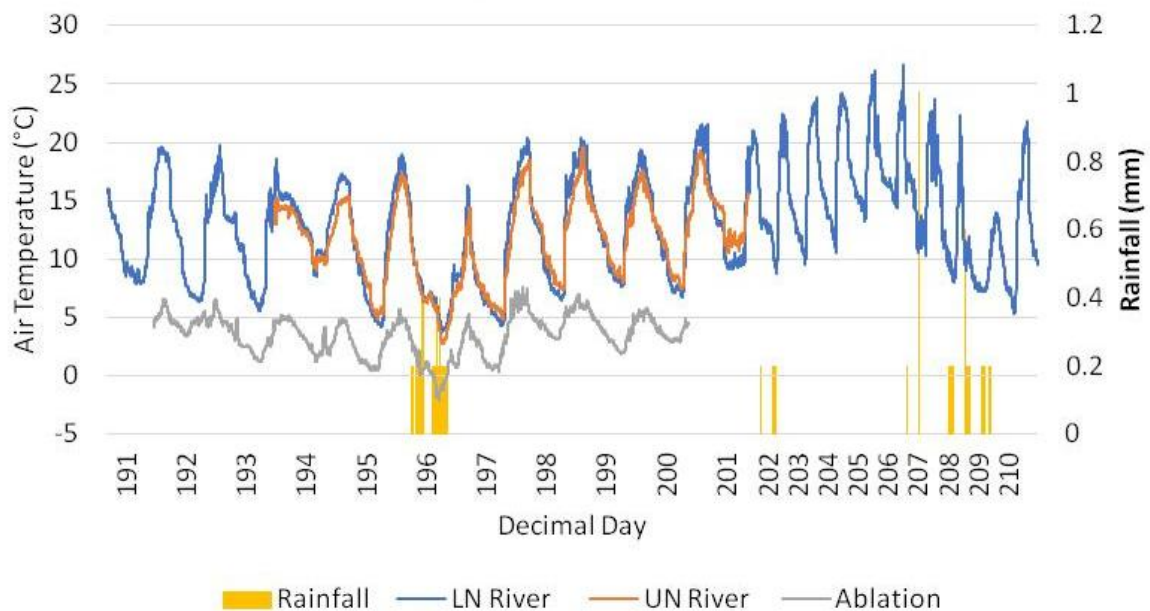


**Figure 22 - Air temperature record at the Ablation Site on the Feegletscher Nord (DOY 191 - 201); Upper North River Site (DOY 193 - 201) and Lower North River site (DOY 190 - 210) of the Feegletscher Nord's proglacial stream and rainfall data recorded at the Lower North River Site in the proglacial area of the Feegletscher Nord (DOY 190 - 210)**

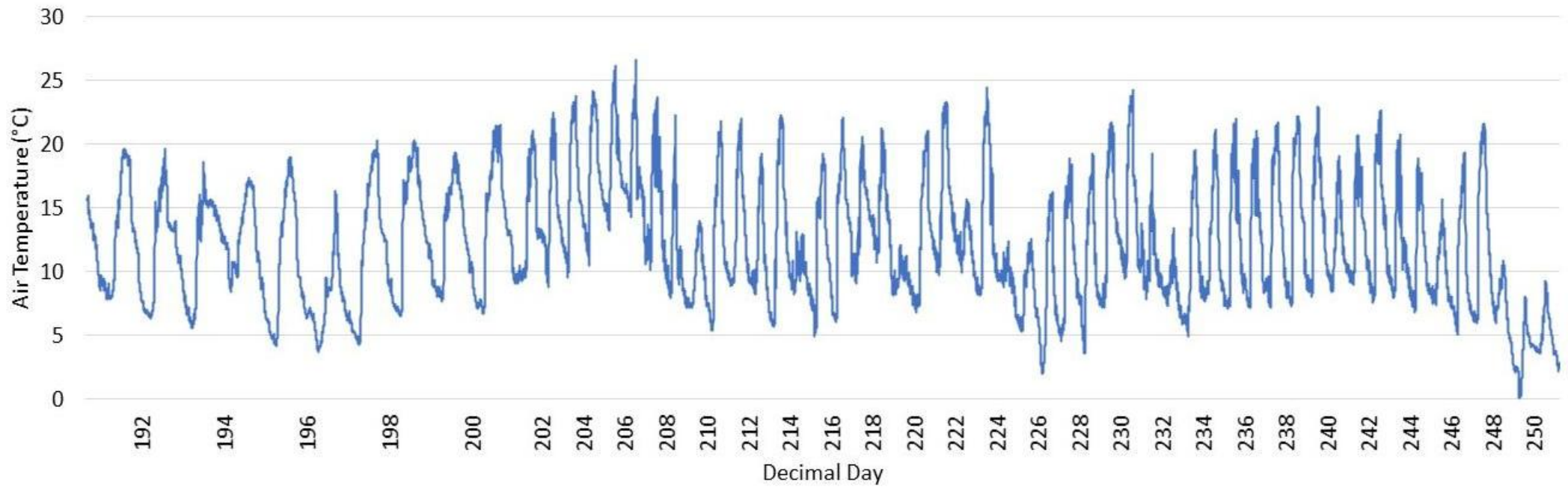


Figure 23 - Air temperature recorded at Lower North River site in the proglacial area of the Feegletscher Nord (DOY 190 - 250)

### 6.1.2 Rainfall

During the period of measurement (DOY 190 - 210), the Lower North site experienced 9 rainfall events across 8 days: DOY 195, 196, 201, 202, 206, 207, 208, and 209 (Figure 22). During the period of study, the Lower North site had a total of 43.818 mm of rain. The largest rainfall event of 24.120 mm occurred on DOY 195 - 196 with 9.246 mm on DOY 195 and 14.874 mm on DOY 196 (Table 1). The rainfall occurring on DOY 196 was the most precipitation experienced in a single day. The smallest rainfall event of 0.201 mm took place on DOY 206 (Table 1). DOY 208 had two precipitation events take place, the first event was a total of 4.020 mm and the second was 7.437 mm, making the overall rainfall for DOY 208 11.457 mm (Table 1).

**Table 1 - Rainfall recorded at the Lower North River site in the proglacial area of the Feegletscher Nord during DOY 190 - 210**

Decimal Day	Quantity of Rainfall (mm)
195	9.246
196	14.874
201	0.402
202	1.608
206	0.201
207	2.814
208	3.216
209	11.457

### 6.1.3 Lapse Rate

The lapse rate at which air temperature differs as an expression of elevation were calculated using time series of air temperature monitored at the Ablation site (2939 m asl); the Upper North Tinytag site (2103m asl); and the Lower North River site (1935 m asl) (Figure 13) (Figure 22 & 23). Lapse rates were calculated between the Lower North River site and the Upper North Tinytag site; the Lower North River site and the Ablation site; and lastly, the Upper North Tinytag site and the Ablation site (Figure 24).

All sites demonstrated diurnal cycles in lapse rates, however, the lapse rates between the Lower North site and Upper North Tinytag site showed the most diurnal variation (Figure

24). Negative values demonstrate a reduction in air temperature with altitude and positive values demonstrate an increase in air temperature with altitude, therefore, suggesting a temperature inversion. The lapse rates recorded at all sites showed a slight but small positive increase throughout the period of measurement. The mean lapse rate between the Lower North River site and the Ablation site was  $-0.821$  °C per 100 m (DOY 191 - 200). Between these two sites, the minimum lapse rate recorded was  $-0.138$  °C per 100 m (DOY 192.2) and the maximum lapse rate was  $-1.451$  °C per 100 m (192.6). Between the Lower North River site and the Upper North Tinytag site the mean lapse rate was  $-0.245$  °C per 100 m (DOY 193 - 201), with a maximum lapse rate of  $+1.519$  °C per 100 m (DOY 201.1) and a minimum lapse rate of  $-2.862$  °C per 100 m (DOY 200.7). The mean lapse rate between the Upper North Tinytag site and the Ablation site was  $-0.951$  °C per 100 m (DOY 193 - 200). The maximum lapse rate between these two sites was  $-0.297$  °C per 100 m and the minimum lapse rate was  $-1.662$  °C per 100 m.

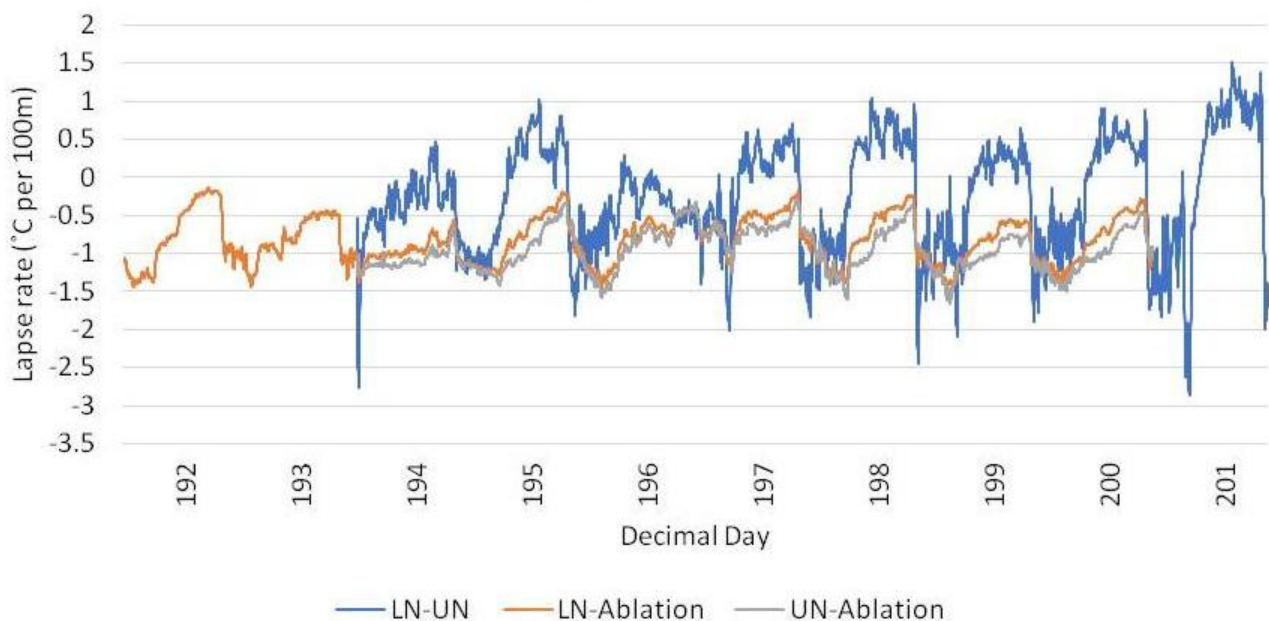


**Figure 24 - Lapse Rate data for Lower North River Site-UN River Site (DOY 193 - 201); Lower North River Site-Ablation Site (DOY 191 - 200); Upper North River Site-Ablation Site (DOY 193 - 200). Negative values demonstrate a reduction in air temperature with altitude and positive values demonstrate an increase in air temperature with altitude**

## 6.2 Glacier Ablation

### 6.2.1 Melt Rate

During the period of measurement (DOY 191 - 200) the mean daily surface melt recorded on Feegletscher was 4.033 cm. The daily maximum surface melt was 7.875 cm (DOY 193) and the daily minimum melt experienced was 2.385 on DOY 196 (Figure 25). The surface melt of Feegletscher reflects the average daily temperature at the Ablation site (Figure 25).

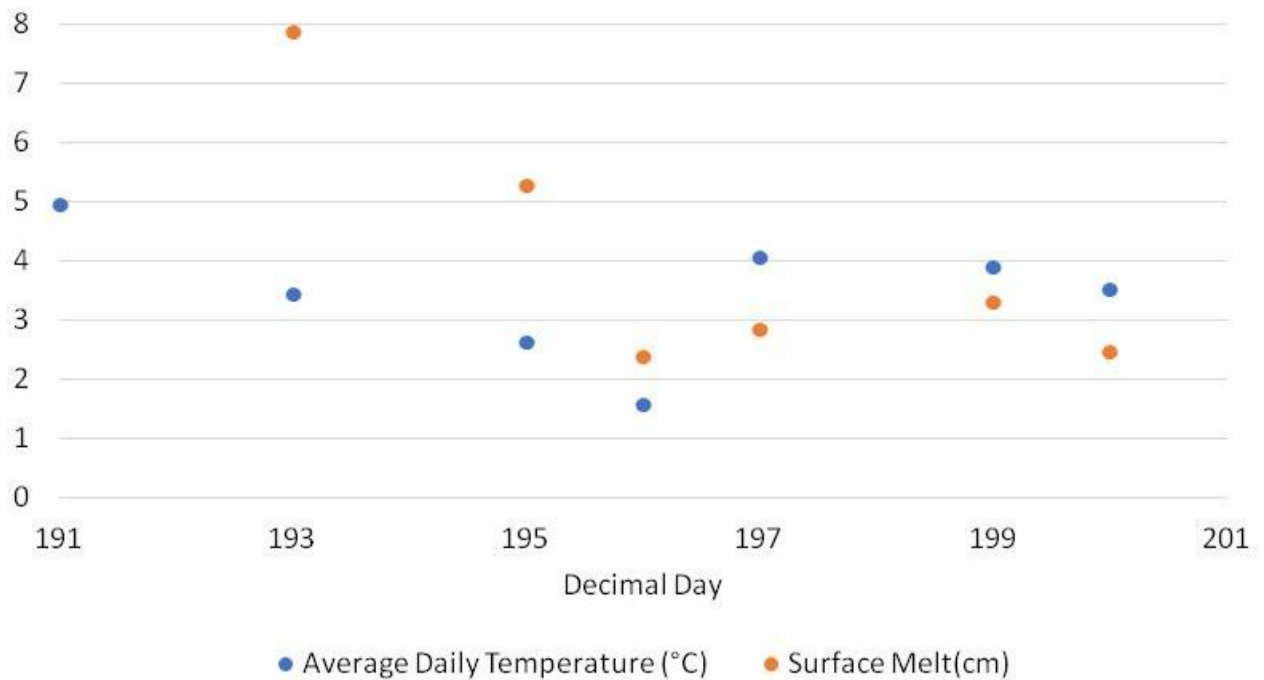


Figure 25 - Average daily temperature at the Ablation Site and recorded surface melt on the Feegletscher Nord during DOY 191 - 201.

### 6.2.2 Drone RGB Imagery

Overall albedo figures were not produced, however, visual inspection of the drone imagery of the Feegletscher shows that DOY 193 (Figure 26) had the highest quantity of glacier surface dust but the lowest amount of bare ice surface. In comparison to Figure 26, there is a clear reduction in glacier surface dust and an increase in the size of bare ice patches on DOY 199 (Figure 27) and DOY 200 (Figure 28). Surface melting is demonstrated by the increased size of bare ice patches from DOY 193 to 200. Gabbi *et al.*, (2015) found that on average the presence of dust at a glacier surface could reduce mean annual albedo by less than 0.01. During DOY 193 to 200, the reduction of dust on the glacier's surface increases

the overall mean albedo, however, the increase in the size of bare ice patches reduces the overall mean albedo (e.g. Warren *et al.*, 1998; Bond & Bergstrom, 2006; Gabbi *et al.*, 2015).

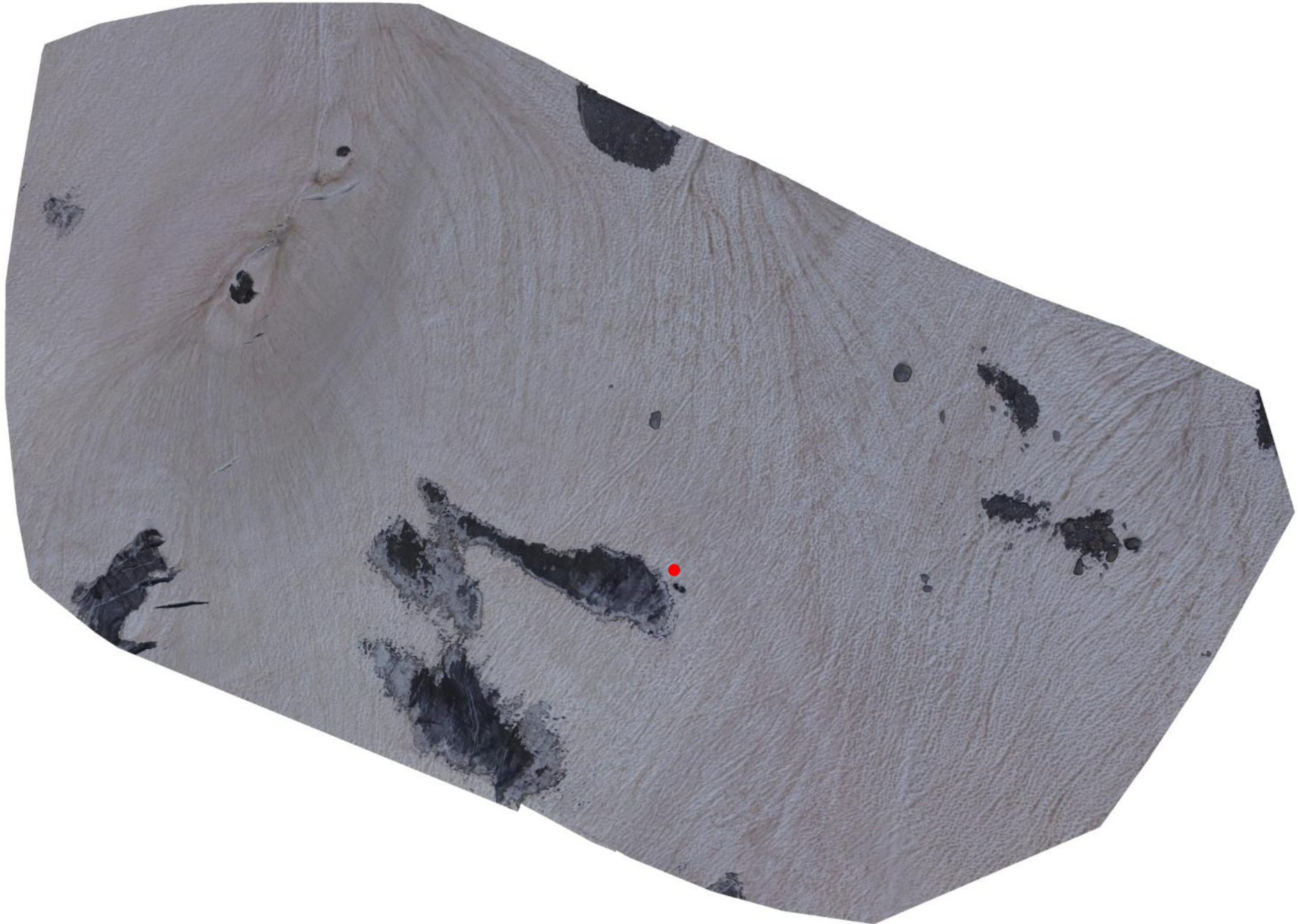


Figure 26 - DOY 193 drone imagery of the albedo site on the Feegletscher. The red dot shows the approximate location of the ablation stake and TinyTag station. Visually shows the highest quantity of glacier surface dust and smallest size of bare ice patches compared to Figures 27 and 28.

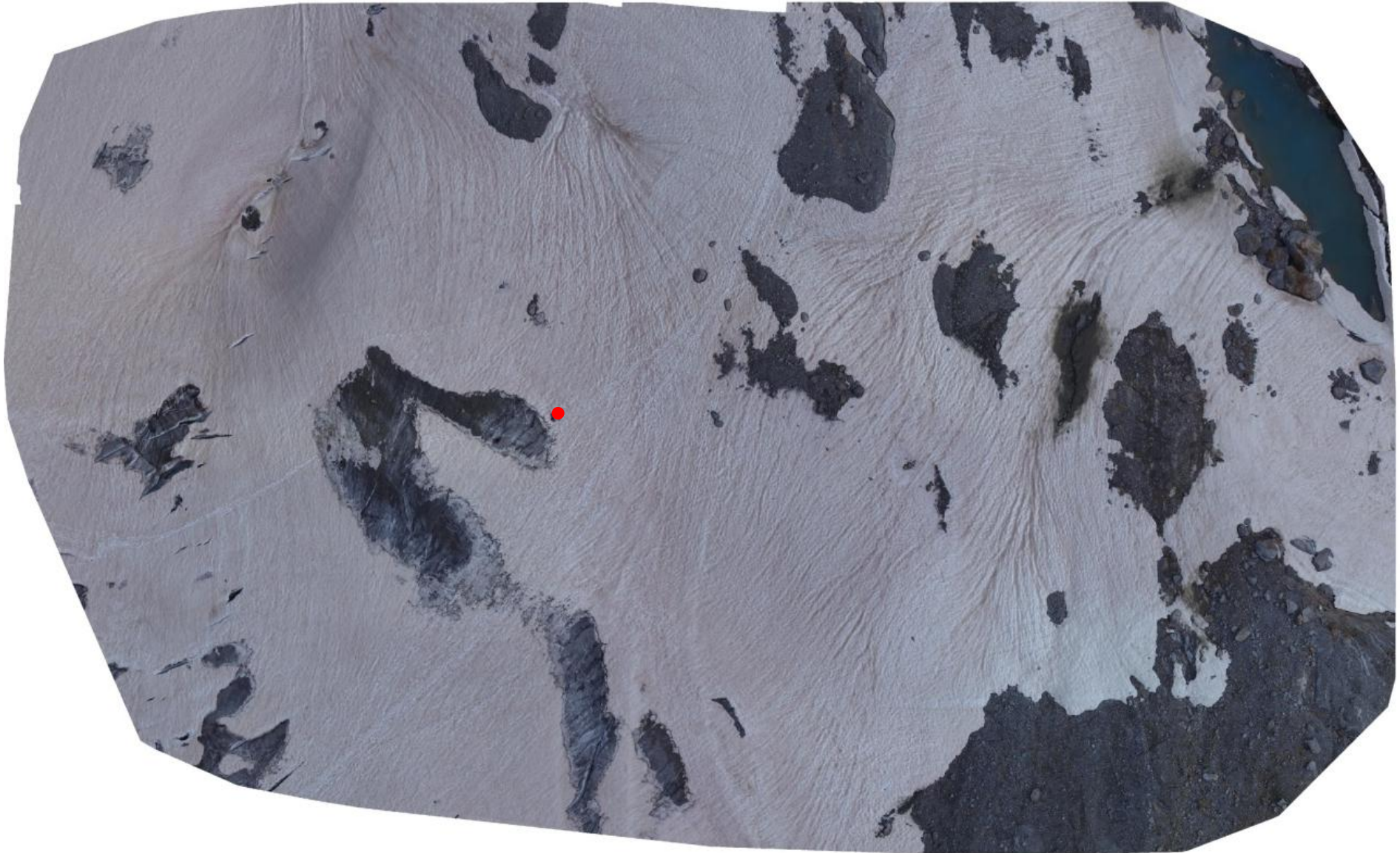


Figure 27 - DOY 199 drone imagery of the albedo site on the Feegletscher and demonstrates that the area of bare ice has increased compared to Figure 26. The red dot shows the approximate location of the ablation stake and TinyTag station. Visually shows a lower quantity of glacier surface dust compared to Figure 26, but a higher quantity compared to Figure 28.

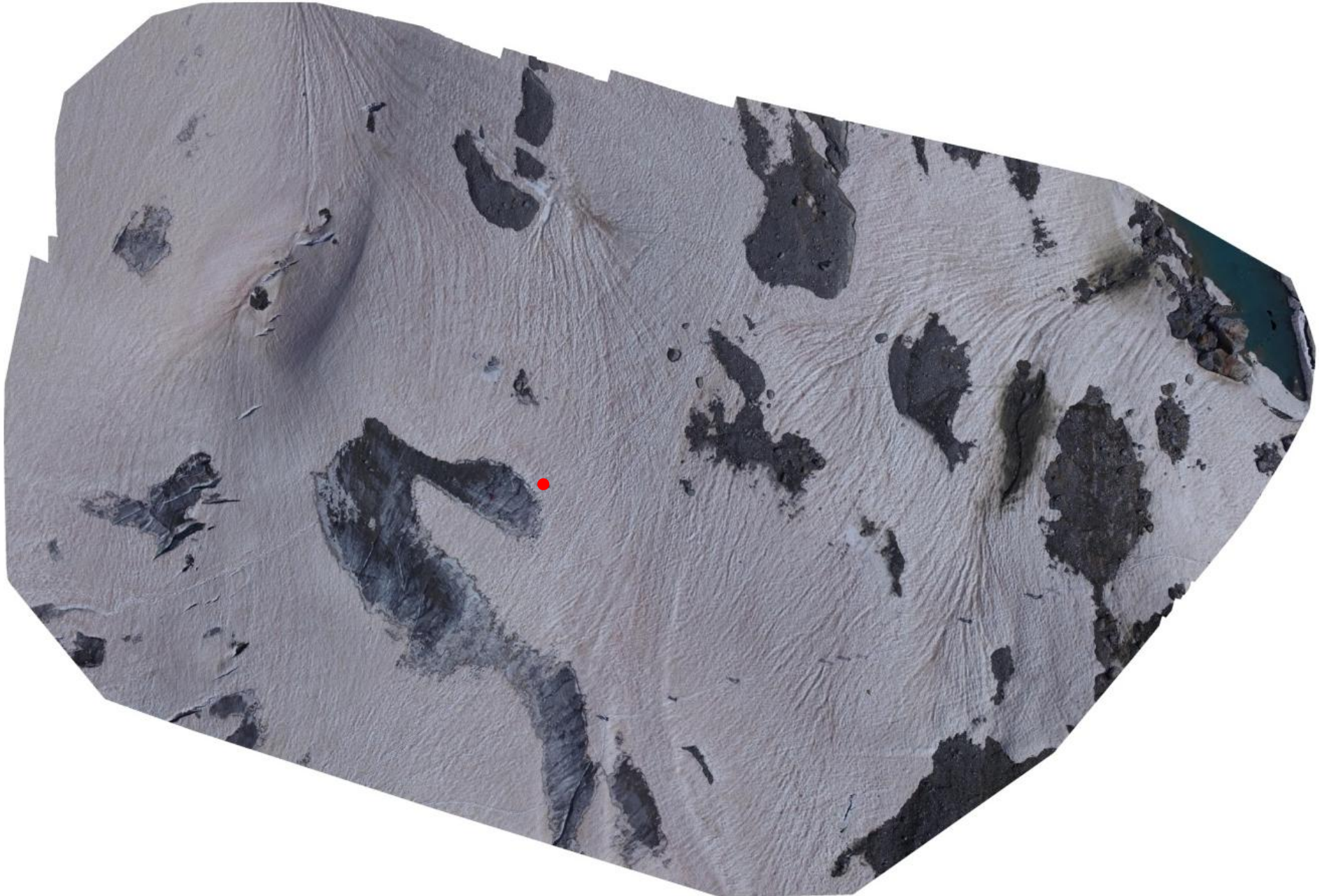


Figure 28 - DOY 200 drone imagery of the albedo site on the Feegletscher and demonstrates that the area of bare ice is increased to Figures 26 and 27. The red dot shows the approximate location of the ablation stake and TinyTag station. Visually shows the lowest quantity of glacier surface dust compared to Figures 26 and 27.

## 6.3 Proglacial Stream Data

### 6.3.1 Discharge

During the total period of measurement of the three sites, the Upper North River exhibited the lowest discharge (Figures 29 and 30). The Upper North River site had a mean discharge of  $0.828 \text{ m}^3 \text{ s}^{-1}$  (DOY 195 - 199) with a maximum discharge of  $1.205 \text{ m}^3 \text{ s}^{-1}$  (DOY 199.6), and a minimum discharge of  $0.413 \text{ m}^3 \text{ s}^{-1}$  (DOY 197.3). During week 1 of discharge measurement for the Upper North River site (DOY 195 - 197), the mean discharge was  $0.779 \text{ m}^3 \text{ s}^{-1}$  with a maximum discharge of  $1.110 \text{ m}^3 \text{ s}^{-1}$  (DOY 196.0) and a minimum discharge of  $0.413 \text{ m}^3 \text{ s}^{-1}$  (DOY 197.3). The second week (DOY 198 - 199) of discharge records showed an increase in all values with a mean discharge of  $0.894 \text{ m}^3 \text{ s}^{-1}$ , a maximum discharge of  $1.205 \text{ m}^3 \text{ s}^{-1}$  (DOY 199.6), and a minimum discharge of  $0.585 \text{ m}^3 \text{ s}^{-1}$  (DOY 198.3).

The Lower North River site had an overall mean discharge of  $1.357 \text{ m}^3 \text{ s}^{-1}$  (DOY 190 - 210) which is  $0.529 \text{ m}^3 \text{ s}^{-1}$  greater than the mean discharge experienced at the Upper North River site. During DOY 190 - 210, this site had a maximum discharge of  $3.781 \text{ m}^3 \text{ s}^{-1}$  (DOY 207.7) which is over three times greater than that of the Upper North River. The Lower North River site had a minimum discharge of  $0.0533 \text{ m}^3 \text{ s}^{-1}$  (DOY 197.3). During week 1 (DOY 190 - 196) of discharge measurement this site had a maximum discharge value of  $2.100 \text{ m}^3 \text{ s}^{-1}$  (DOY 191.6), a minimum discharge of  $0.273 \text{ m}^3 \text{ s}^{-1}$  (DOY 196.7), and a mean discharge value of  $0.851 \text{ m}^3 \text{ s}^{-1}$ . During week 2 (DOY 197 - 203), the mean discharge increased to  $1.026 \text{ m}^3 \text{ s}^{-1}$  and the maximum discharge increased by  $0.650 \text{ m}^3 \text{ s}^{-1}$  to  $2.650 \text{ m}^3 \text{ s}^{-1}$  (DOY 203.6). During the same period, the minimum discharge for the Lower North River was the overall minimum value described above. During week 3 (DOY 204 - 210), the Lower North site of the Feegletscher proglacial stream had a mean discharge of  $2.152 \text{ m}^3 \text{ s}^{-1}$  which is over 2 times greater than DOY 197 - 203 and an increase of over 2.5 times compared to DOY 190 - 197.

The South River site had the highest overall mean discharge with a value of  $2.708 \text{ m}^3 \text{ s}^{-1}$  (DOY 191 - 236), which is approximately two times larger than the overall mean discharge recorded at the Lower North River site, and over three times larger than that of the Upper North River site. The South River site recorded a maximum discharge of  $7.305 \text{ m}^3 \text{ s}^{-1}$  during DOY 205.8. During the whole period of study, the South River site experienced three large fluctuations in discharge during the DOY 192.7, DOY 218.9, and DOY 232.9 that

demonstrated sudden deviation from the dominant and generally smooth diurnal discharge cycle and were unrelated to the precipitation events. During week 1 (DOY 191 - 196) of discharge measurement, the South River site recorded a mean of  $2.900 \text{ m}^3 \text{ s}^{-1}$ , a maximum discharge of  $5.226 \text{ m}^3 \text{ s}^{-1}$  (DOY 192.8), and a minimum discharge value of  $1.592 \text{ m}^3 \text{ s}^{-1}$ . The mean discharge showed a slight increase in week 2 (DOY 197 - 203) of measurement, with a value of  $2.934 \text{ m}^3 \text{ s}^{-1}$ . During this period the maximum discharge experienced was  $5.210 \text{ m}^3 \text{ s}^{-1}$  (DOY 203.8) and the minimum discharge experienced was  $1.0524 \text{ m}^3 \text{ s}^{-1}$  (DOY 197.3). The mean discharge for week 3 (DOY 204 - 210) was a value of  $3.831 \text{ m}^3 \text{ s}^{-1}$ , and this meant the mean discharge for week 3 increased by  $0.931 \text{ m}^3 \text{ s}^{-1}$  compared to DOY 191 - 196 and increased by  $0.897 \text{ m}^3 \text{ s}^{-1}$  compared to DOY 197 - 203. Week 3 had a maximum discharge of  $7.305 \text{ m}^3 \text{ s}^{-1}$  (DOY 205.8) and a minimum discharge of  $0.943 \text{ m}^3 \text{ s}^{-1}$  (DOY 210.3).

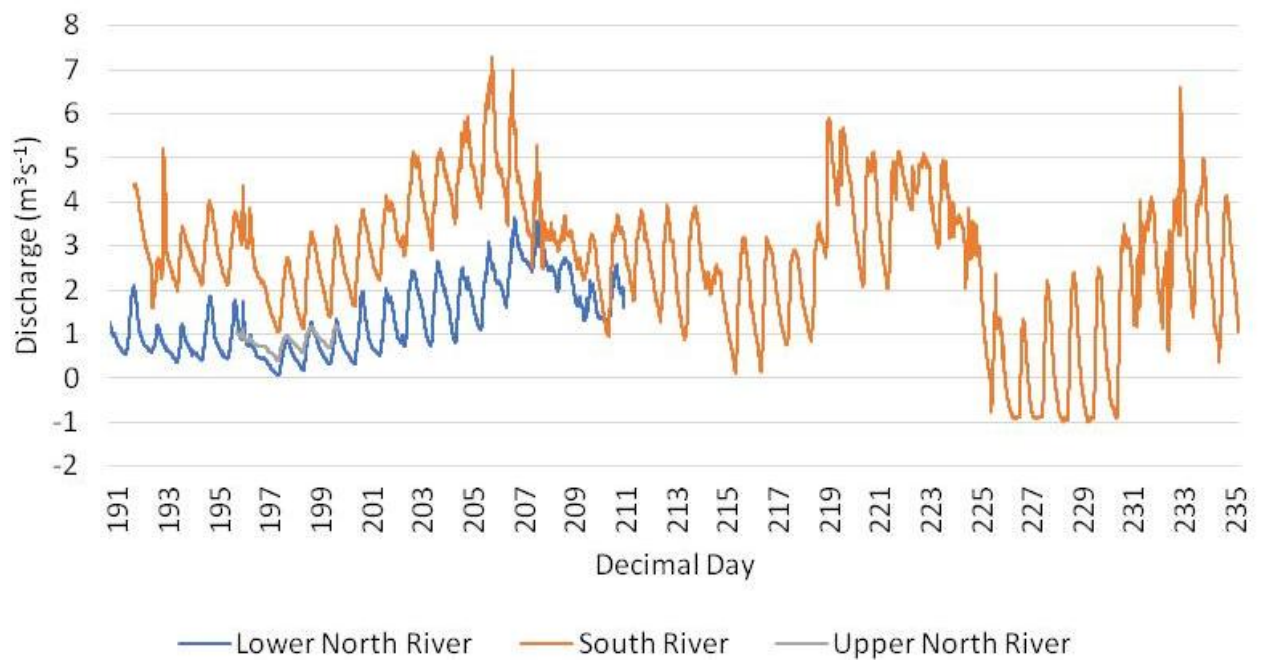


**Figure 29 - Calibrated discharge for the Upper North River site (DOY 195 - 199) and Lower North River site of the Feegletscher Nord's proglacial stream (DOY 190 - 210) and the South River site of the Feegletscher Süd's proglacial stream (DOY 191 - 236).**

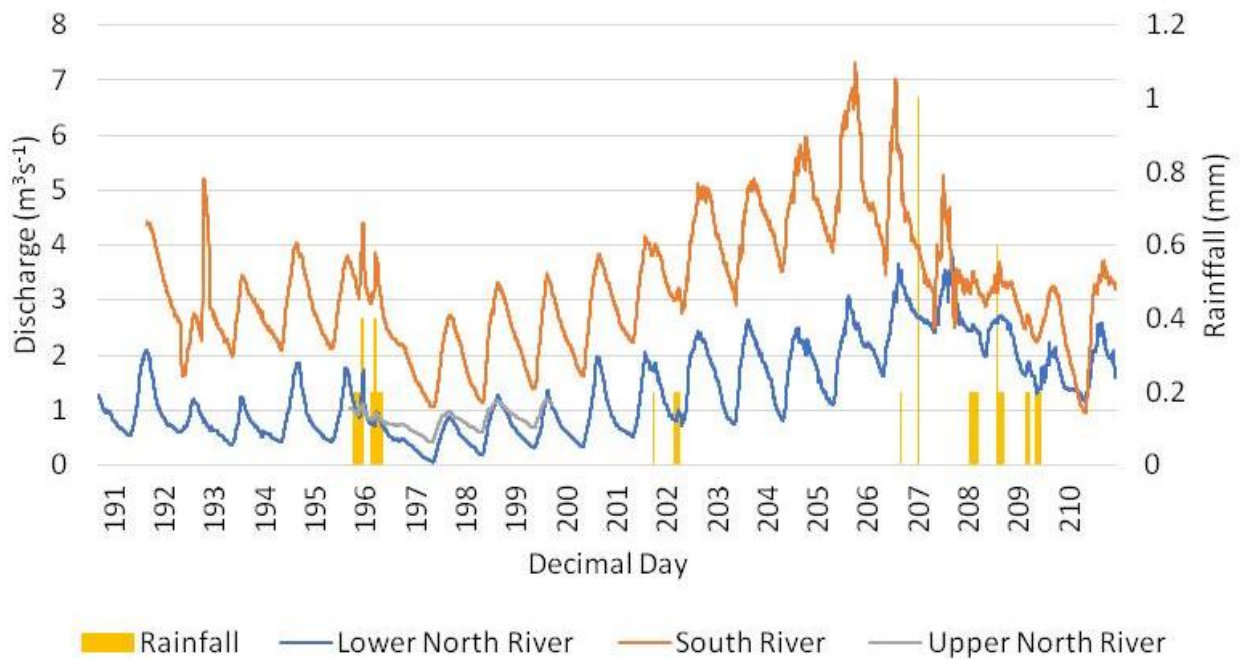
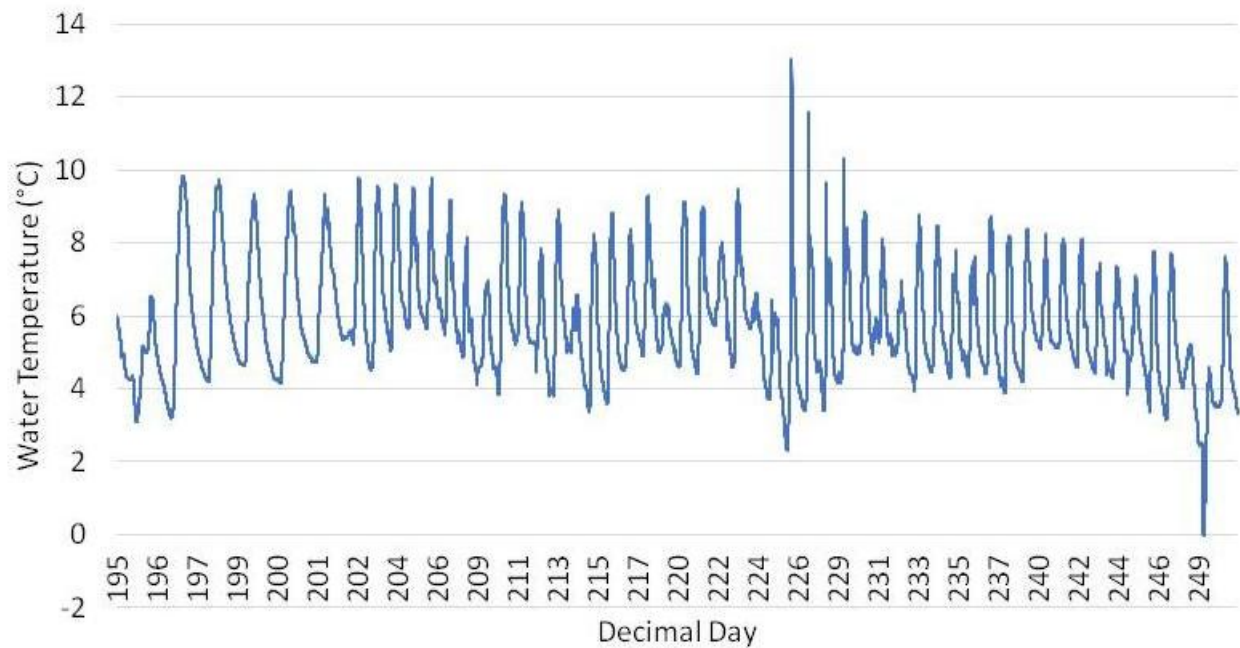


Figure 30 - Calibrated discharge record at the Upper North River site (DOY 195 - 199) and Lower North River site (DOY 190 - 210) of the Feegletscher Nord's proglacial stream; the South River site of the Feegletscher Süd's proglacial stream (191 - 210) and rainfall data recorded at the Lower North River Site (DOY 190 -210).

### 6.3.2 Water Temperature

Water temperature at the South River site was recorded from DOY 195 to 251 (Figure 32) and during this period the mean water temperature recorded was 5.82 °C, the maximum water temperature was 13.06 °C (DOY 226.5), and the minimum water temperature was -0.04 °C (249.4). During week 1 (DOY 191 - 196) of water temperature measurement, the South River site had a mean temperature of 4.79 °C, a maximum temperature of 6.55 °C (DOY 196.3), and a minimum temperature of 3.10 °C (DOY 196.7). These values all increased during week 2 (DOY 197 - 203). The mean water temperature increased by 1.54 °C to 6.33 °C, the maximum temperature experienced a large increase of 3.27 °C to 9.82 °C (DOY 197.6), and the minimum temperature increased slightly by 0.09 °C to 3.19 °C (DOY 197.2). Week 3 (204 - 210) showed a further increase in both the mean and minimum water temperature but experienced a small reduction of 0.02 °C in the maximum water temperature. The average water temperature was 6.44 °C, the maximum temperature was 9.80 °C (DOY 206.6), and the minimum temperature was 3.86 °C (DOY 210.3). The water temperature readings demonstrate a clear diurnal cycle throughout the whole duration of measurement (DOY 195 - 251), and the water temperature shows a minimal negative trend, however, this was small in value.



**Figure 31 - Water temperature recorded at the South River site of the Feegletscher Süd's proglacial stream (DOY 195 - 251).**

### **6.3.3 Suspended Sediment Concentration**

During the study period (DOY 195 - 199), the Upper North River site had a mean SSC of 0.0923 g/l with a maximum SSC of 0.355 g/l (DOY 195.8), and a minimum of 0.0241 g/l (DOY 195.7) (Figure 33). The Lower North River site had an overall mean SSC of 0.0654 g/l (DOY 190 -209), which is 0.0269 g/l less than the Upper North River site (Figure 34). The Lower North River site experienced a maximum SSC of 1.98 g/l (DOY 202.6) and a minimum SSC of 0.0122 g/l (DOY 197.2). The South River site had the highest overall mean SSC of 0.125 g/l (DOY 191 - 251) (Figure 35), which is 0.0327 g/l more than the Upper North River site, and 0.0596 g/l more than the Lower North River site. During the whole period of study, the South River site experienced three large fluctuations in SSC that were much larger in value compared to the mean and that appeared to not be driven by the usual air temperature melt forcing observed throughout the bulk of the observation period. These occurred on DOY 192.7, DOY 218.9, and DOY 232.9. The South River site experienced the greatest maximum SSC during the first of these fluctuations, with a value of 8.98 g/l (DOY 192.8). The minimum SSC at this site was 0.00158 g/l (DOY 191.8).

During week 1 of SSC measurement, the Upper North River site had a mean concentration of 0.115 g/l (195 - 196), a maximum concentration of 0.355 g/l (195.8), and a minimum of

0.0241 g/l (195.7). The Upper North River site had a week 2 (DOY 197 - 199) mean SSC of 0.0815 g/l with a maximum value of 0.124 g/l (197.5), and a minimum of 0.0619 g/l (197.2).

During week 1 (DOY 190 - 196) measurement of SSC, the Lower North River site had a mean value of 0.0515 g/l, a maximum concentration value of 0.131 (DOY 194.5), and a minimum concentration value of 0.0132 (DOY 196.9). Week 2 (DOY 197 - 203) showed a slight increase in the mean SSC of approximately 0.006 g/l to give a mean value of 0.0575 g/l. During this period, the Lower North River site experienced its overall maximum value for SSC of 1.98 (DOY 202.6). This maximum SSC is over 5.5 times greater than that for the Upper North River site with a difference of approximately 1.63 g/l. For week 2, the Lower North River site experienced a minimum SSC of 0.0122 (DOY 197.2). During week 3 (DOY 204 - 209), the mean SSC was 0.0939 g/l, which is the highest mean compared to DOY 190 - 196 and DOY 197 - 203. Week 3 experienced a maximum SSC value of 1.95 g/l which is 1.82 g/l more compared to DOY 190 - 196, but 0.04 g/l less than DOY 197 - 203). The minimum SSC for the Lower North River site during week 3 was 0.018 (DOY 208.3).

During week 1 (DOY 191 - 196) measurement of SSC, the South River site had an overall mean of 0.0997 g/l, a maximum concentration of 8.98 g/l (DOY 192.8), and a minimum concentration of 0.00158 g/l (DOY 191.8). During week 2 (DOY 196 - 203), the mean SSC of the South River site experienced a decrease of approximately 0.0251 g/l to give a value of 0.0746 g/l. DOY 196 - 203 exhibited a maximum SSC of 0.370 g/l (DOY 199.5) and a minimum SSC of 0.0236 g/l (DOY 198.3). During week 3 (DOY 204 - 210), the South River site experienced a mean SSC of 0.147 g/l, which is approximately 1.5 times greater than DOY 191 - 196 and approximately 2 times greater than DOY 196 - 203. During this time, the South River site had a maximum SSC value of 2.96 g/l (DOY 207.7) and a minimum concentration of 0.0395 g/l (DOY 204.3).

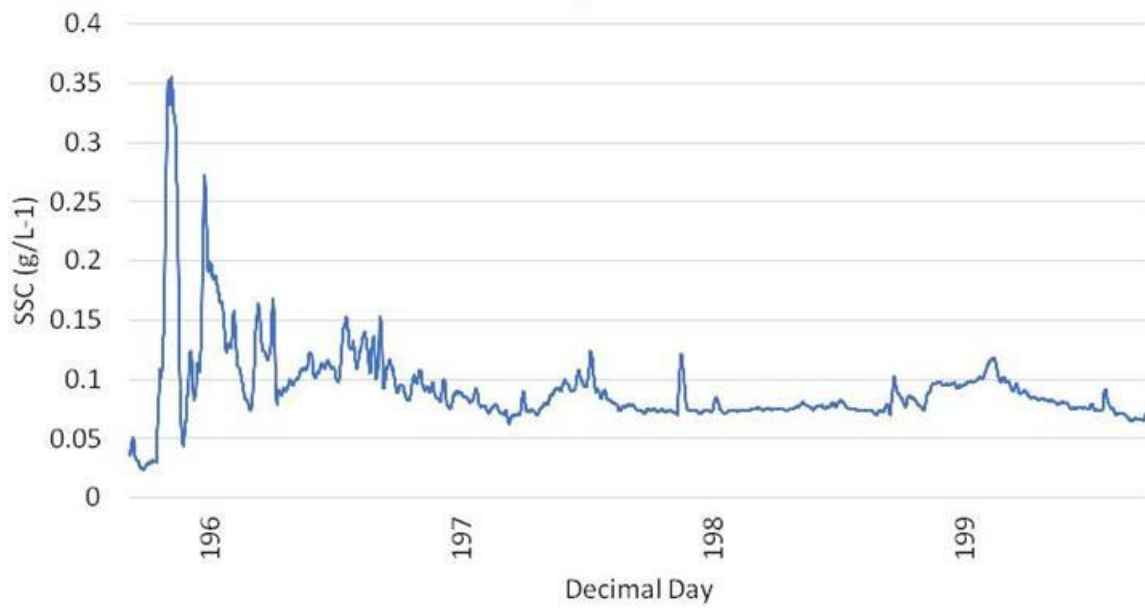


Figure 32 - Calibrated suspended sediment concentration (SSC) for the Upper North River site during DOY 195 - 199 (Feegletscher Nord, 2019).

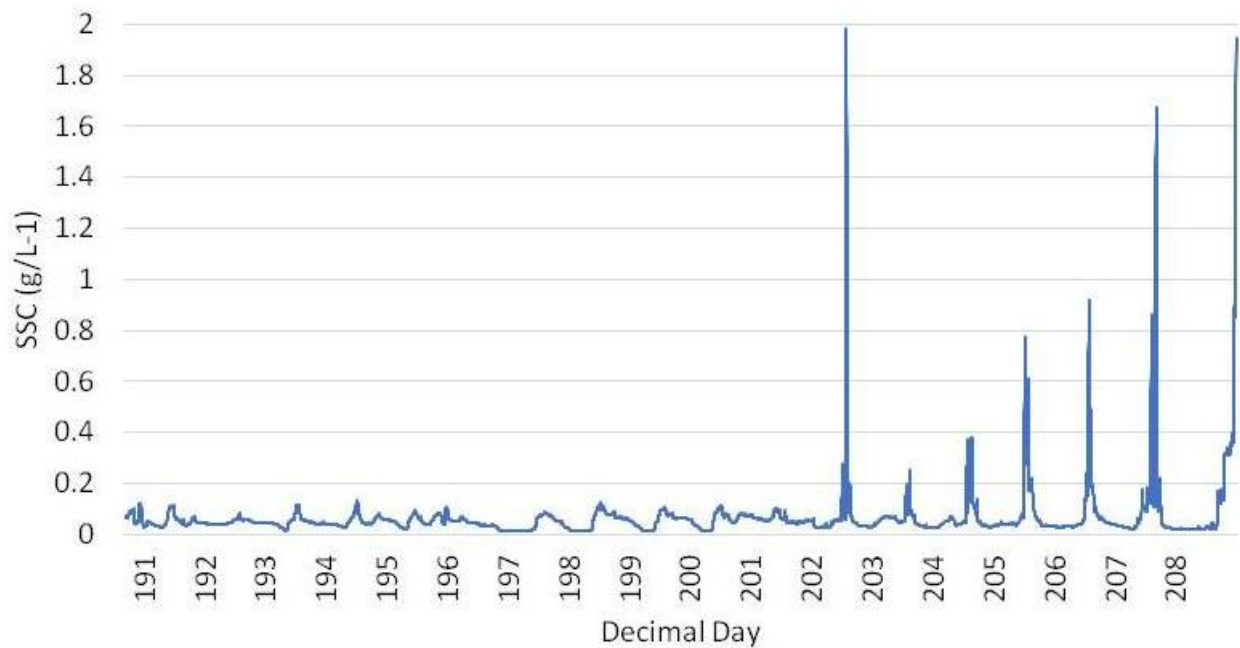


Figure 33 - Calibrated suspended sediment concentration (SSC) for the Lower North River site location during DOY 190 - 209 (Feegletscher Nord, 2019).

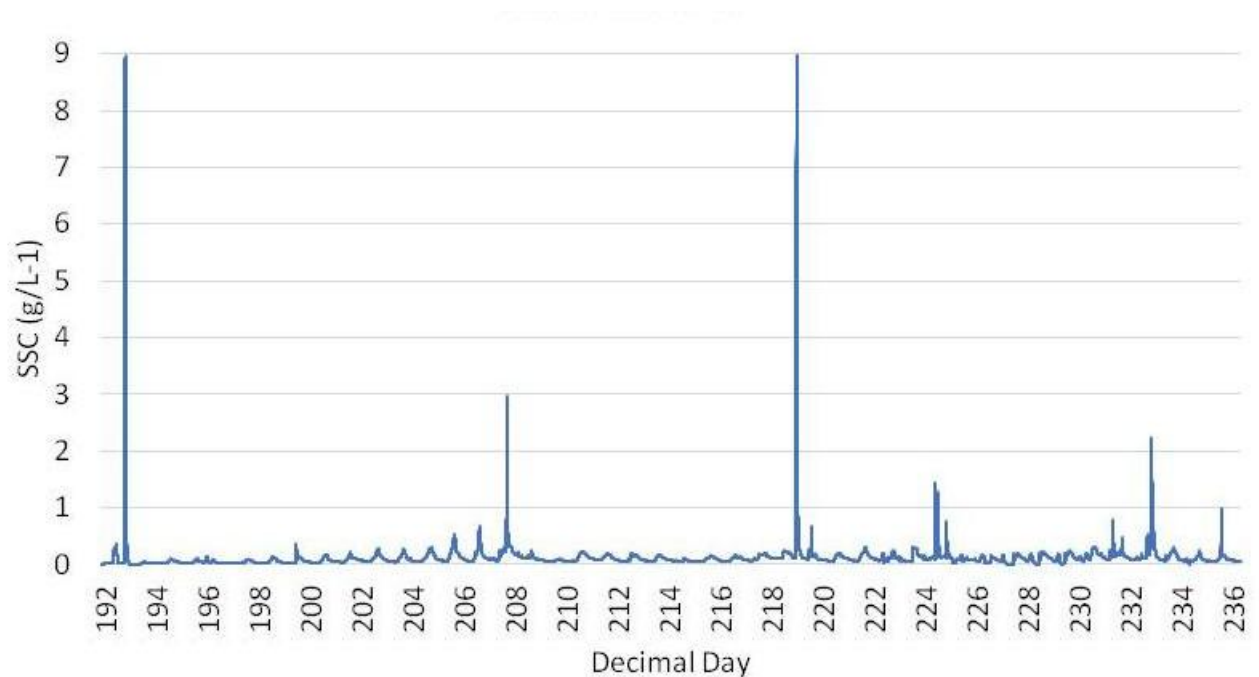


Figure 34 - Calibrated suspended sediment concentration (SSC) for the South River site location during DOY 191 - 236 (Feegletscher Süd, 2019).

#### 6.3.4 Suspended Sediment Flux

During the whole period of measurement, the Upper North River site experienced an overall mean SSF of 99.38 g/s (DOY 195 - 199), a maximum flux of 144.58 g/s (DOY 199.6), and a minimum flux of 49.60 g/s (DOY 197.32) (Figure 36 and 38). The Lower North River had an overall mean SSF of 13.07 g/s (DOY 190 - 209), a maximum SSF of 733.94 g/s (DOY 207.7), and a minimum SSF of 0.0945 g/s (DOY 197.4) (Figure 37 and 39). This maximum SSF is approximately 5 times greater than the maximum flux recorded at the Upper North site, and the minimum flux is over 524 times smaller than the Upper North site minima. During the whole period of measurement, the South River site had a mean SSF of 49.18 g/s (DOY 191 - 236), which almost 3.75 times more compared to the Lower North River site, and approximately half the mean value experienced than the Upper North River site (Figure 38 and 39). The maximum SSF at the South River site was approximately 43 times greater than the maximum value of the Upper North River, with a value of 6286.96 (DOY 218.9). This value is approximately 8.5 times more than the maximum recorded at the Lower North River site. During DOY 191 - 249, the minimum value for SSF at the South River site was 0.0108 (DOY 238.3).

During week 1 (DOY 195 - 196), the Upper North River site had an overall mean SSF of 99.50 g/s, a maximum flux of 133.26 (DOY 195.9), and a minimum flux of 72.00 (DOY 196.9). During week 2 (DOY 197 - 199), the Upper North River had a slightly lower overall mean SSF of 99.32 g/s with the maximum and minimum flux values described above.

During week 1 (DOY 190 - 196), the Lower North River site had a mean SSF of 5.63 g/s, a maximum SSF of 19.62 g/s (DOY 196.6), and a minimum SSF of 0.45 g/s (196.9). Week 2 (DOY 197 - 203) showed an increase in both the mean and the maximum SSF values, but a decrease in the minimum flux. The overall mean increased by approximately 1.3 times to give a value of 8.57 g/s, and the maximum increased by over 27.5 times to give a value of 543.30 g/s (DOY 202.6). Week 2 of measurement for the Lower North River site had the overall minimum SSF value described above. Week 3 (DOY 204 - 209) experienced a further increase in the average, maximum, and minimum values of SSF. The average value experienced was 28.77 g/s which is approximately 5 times greater than DOY 190 - 203 and over 3 times greater than DOY 197 - 204. The maximum value experienced in week 3 was 733.94 g/s (DOY 207.7) which is the maximum SSF for the whole measurement period of the Lower North River site. During week 3, the Lower North River site had a minimum SSF of 4.33 g/s, which is approximately 9.6 times greater than week 1 and 45.8 times greater than week 2.

During week 1 (DOY 191 - 196) measurement of SSF, the South River site had an overall mean of 50.12 g/s, a maximum flux of 5565.19 g/s (DOY 192.8), and a minimum flux of 0.73 g/s (DOY 193.2). During week 2 (DOY 197 - 203), the mean SSF of the South River site experienced a decrease of 19.2 g/s to give a value of 30.92 g/s. DOY 197 - 203 exhibited a maximum SSF of 173.53 g/s (DOY 202.6) and a minimum SSF of 3.30 g/s (DOY 198.3). During week 3 (DOY 204 - 210), the South River site experienced a mean SSF of 79.70 g/s, which is approximately 1.6 times greater than DOY 191 - 196 and approximately 2.6 times greater than DOY 197 - 203. During this time, the South River site had a maximum SSF value of 79.70 g/s (DOY 207.7) and a minimum flux of 14.76 g/s (DOY 209.4).

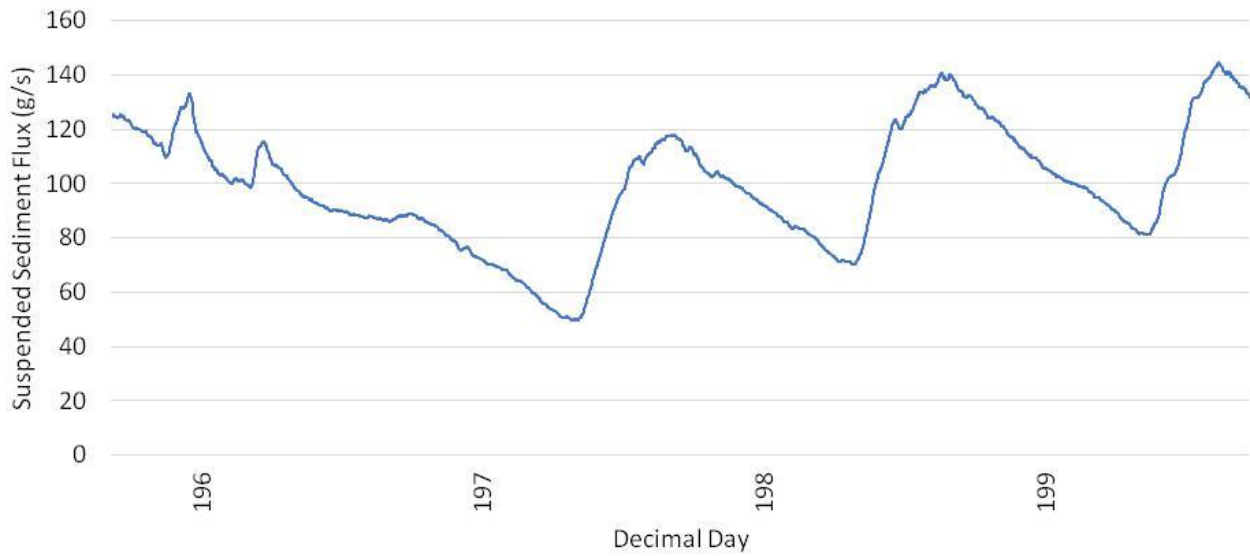


Figure 35 - Suspended Sediment Flux for the Upper North River site location during DOY 195 - 199 (Feegletscher Nord, 2019).

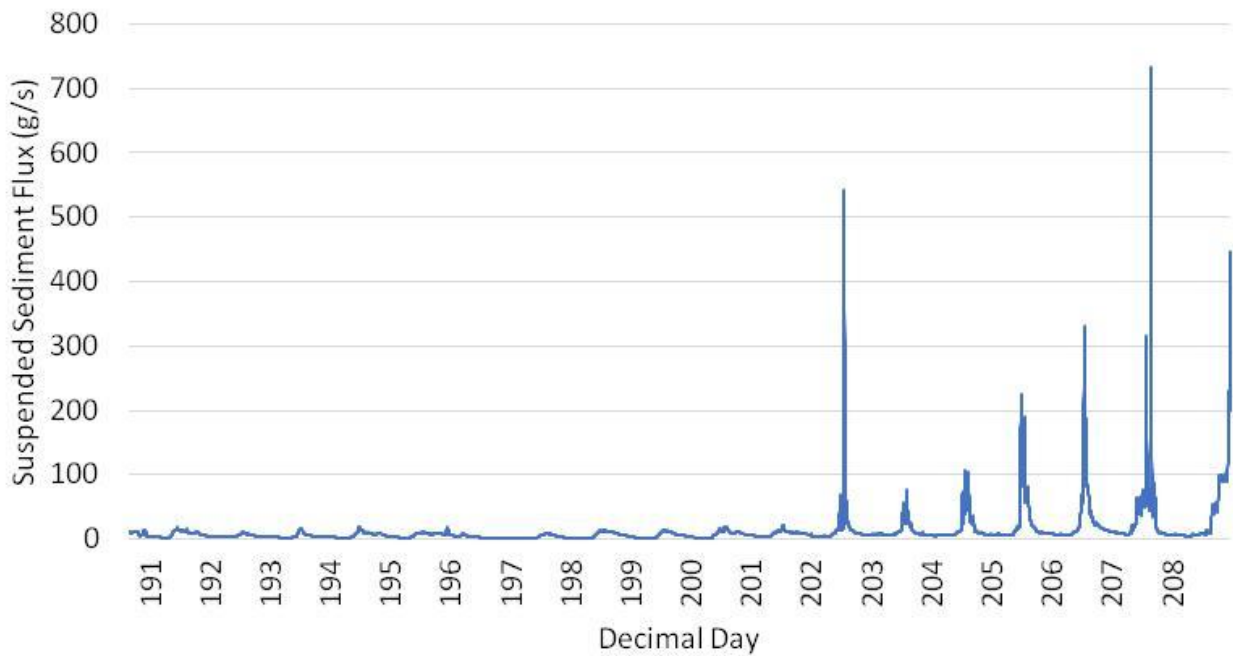


Figure 36 - Suspended Sediment Flux recorded at the Lower North River site location during DOY 190 - 209 (Feegletscher Nord, 2019).

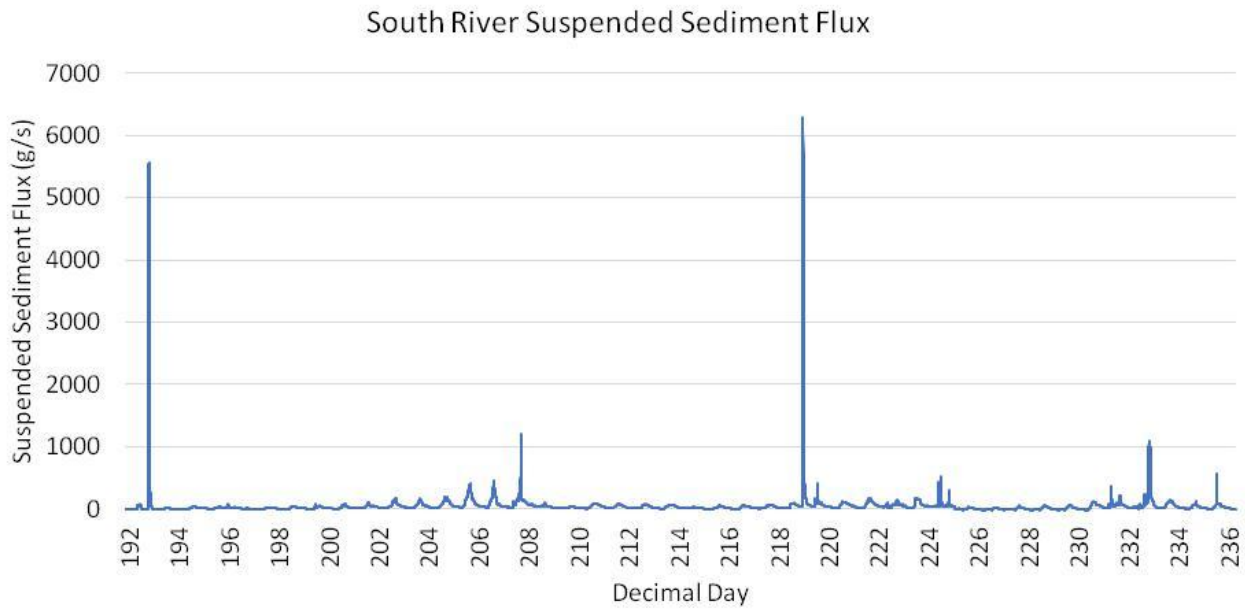


Figure 37 - Suspended Sediment Flux for the South River site location during DOY 191 - 236 (Feegletscher Süd, 2019).

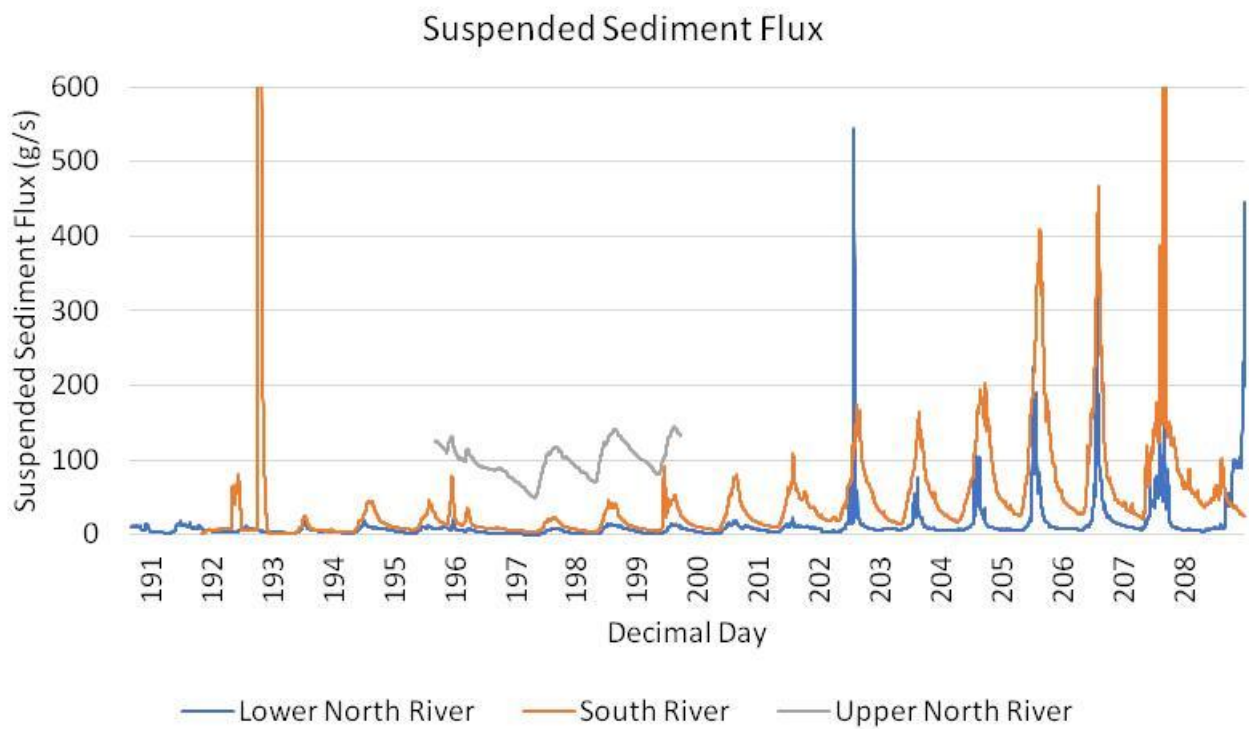


Figure 38 - Suspended Sediment Flux recorded at the Upper North River Site (DOY 195 -199); Lower North River site (DOY 190 - 209); South River (DOY 191 - 209). Suspended Sediment Flux axis is limited to 600 g/s and therefore refer to Figure 38 for maximum values for the South River.

#### 6.4 Suspended Sediment Dynamics

During the monitoring period of the Upper North River site, a precipitation event took place that spanned over DOY 195 and 196, and it had the potential to impact the collected data for both SSC and discharge. The recording of both variables started at the Upper North River site at 195.68 (16:24 PM) when the sensors were installed (Figure 40 and Appendix A). During the DOY 195, the maximum discharge of  $1.110 \text{ m}^3\text{s}^{-1}$  was reached at 195.96 (23:00 PM) and the maximum SSC of  $0.355 \text{ g l}^{-1}$  was reached at 195.85 (20:24 PM). A total of 13.87 mm of precipitation occurred from 195.76 (18:16 PM) - 196.31 (8:10 AM) which impacted both the SSC and discharge values by creating a smaller secondary peak in SSC and a secondary peak in discharge. However, because the sensors were not installed until 195.68 (16:24 PM) the data does not represent the whole hydrological day, and therefore it is unclear if the recorded maximum values were the peak values for the DOY 195. The maximum values recorded showed that SSC values reached their maximum prior to the hydrological peak, but due to the precipitation event SSC also peaked after the hydrological peak. The incomplete DOY 195 showed an overall anticlockwise hysteresis relationship for both loops present (Figure 40 and Appendix A).

Due to the precipitation event, the Upper North River site's hydrological day 196 (Figure 40) started at 196.18 (04:16 AM), which is the earliest diurnal hydrological start for the Upper North River site. During the hydrological day, there was a total of 10.45 mm of precipitation. DOY 196 experienced a maximum discharge value of  $0.963 \text{ m}^3\text{s}^{-1}$  and a maximum SSC value of  $0.168 \text{ g l}^{-1}$ . Discharge peaked first at 196.22 (05:22 AM) and the SSC peaked second at 196.26 (06:08 AM). The hysteresis loop showed an overall anticlockwise relationship in which both the maximum of discharge and SSC were reached and followed by a sudden drop-off and constant fluctuation in SSC until the end of the hydrological day.

At the Upper North River site, a typical clockwise hysteresis relationship between SSC and discharge occurred on the hydrological day of 197 and 199. The hydrological day 197 at the Upper North River site (Figure 40 and Appendix A) started at 197.33 (07:52 AM) and ended at 198.32 (07:36 AM), and during this period the peak SSC and discharge values were  $0.124 \text{ g l}^{-1}$  (197.52 - 12:22 PM) and  $0.982 \text{ m}^3\text{s}^{-1}$  (197.68 - 16:26 PM). The hydrological day 199 began at 199.34 (08:12 AM) and ended when the sensors were removed at 199.68 (17:30 PM), and during this period the peak SSC and discharge values were  $0.092 \text{ g l}^{-1}$  at 199.56

(13:32 PM) and  $1.205 \text{ m}^3\text{s}^{-1}$  at 199.62 (14:50 PM) (Figure 41 and Appendix A). This SSC value was the lowest diurnal maximum experienced at the Upper North River site, and in contrast, this discharge value was the highest diurnal discharge value recorded at the Upper North River site. Both hydrological days experienced SSC reaching a maximum value prior to values in discharge. Both demonstrated small fluctuations in SSC on the rising limb before reaching the peak value, and then on the falling limb, minimal fluctuations in SSC were apparent apart from a large fluctuation for the hydrological day 197 that was not linked to a change in discharge.

The penultimate day of recording SSC and discharge at the Upper North site was the hydrological day 198 and it experienced a pattern between the two variables that was unlike any of the other days, and an overall anticlockwise relationship between the two variables occurred (Figure 40). Hydrological day 198 at the Upper North River site (Figure 40) began at 198.32 (07:36 AM) and ended at 199.34 (08:12 AM) which is the latest end to any hydrological day at the Upper North River site (Appendix A). During this hydrological day, the site experienced the highest overall discharge value of  $1.172 \text{ m}^3\text{s}^{-1}$  which occurred at 198.63 (15:10 PM). SSC peaked much later at 199.11 (02:42 AM) with a value of  $0.118 \text{ g l}^{-1}$ .

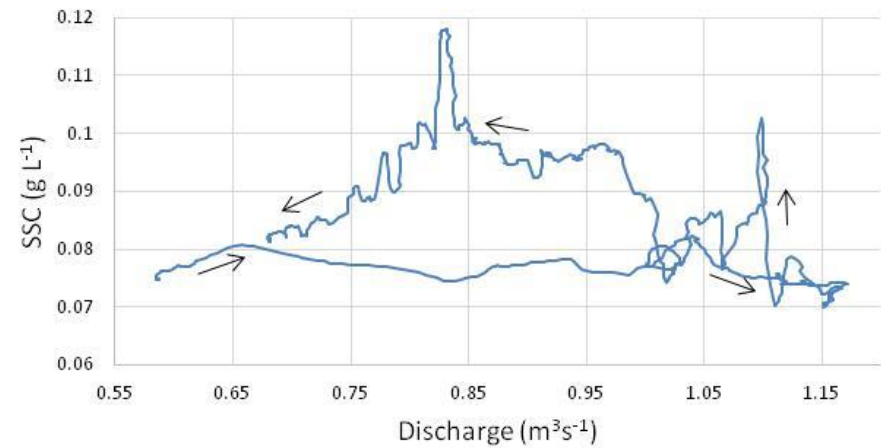
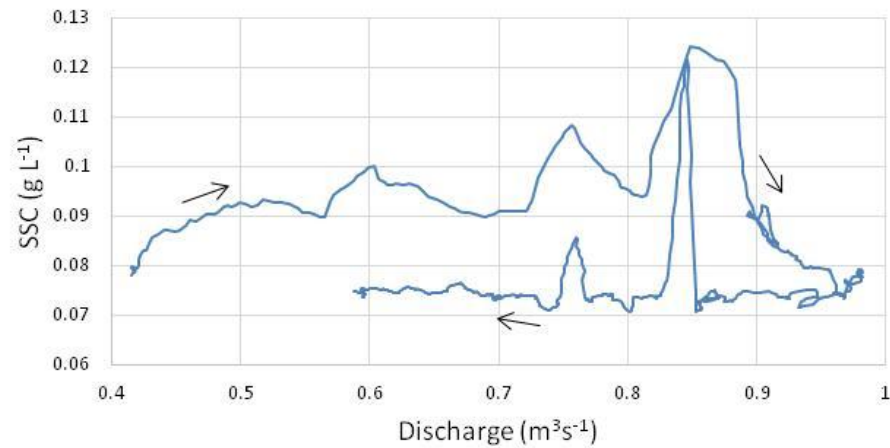
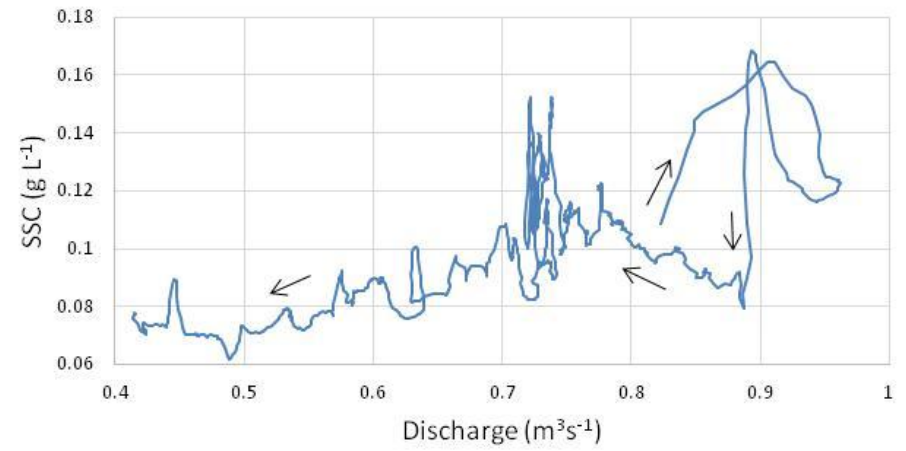
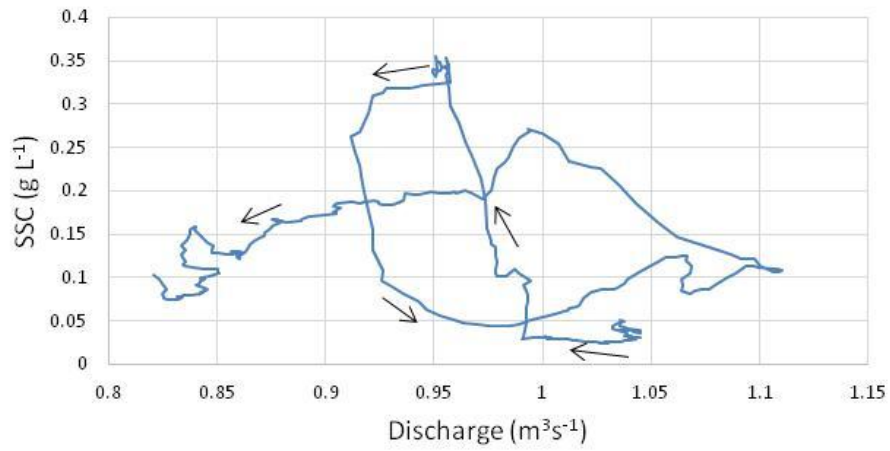
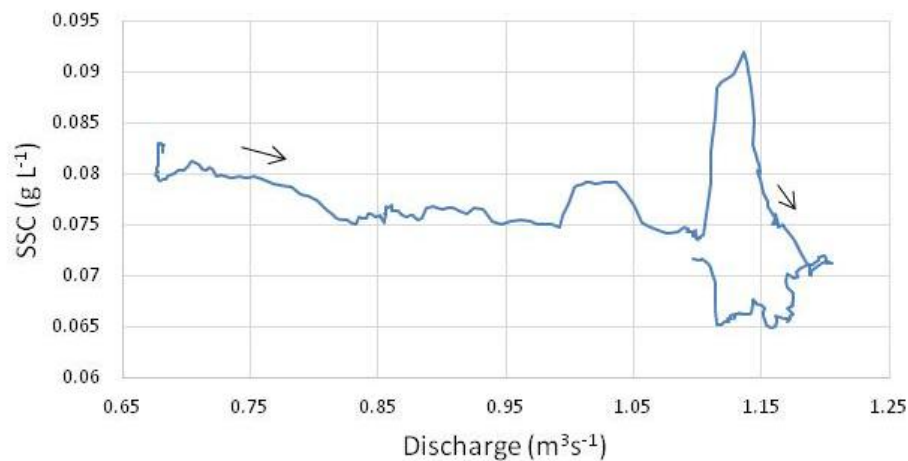


Figure 39 - Simple line graphs between smoothed discharge and suspended sediment concentration (SSC) series recorded at the Upper North River site for each of the selected hydrological day sub-periods (DOY 195 - 198). Black arrows indicate the direction of hysteresis between the two variables.



**Figure 40 - Simple line graph between smoothed discharge and suspended sediment concentration (SSC) series recorded at the Upper North River site for each of the selected hydrological day sub-period of DOY 199. Black arrows indicate the direction of hysteresis between the two variables.**

The Lower North River site also experienced the same precipitation event that occurred at the Upper North River site (DOY 195 - 196) (Figure 43 and Appendix B). The precipitation event started at 195.76 (18.16 PM) and caused a total of 12.86 mm of rain during the hydrological day 195 at the Lower North River site that site started at 195.32 (07:34 AM) and ended at 196.17 (04:00 AM). This hydrological day experienced two main peaks in discharge with values of  $1.77 \text{ m}^3\text{s}^{-1}$  at 195.60 (14:30 PM) and  $1.75 \text{ m}^3\text{s}^{-1}$  at 195.96 (23:02 PM) after the precipitation event had started. SSC experienced three main peaks, with two occurring during the precipitation event. The first peak of  $0.0935 \text{ g l}^{-1}$  was at 195.48 (11:26 AM), and then the second peak of  $0.863 \text{ g l}^{-1}$  occurred much later at 195.88 (21:04 PM), followed by the last, and the biggest peak of  $0.109 \text{ g l}^{-1}$  at 195.99 (23:48 PM). The hysteresis between SSC and discharge is characterised by two loops, firstly a clockwise loop that occurred before the precipitation event, and that was followed by an anticlockwise loop after the precipitation event had started.

Due to the precipitation event, the hydrological day 196 at the Lower North River site (Figure 43 and Appendix B) started at 196.17 (04:00 AM) and ended at 197.34 (08:06 AM). The start of this hydrological day was the earliest diurnal hydrological start for the Lower North River site. The precipitation event caused a total of 11.27 mm of rain from 196.17 (04:00 AM) until 196.34 (08:10 AM). A maximum discharge value of  $0.986 \text{ m}^3\text{s}^{-1}$  occurred at 196.23 (05:32 AM) followed by the maximum SSC value of  $0.069 \text{ g l}^{-1}$  at 196.24 (05:48 AM),

meaning that discharge reached its maximum value prior to SSC. The overall hysteresis relationship between SSC and discharge is anticlockwise in nature, and the falling limb demonstrates minimal fluctuations and extends much beyond the starting point.

At the Lower North River site, two common forms characterise the hysteresis relationships present, with the first common form, demonstrated a clockwise hysteresis relationship between SSC and discharge that occurred on the hydrological days of 193, 197, 198, 199, and 200 (Figures 42 - 44 and Appendix B). There were variations between the overall hydrological day lengths and the values of both SSC and discharge, but the overall form and characteristics of the hysteresis relationships were similar in nature. For multiple examples, the hydrological days 198 and 199 are detailed below (Figure 44). The hydrological day 198 at the Lower North River site started at 198.31 (07:24 AM) and ended at 199.35 (08:20 AM). This hydrological day experienced a maximum SSC of  $0.128 \text{ g l}^{-1}$  at 198.52 (12:35 PM) and a maximum discharge of  $1.273 \text{ m}^3\text{s}^{-1}$  which peaked after SSC at 198.63 (15:10 PM). The hydrological day 199 at the Lower North River site started at 199.35 (08:20 AM) and ended at 200.31 (07:28 AM). During this period the Lower North River site experienced a peak SSC of  $0.109 \text{ g l}^{-1}$  and a peak discharge of  $1.359 \text{ m}^3\text{s}^{-1}$ . Again, out of the two variables, the maximum value of SSC occurred first at 199.58 (14:00 PM), followed by the maximum value of discharge at 199.63 (15:02 PM). On both hydrological days, the hysteresis between SSC and discharge showed a clockwise relationship and the rising and falling limbs showed similar SSC values for the same discharge value during the beginning and end of the hydrological day. However, for the rest of the hydrological day, the rising and falling limbs did not demonstrate similar values of SSC values for the same discharge.

The second common form also demonstrated a clockwise hysteresis relationship between SSC and discharge that occurred on the hydrological days of 202, 203, 204, 205, 206, and 207 (Figures 45 - 50). In comparison to the hydrological days of 193, 197-200, these hydrological days experienced an increase in overall mean temperatures of  $4.048 \text{ }^\circ\text{C}$ , an increase in mean discharge of  $1.417 \text{ m}^3\text{s}^{-1}$ , and an increase in SSC of  $0.0261 \text{ g l}^{-1}$ . There were variations between the overall hydrological day lengths and the values of both SSC and discharge, but the overall form and characteristics of the hysteresis relationships were similar in nature. The hysteresis between SSC and discharge that occurred on these days reflects a much different relationship compared to any other hydrological day at the Lower

North River, the Upper North site, and the South River site. In comparison with the hydrological days of 193, 197 - 200 (Figures 42 - 44), these hydrological days demonstrated an earlier hydrological start with an average time of 07:12 AM compared to 08:00, however, they showed a later start to the rising limb SSC with an average time of 12:28 PM compared to 08:38 AM. For multiple examples, the hydrological days 203 and 205 are detailed below (Figures 45, 47, and 48). The hydrological day 203 at the Lower North River site started at 203.31 (06:46 AM) and ended at 204.28 (06:46 AM). During this period the recorded discharge peaked before SSC. A peak discharge value of  $2.650 \text{ m}^3\text{s}^{-1}$  was recorded at 203.60 (14:20 PM), and compared to previous hydrological days at the Lower North River site this value is the highest diurnal peak value. At 203.63 (15:00 PM) the peak of SSC was recorded at  $0.251 \text{ g l}^{-1}$ . The SSC values at the start and end of the hydrological day both reflect each other closely with minimal separation between the rising and falling limbs at the same discharge values during this time (Figure 47). However, before and after this period rapid fluctuations in SSC occurred during 203.52 (13:30 PM) - 203.64 (15:26 PM) (Figure 48).

The hydrological day 205 at the Lower North River site started at 205.29 (07:04 AM) and ended at 206.31 (07:22 AM) (Figures 45, 48, 49, and Appendix B). During this period the peak in SSC occurred before the peak in discharge, with values of  $0.774 \text{ g l}^{-1}$  (205.53 - 12:40 PM) and  $3.090 \text{ m}^3\text{s}^{-1}$  (205.62 (14:50 PM)). The discharge and SSC values hydrological day maximums were the highest and second highest compared to any previous hydrological day at the Lower North River site. The hysteresis between SSC and discharge shows a similar characteristic to hydrological days 202 - 204 (Figure 45, 47- 49), however, unlike 204 only two significant, rapid spikes in SSC were recorded during the period of 205.50 (12:04 PM) and 204.59 (14:14 PM) (Figure 45, 49). The overall relationship between SSC and discharge is clockwise.

The South River catchment also experienced the same precipitation event that was recorded at the Upper North River and Lower North River site (DOY 195 - 196) that started at 195.76 (18.16 PM) and caused a total of 10.653 mm of rain during the hydrological day (Figure 52 and Appendix C). The hydrological day 195 at the South River site started at 195.33 (07:54 AM) and ended at 196.10 (02:30 AM) due to a precipitation event. This hydrological day experienced two main peaks in the discharge of  $3.803 \text{ m}^3\text{s}^{-1}$  at 195.66 (15:50 PM), and the second peak of  $4.391 \text{ m}^3\text{s}^{-1}$  occurring at 195.96 (23:08 PM) after the

precipitation event had started. SSC also experienced two main peaks with one occurring before and during the precipitation event. The first peak of  $0.109 \text{ g l}^{-1}$  was at 195.59 (14:04 PM), and then the second, larger peak of  $0.147 \text{ g l}^{-1}$  occurred much later at 195.88 (23:10 PM). Therefore, before the precipitation event, SSC peaked first compared to discharge, however, during the precipitation event discharge peaked before SSC. The hysteresis between SSC and discharge is characterised by two peaks in both variables which are displayed by two loops, firstly a clockwise loop followed by an anticlockwise loop.

The hydrological day 196 at the South River site start was the earliest diurnal hydrological start for the South River site with a time of 196.10 (02:30 AM) (Figure 52 and Appendix C). However, the end of the hydrological day was similar to most other days at the South River site with a start time of 197.34 (08:04 AM). The precipitation event caused a total of 13.27 mm of rain from 196.10 (02:30 AM) to 196.31 (07:30 AM). A maximum discharge value of  $3.873 \text{ m}^3\text{s}^{-1}$  occurred at 196.21 (05:02 AM) followed by the maximum SSC value of  $0.080 \text{ g l}^{-1}$  at 196.22 (05:18 AM). Therefore, discharge reached its maximum value prior to SSC, and also, both variables peaked first compared to any other selected hydrological day at the South River site. The hysteresis between SSC and discharge shows an anticlockwise loop near the start of the hydrological day, which is followed by the falling limb extending much beyond the starting point. The falling limb is characterised by many small fluctuations in SSC.

At the South River site, one common form characterises the hysteresis relationships present. The common form demonstrated a clockwise hysteresis relationship between SSC and discharge that showed a clear difference in SSC for a given value of discharge on the rising and falling limbs. This occurred on the hydrological days of 192 - 194, 197, 198, 200 - 205, and 210 (Figure 51 - 55 and Appendix C). Much like the Upper and Lower North River sites, there were variations between the overall hydrological day lengths and the values of both SSC and discharge, but the overall form and characteristics of the hysteresis relationships were again similar. For multiple examples, the hydrological days 200 and 203 are detailed below. The hydrological day 200 at the South River site started at 200.33 (07:48 AM) and ended at 201.31 (07:24 AM). During this time, the South River site experienced a maximum value in SSC of  $0.177 \text{ g l}^{-1}$  at 200.60 (14:28 PM) followed by a maximum discharge value of  $3.842 \text{ m}^3\text{s}^{-1}$  at 200.67 (16:06 PM). The hysteresis between SSC and discharge shows

an overall clockwise relationship and is characterised by four peaks in SSC, with two before and one after the hydrological daily peak in SSC occurred. There is minimal fluctuation in SSC on the falling limb and sediment values are clearly lower at the same discharge when compared to the rising limb.

The hydrological day 203 at the South River site started at 203.37 (08:50 AM) and ended at 204.30 (07:12 AM) (Figure 54 and Appendix C). During this period, SSC peaked at a value of  $0.270 \text{ g l}^{-1}$  at 203.64 (15:28 PM), followed by discharge peaking at a value of 5.210 at 203.75 (18.04 PM). The hysteresis between SSC and discharge overall closely reflects hydrological day 202. The dominant loop shows a clockwise relationship between SSC and discharge, however, there are four smaller loops that show a combination of clockwise and anticlockwise relationships. SSC is characterised by one main peak followed by two smaller peaks which are represented by the last two loops mentioned above.

At the South River site, the hydrological day 199 (Figure 53) was the only period that demonstrated an overall clockwise hysteresis relationship but showed a different form compared to hydrological days 192 - 194, 197, 198, 200 - 205, and 210 (Figure 51 - 55). The hydrological day 199 at the South River site started at 199.34 (08:14 AM) and ended at 200.33 (07:48 AM). During this hydrological day, SSC reached a peak value of  $0.370 \text{ g l}^{-1}$  at 199.45 (10:45 AM), which is the second highest hydrological day peak value compared to previous days at the South River site. Later in the day, a peak in the discharge of  $3.477 \text{ m}^3\text{s}^{-1}$  was reached at 199.63 (15:10 PM). The hysteresis between SSC and discharge shows an overall clockwise relationship, but the overall shape does not reflect any previous day. It is firstly characterised by one dominant, large peak in SSC, followed by two smaller peaks with the first of those being more dominant than the final. Minimal fluctuations in SSC are present after the peak in discharge is reached.

At the South River site, two hydrological days are dominated by an anticlockwise relationship between SSC and discharge. The hydrological days 206 and 207 (Figures 54 - 55) both show an overall form and characteristics that are not demonstrated on any other South River site hydrological days shown in Figures 51 - 55. The hydrological day 206 at the South River site started at 206.36 (08:34 AM) and ended at 207.33 (07:52 AM), and during this period discharge peaked before SSC. Discharge peaked at 206.57 (13:40 PM) with a

value of 7.019, which is the second highest hydrological daily peak for any site, and this was followed by a SSC peak of  $0.671 \text{ g l}^{-1}$  at 206.60 (14:28 PM). The hysteresis between SSC and discharge shows an overall anticlockwise relationship with a small clockwise loop at the peak of SSC. The hysteresis is characterised by two small peaks in SSC followed by a larger, dominant peak.

The hydrological day 207 at the South River site started at 207.33 (07:52 AM) and ended at 208.34 (08:10 AM) (Figure 55 and Appendix C). Much like the previous hydrological day, discharge again peaked prior in comparison to SSC, with a value of 5.276 at 207.51 (12:18 PM) and  $2.963 \text{ g l}^{-1}$  at 207.69 (16:38 PM). This maximum value of SSC is the second highest value for the hydrological days selected at the South River site. The hysteresis between SSC and discharge shows an overall anticlockwise relationship which does not reflect any other hydrological day in appearance. Discharge showed many fluctuations and small peaks throughout the whole hydrological day, but especially after the main peak has been reached.

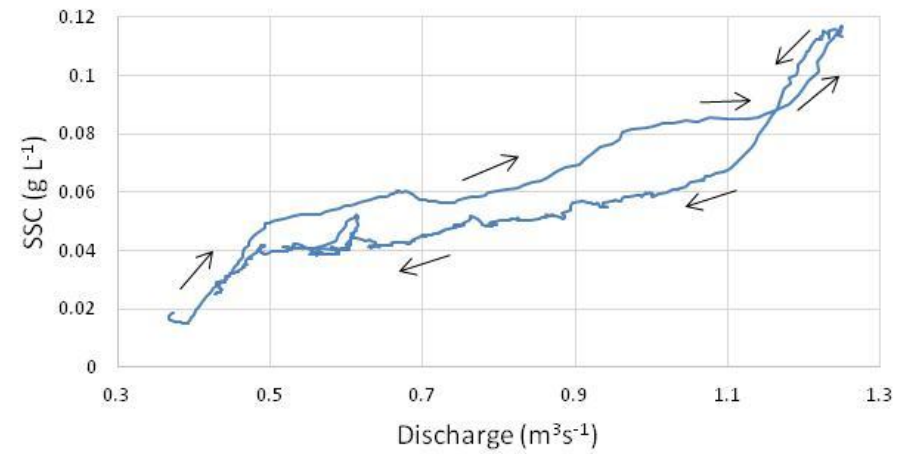
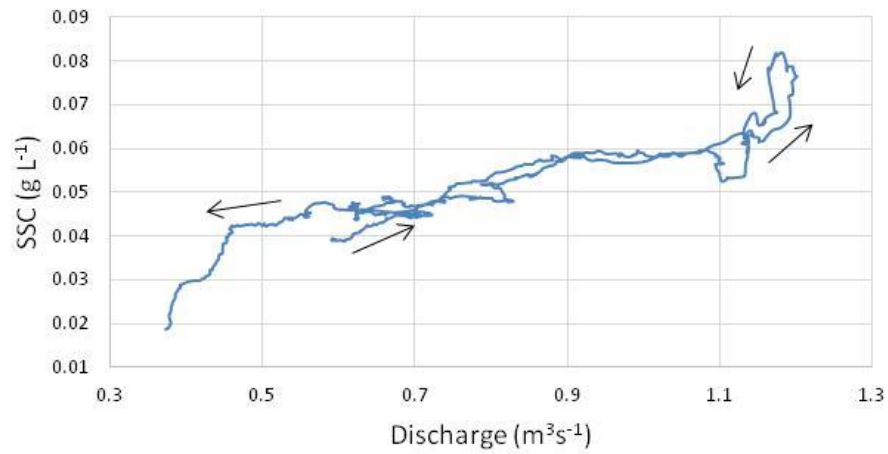
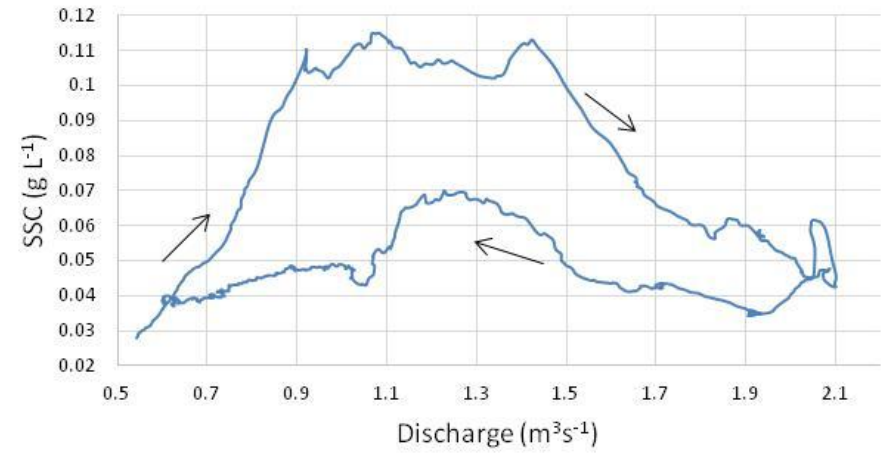
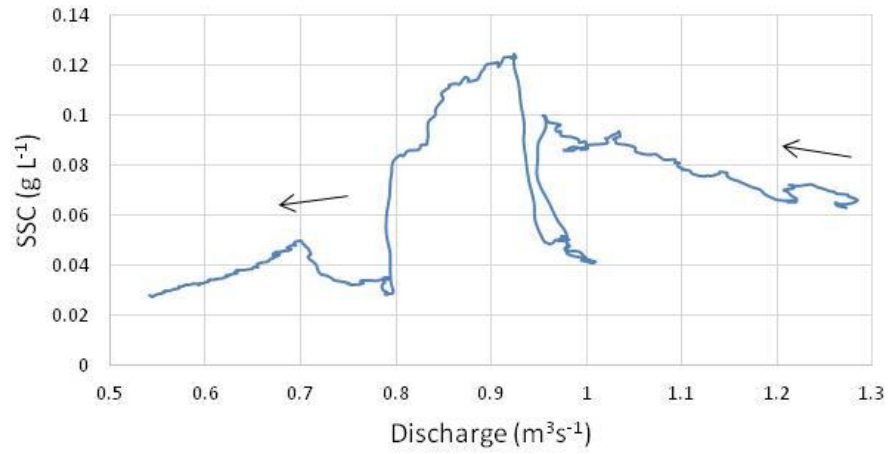


Figure 41 - Simple line graphs between smoothed discharge and suspended sediment concentration (SSC) series recorded at the Lower North River site for each of the selected hydrological day sub-periods (DOY 190 - 193). Black arrows indicate the direction of hysteresis between the two variables.

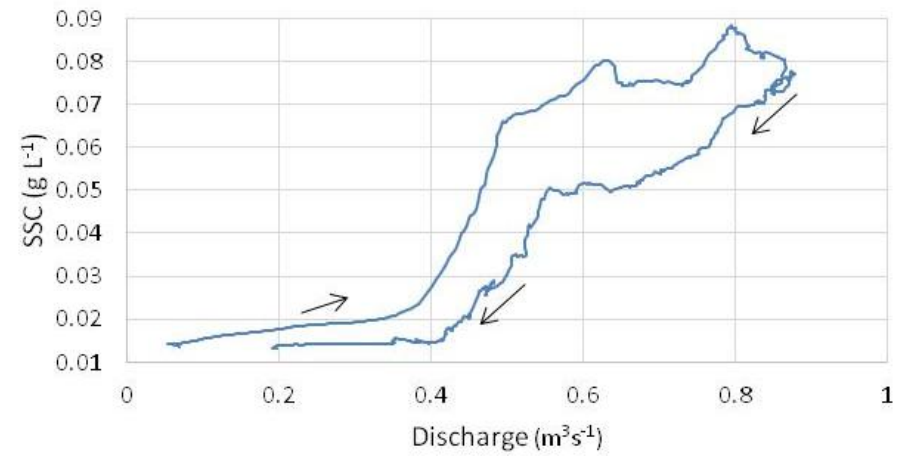
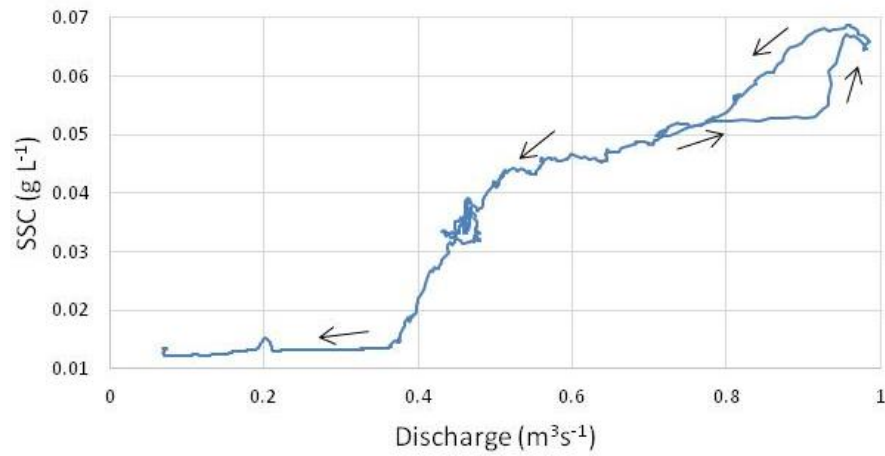
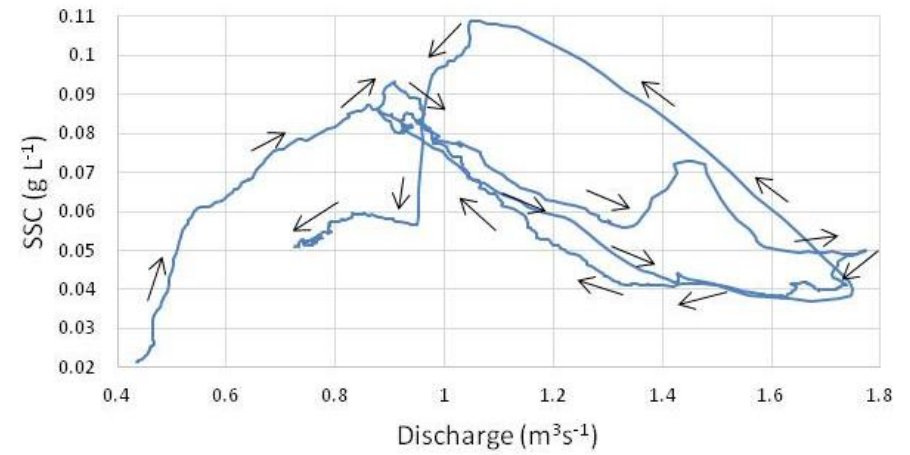
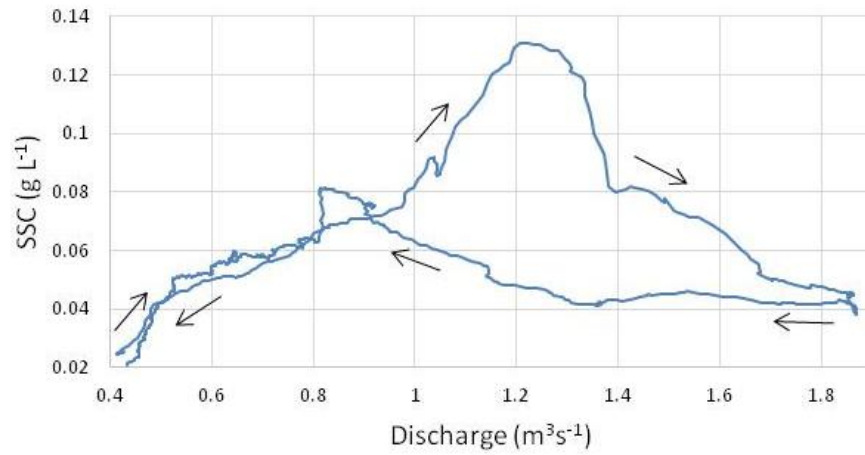


Figure 42 - Simple line graphs between smoothed discharge and suspended sediment concentration (SSC) series recorded at the Lower North River site for each of the selected hydrological day sub-periods (DOY 194 - 197). Black arrows indicate the direction of hysteresis between the two variables.

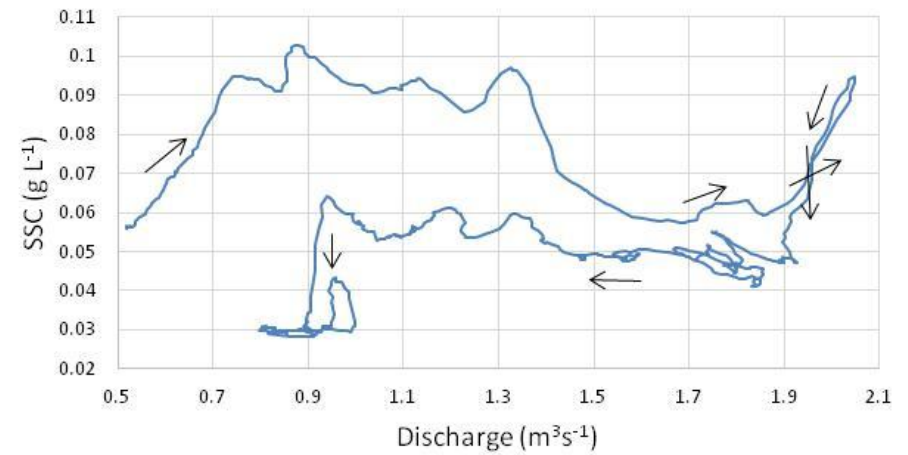
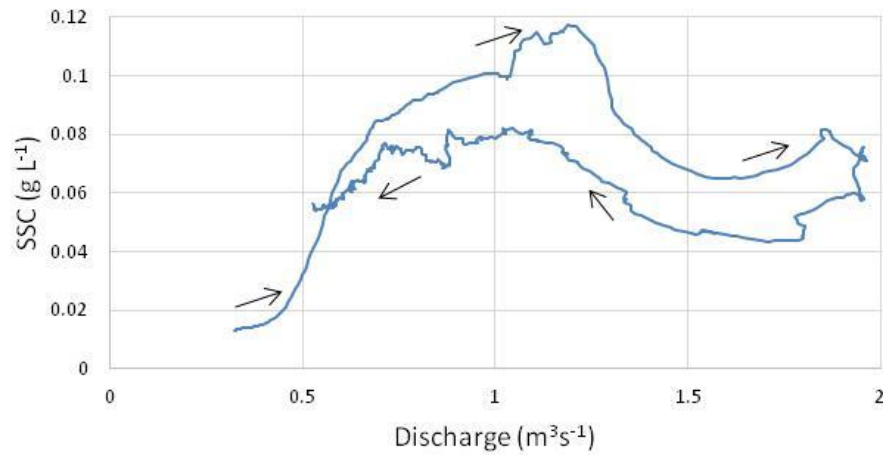
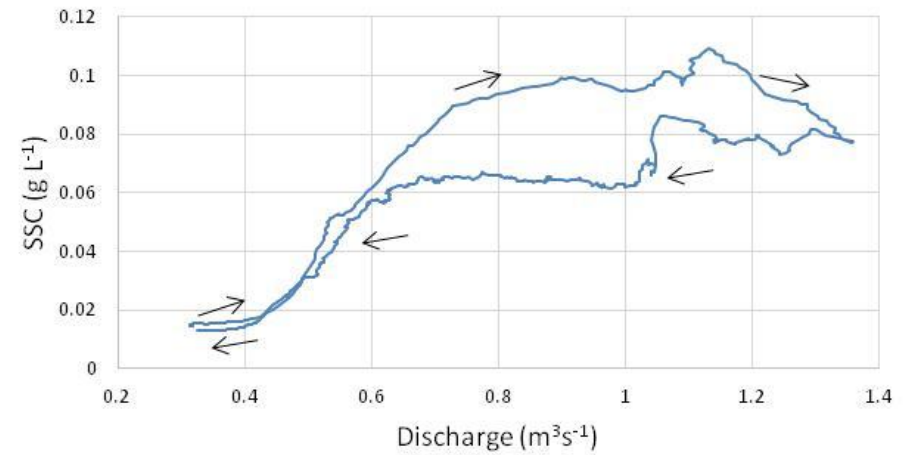
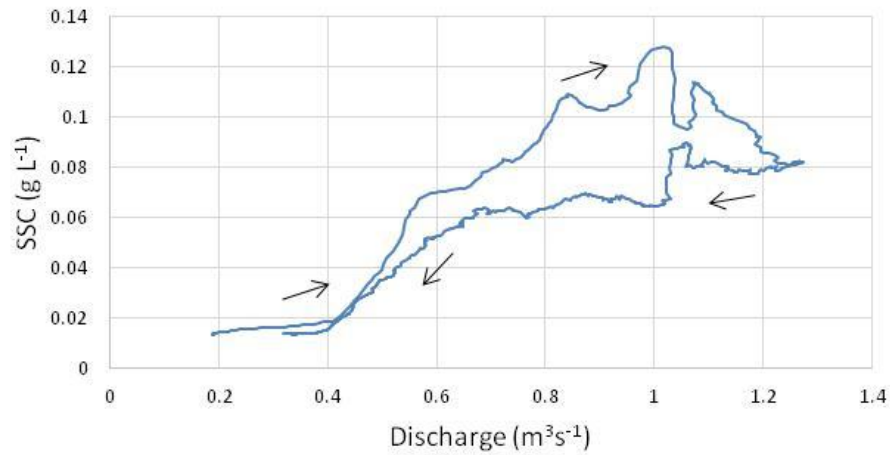


Figure 43 - Simple line graphs between smoothed discharge and suspended sediment concentration (SSC) series recorded at the Lower North River site for each of the selected hydrological day sub-periods (DOY 198 - 201). Black arrows indicate the direction of hysteresis between the two variables.

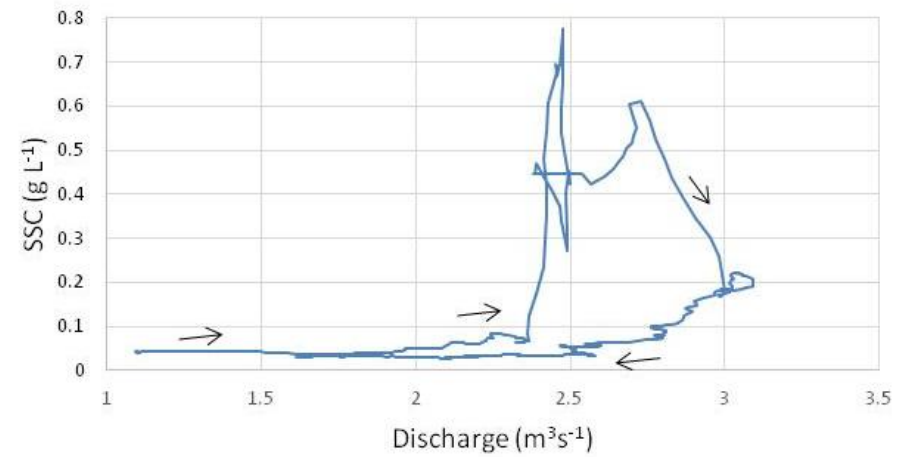
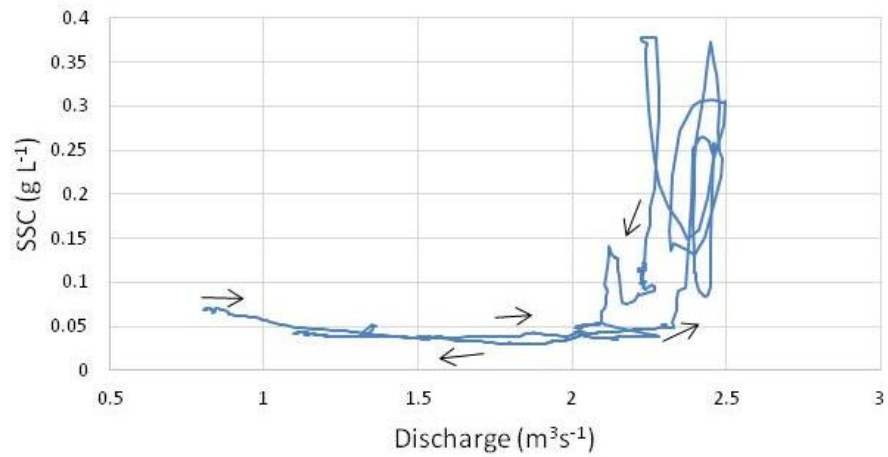
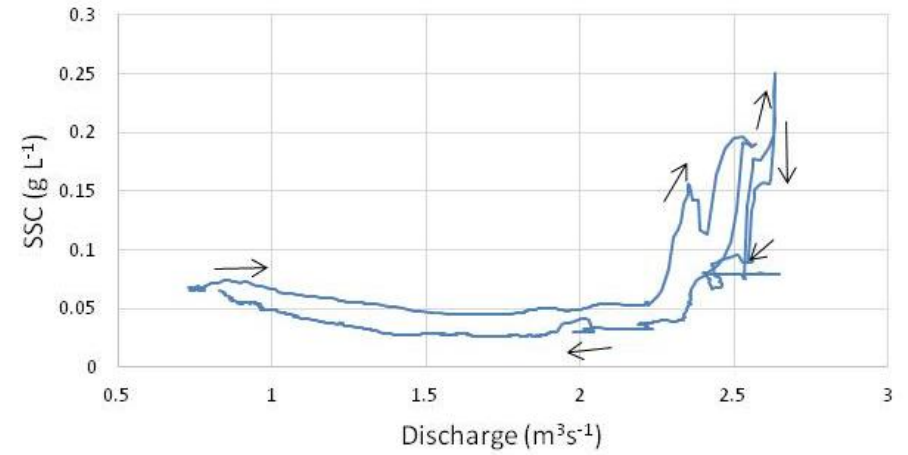
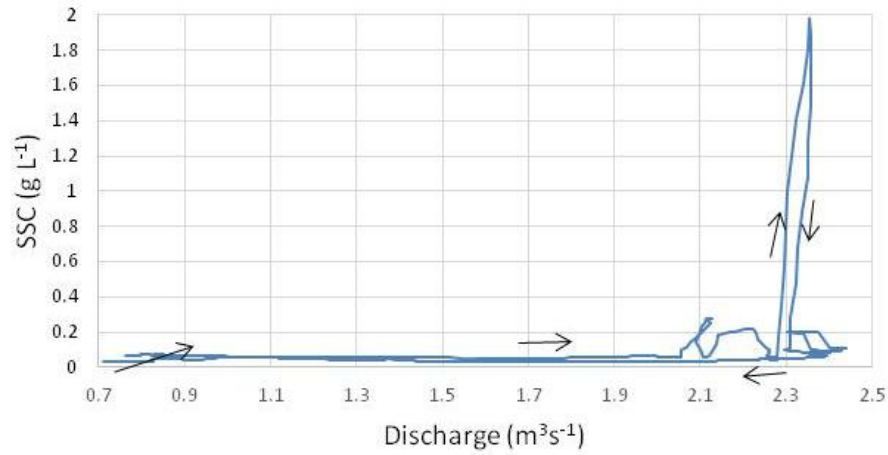


Figure 44 - Simple line graphs between smoothed discharge and suspended sediment concentration (SSC) series recorded at the Lower North River site for each of the selected hydrological day sub-periods (DOY 202 - 205). Black arrows indicate the direction of hysteresis between the two variables.

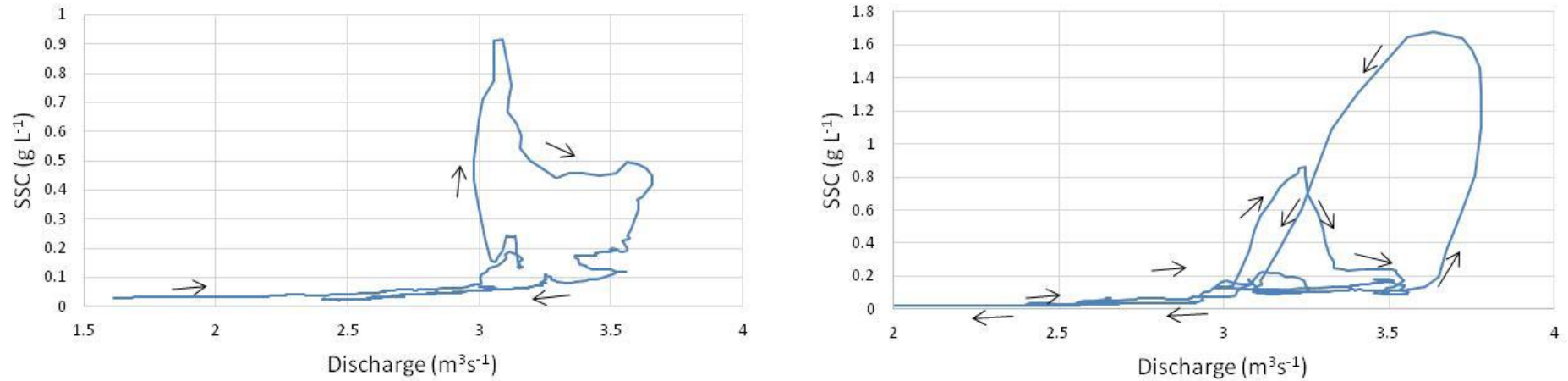


Figure 45 - Simple line graphs between smoothed discharge and suspended sediment concentration (SSC) series recorded at the Lower North River site for each of the selected hydrological day sub-periods (DOY 206 - 207). Black arrows indicate the direction of hysteresis between the two variables.

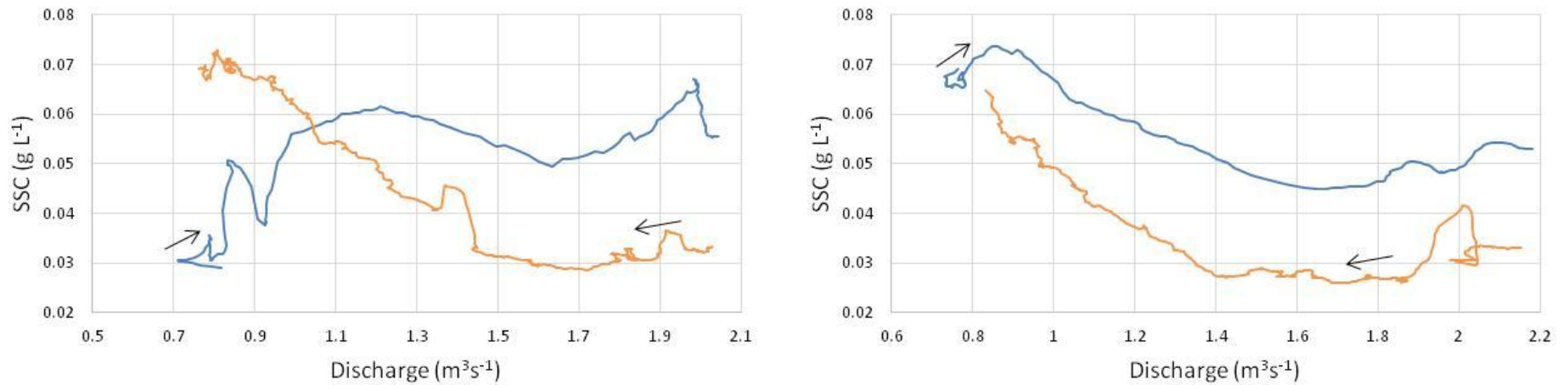


Figure 46 - Breakdowns of selected simple line graphs between smoothed discharge and suspended sediment concentration (SSC) series recorded at the Lower North River site. Blue represents the beginning section and orange represents the end section of the sub-periods up to the breakdowns found in Figure 45 (DOY 202-203). Black arrows indicate the direction of hysteresis between the two variables.

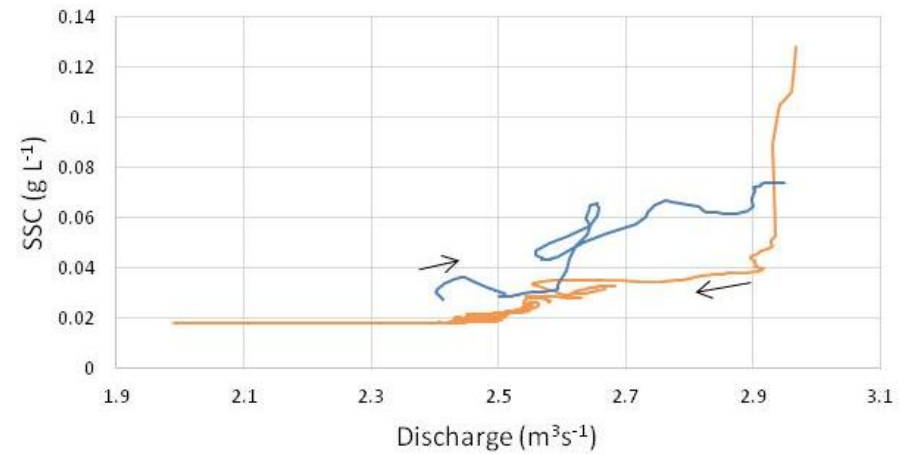
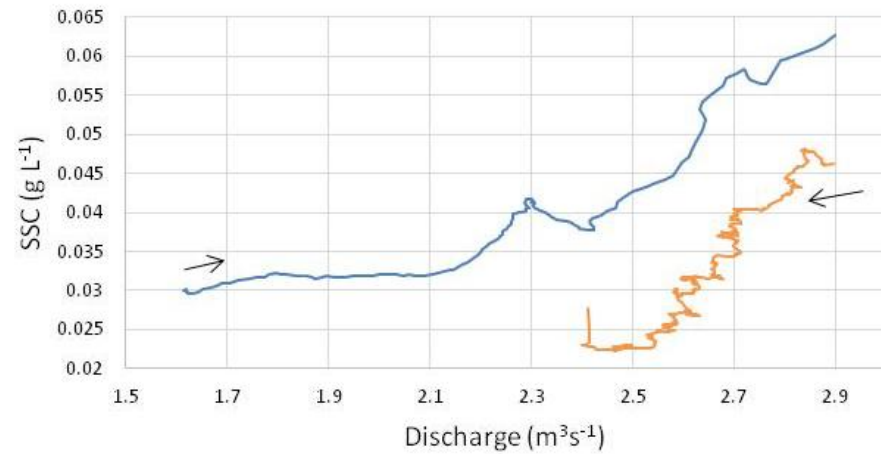
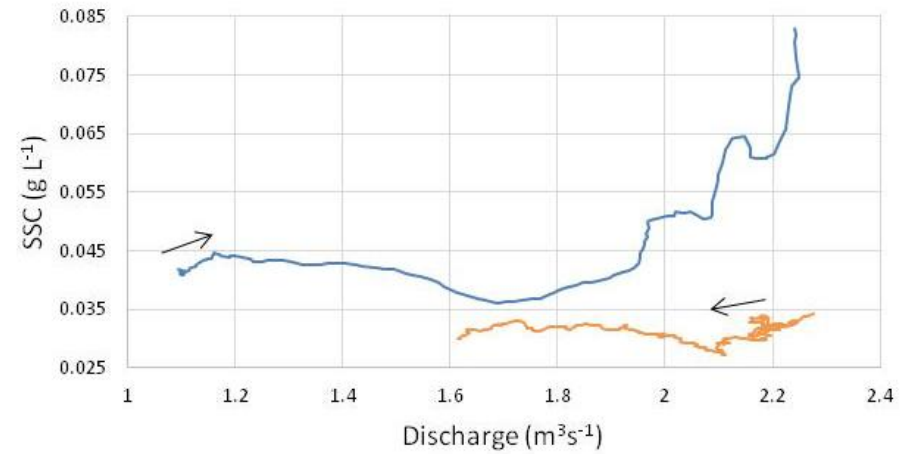
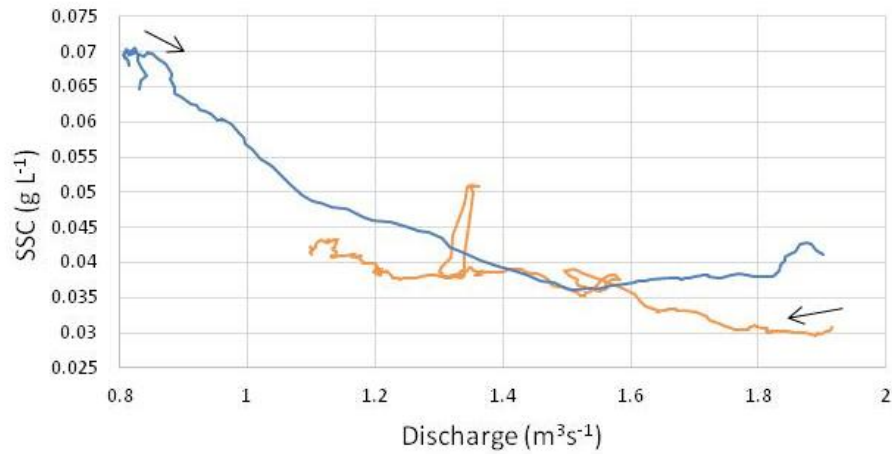


Figure 47 - Breakdowns of selected simple line graphs between smoothed discharge and suspended sediment concentration (SSC) series recorded at the Lower North River site. Blue represents the beginning section and orange represents the end section of the sub-periods up to the breakdowns found in Figures 45 and 46 (DOY 204-207). Black arrows indicate the direction of hysteresis between the two variables.

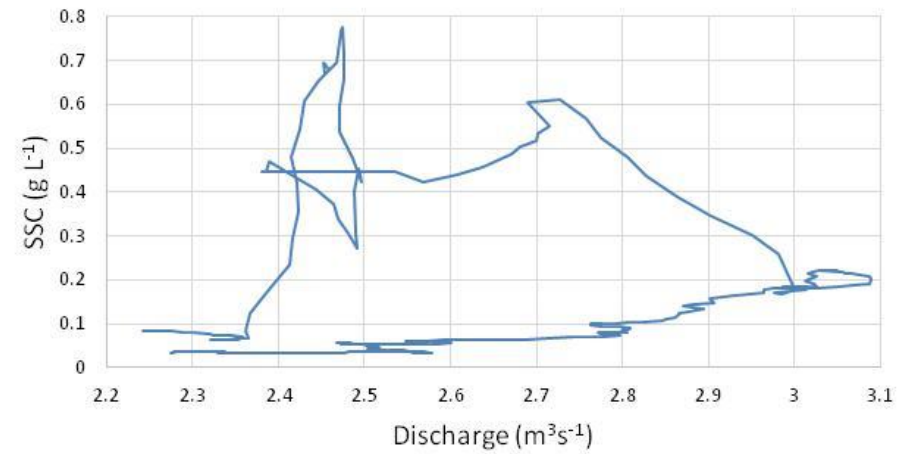
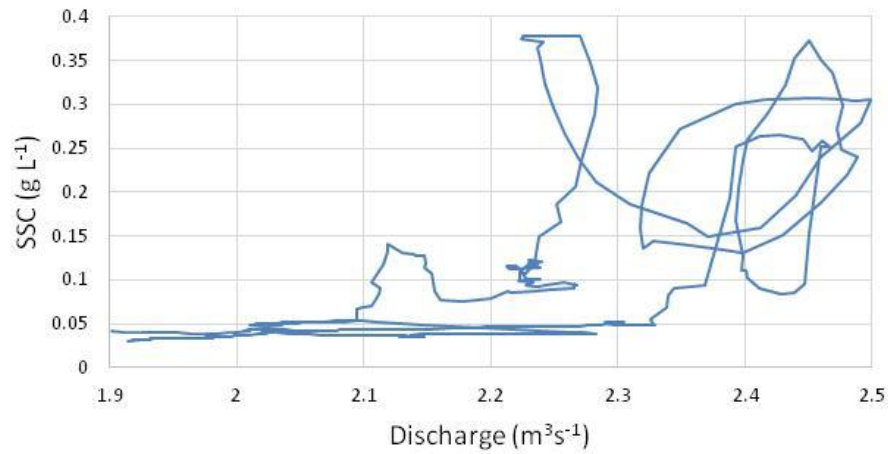
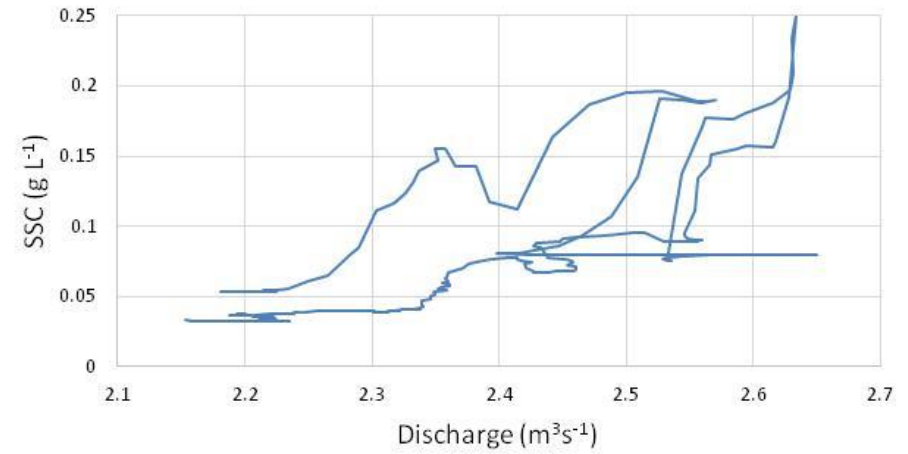
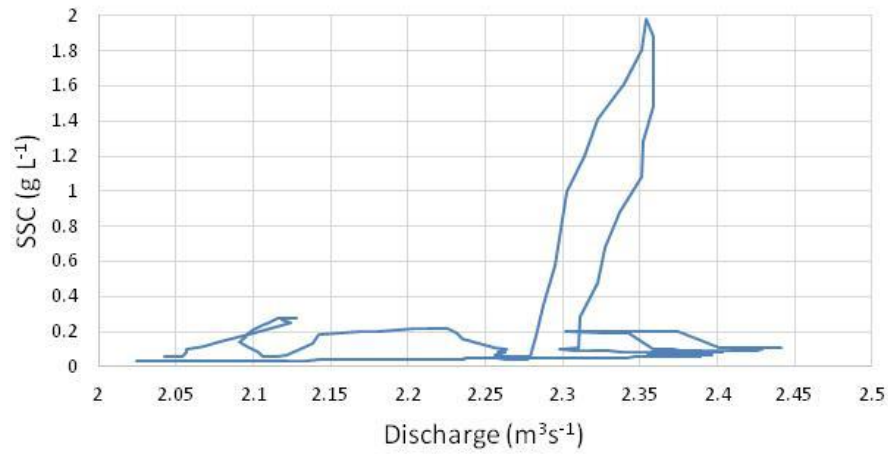


Figure 48 - Breakdowns of selected simple line graphs between smoothed discharge and suspended sediment concentration (SSC) series recorded at the Lower North River site (DOY 202-205) . Breakdown sections are before and after sections in Figures 47 - 48. Black arrows indicate the direction of hysteresis between the two variables.

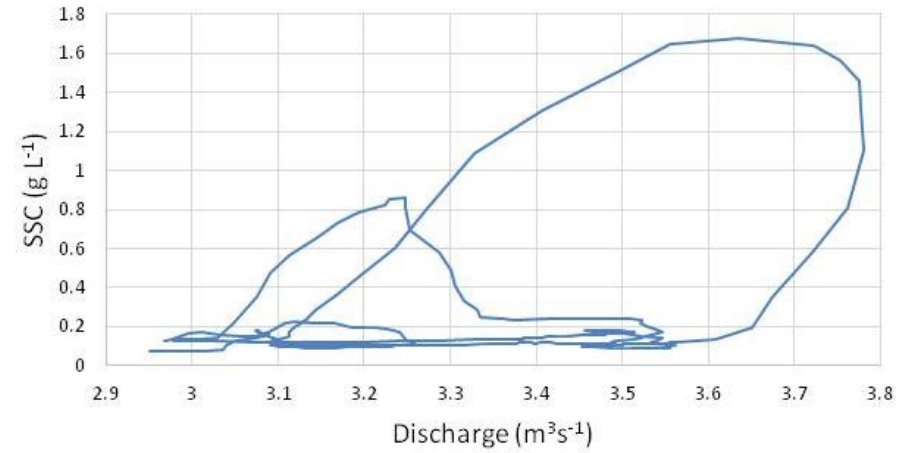
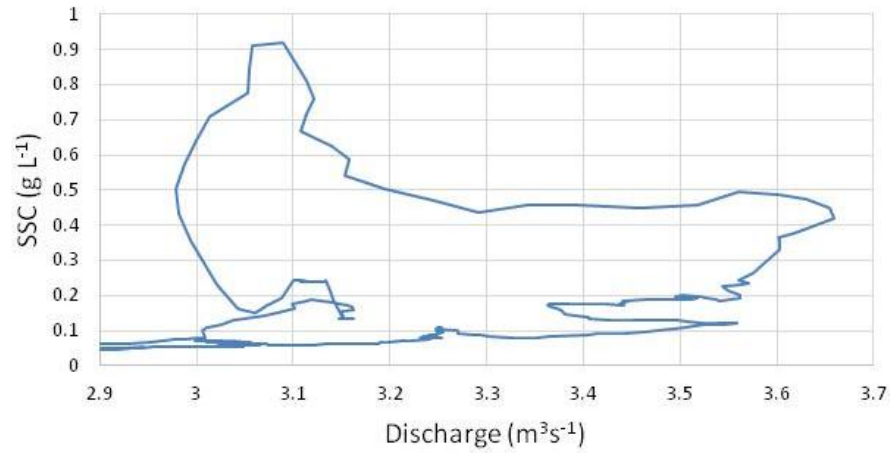


Figure 49 - Breakdowns of selected simple line graphs between smoothed discharge and suspended sediment concentration (SSC) series recorded at the Lower North River site (DOY 206-207) . Breakdown sections are before and after sections in Figure 48. Black arrows indicate the direction of hysteresis between the two variables.

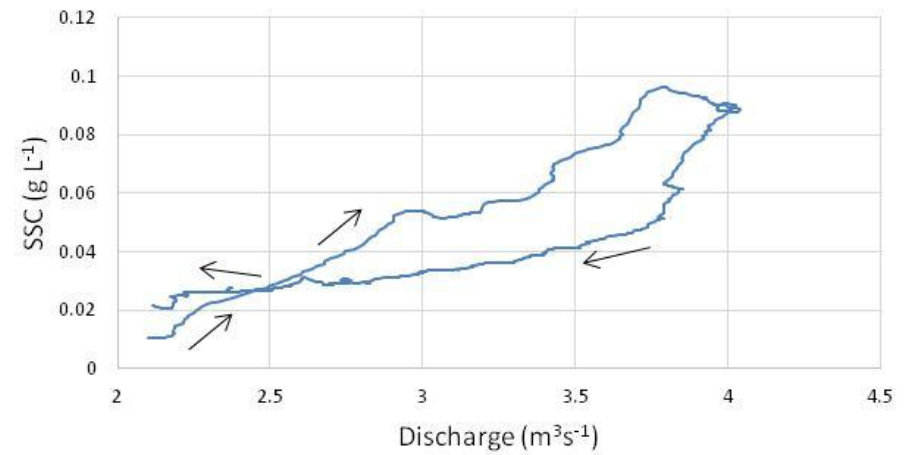
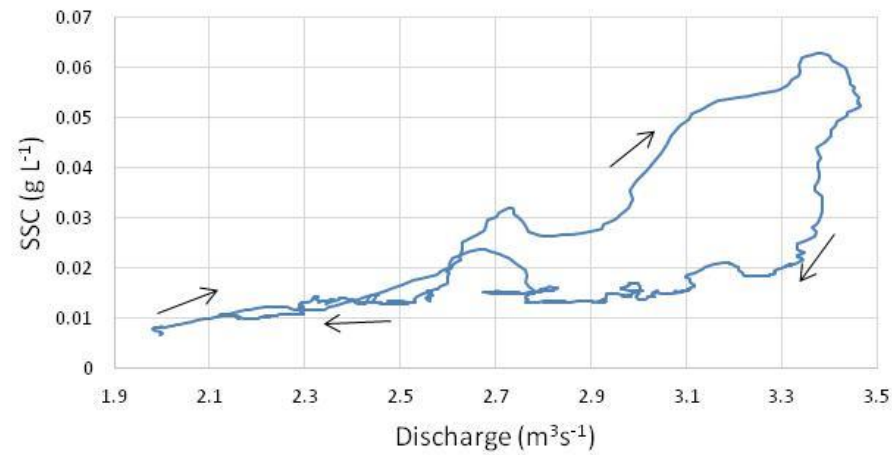
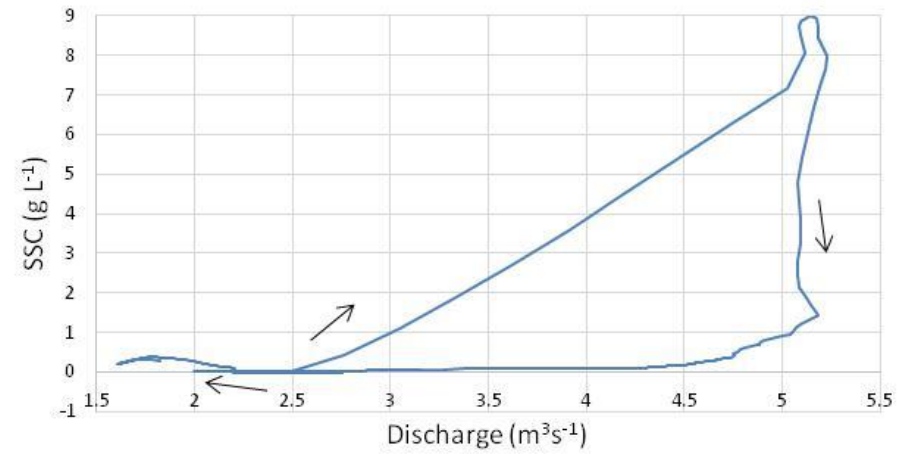
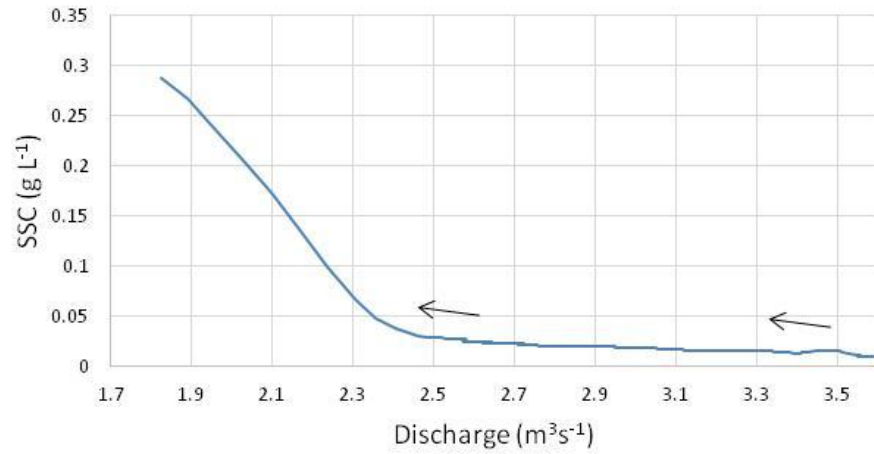


Figure 50 - Simple line graphs between smoothed discharge and suspended sediment concentration (SSC) series recorded at the South River site for each of the selected hydrological day sub-periods (DOY 191 - 194). Black arrows indicate the direction of hysteresis between the two variables.

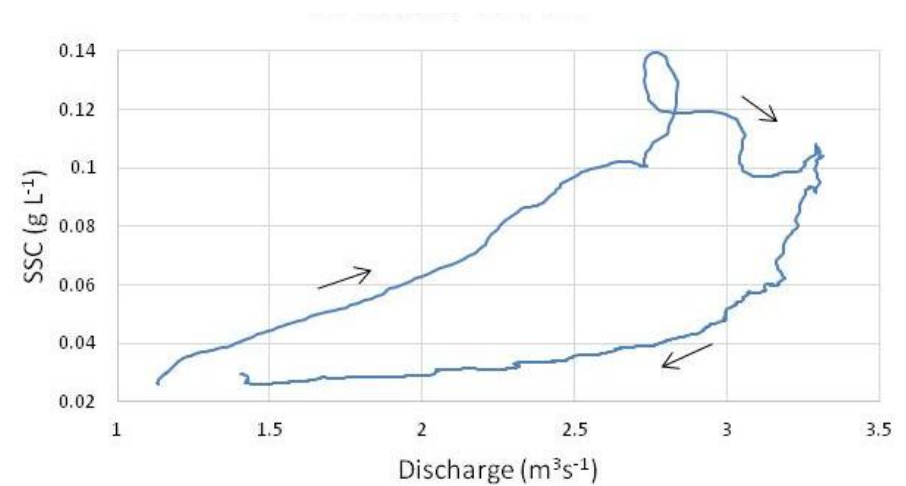
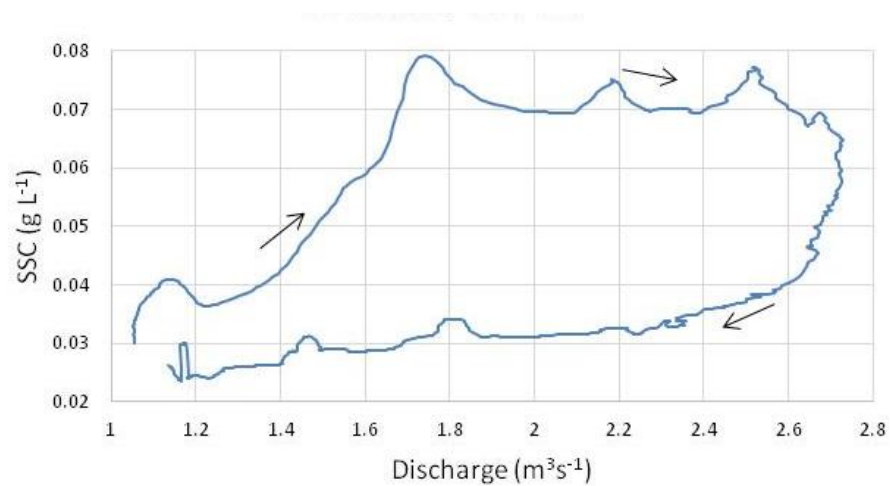
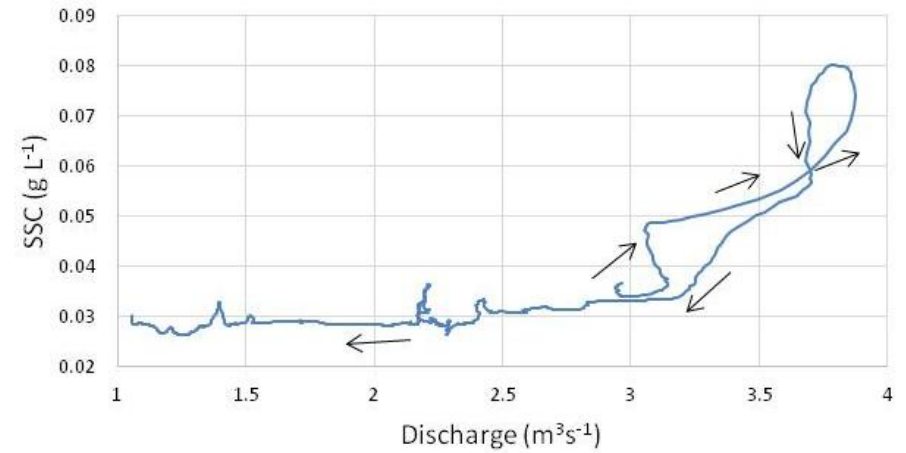
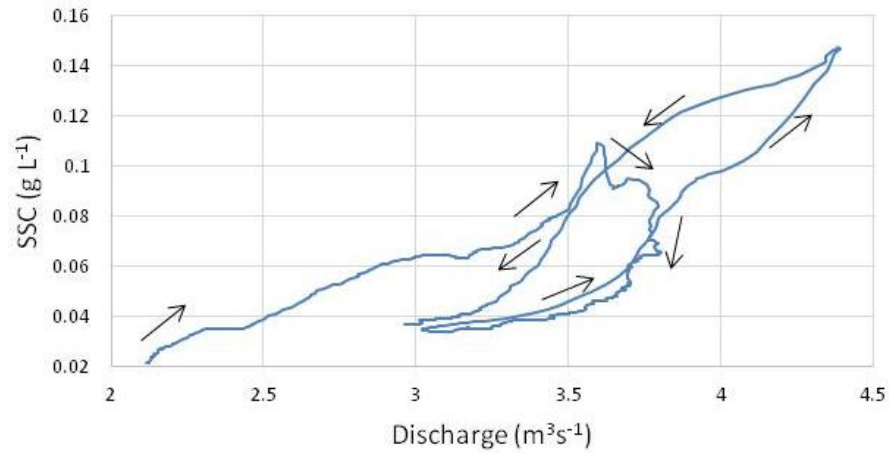


Figure 51 - Simple line graphs between smoothed discharge and suspended sediment concentration (SSC) series recorded at the South River site for each of the selected hydrological day sub-periods (DOY 195 - 198). Black arrows indicate the direction of hysteresis between the two variables.

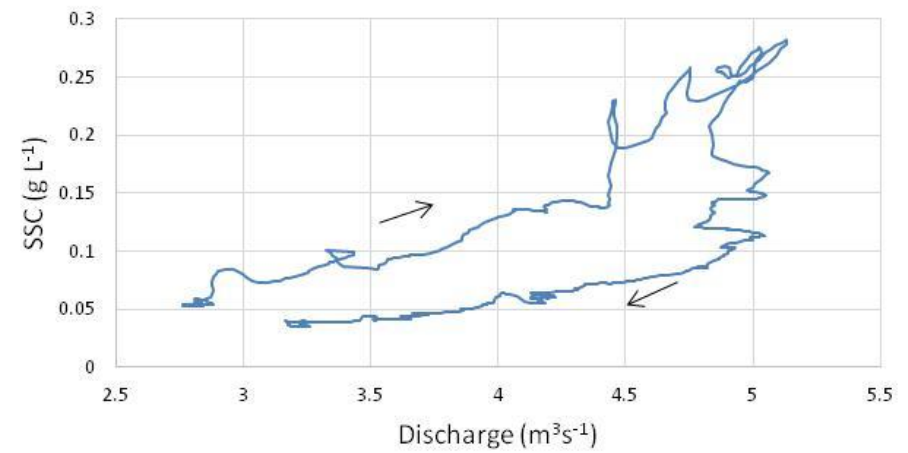
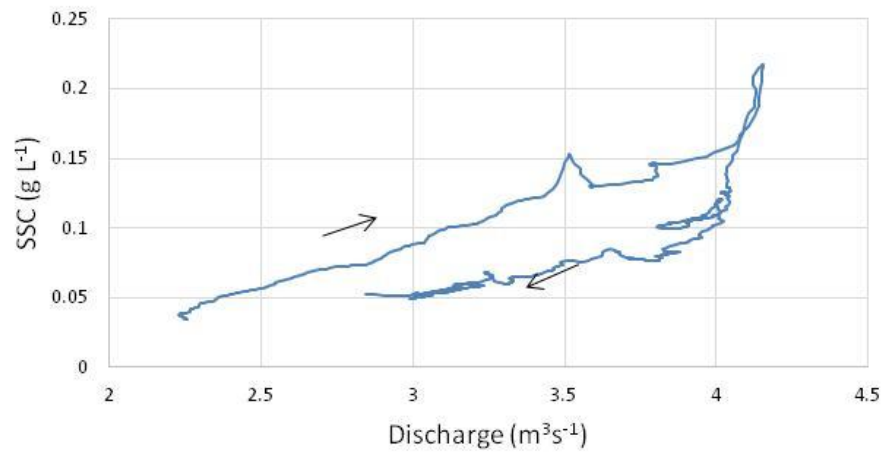
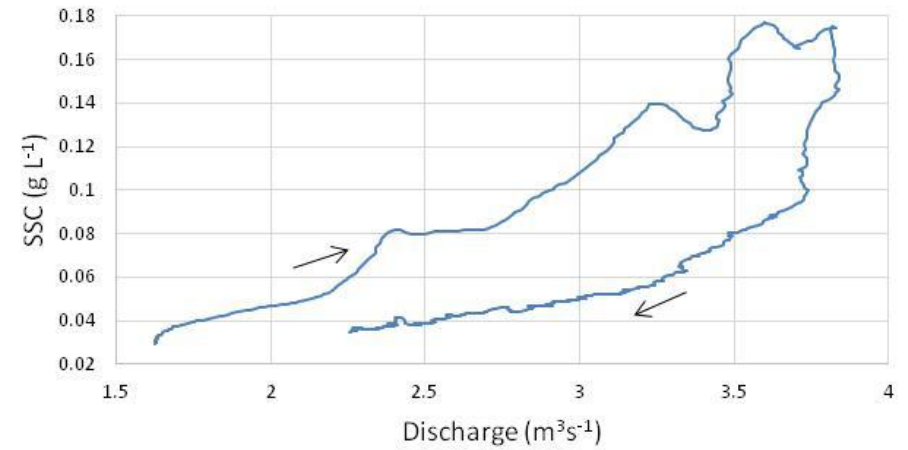
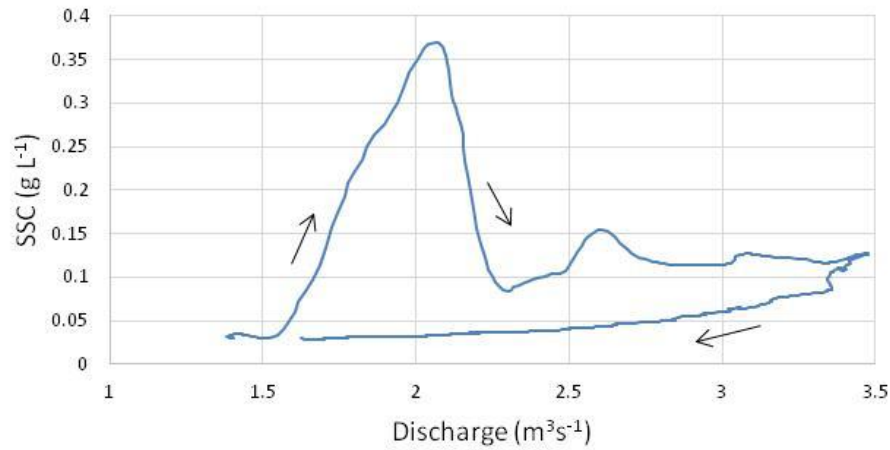


Figure 52 - Simple line graphs between smoothed discharge and suspended sediment concentration (SSC) series recorded at the South River site for each of the selected hydrological day sub-periods (DOY 199 - 202). Black arrows indicate the direction of hysteresis between the two variables.

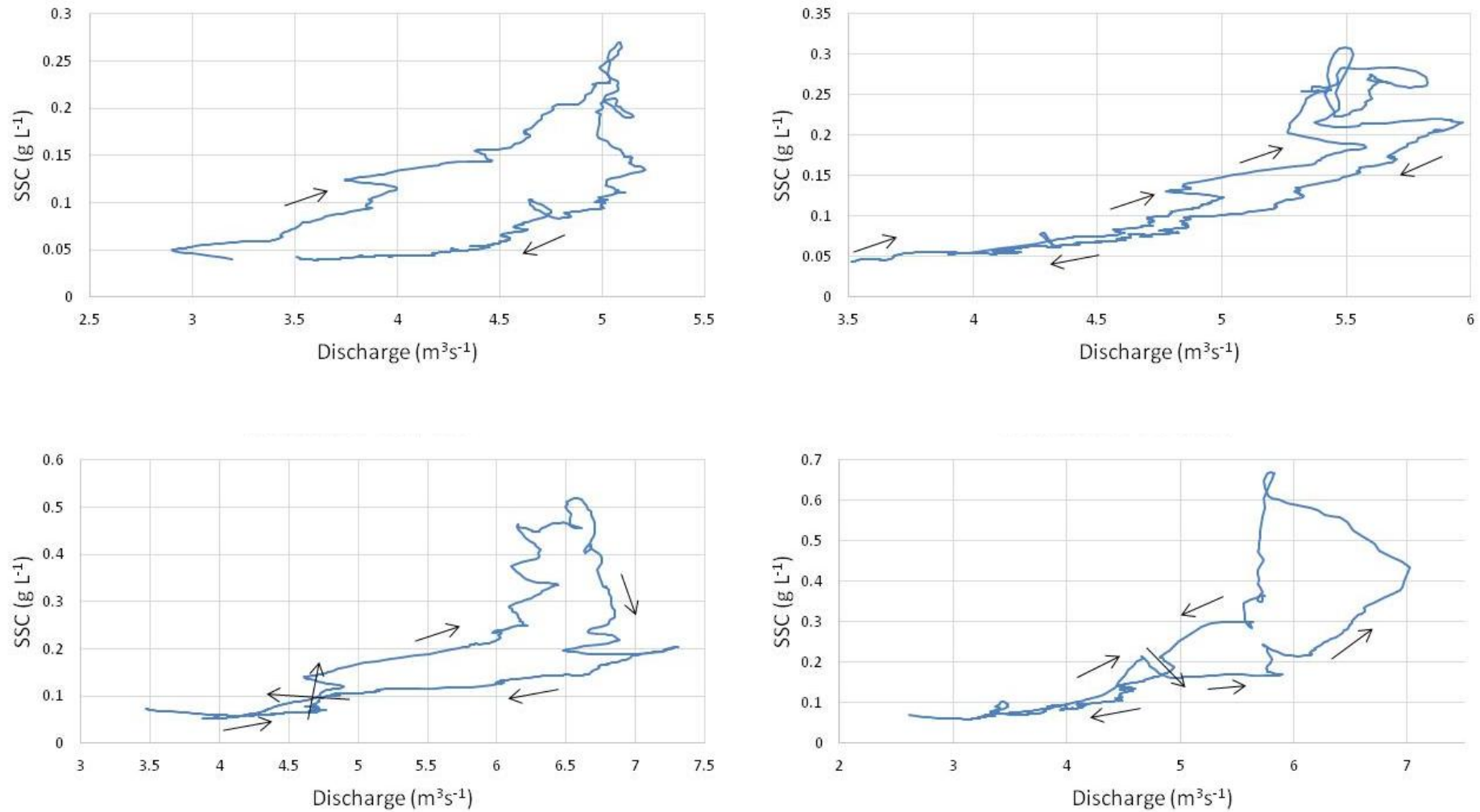


Figure 53 - Simple line graphs between smoothed discharge and suspended sediment concentration (SSC) series recorded at the South River site for each of the selected hydrological day sub-periods (DOY 203 - 206). Black arrows indicate the direction of hysteresis between the two variables.

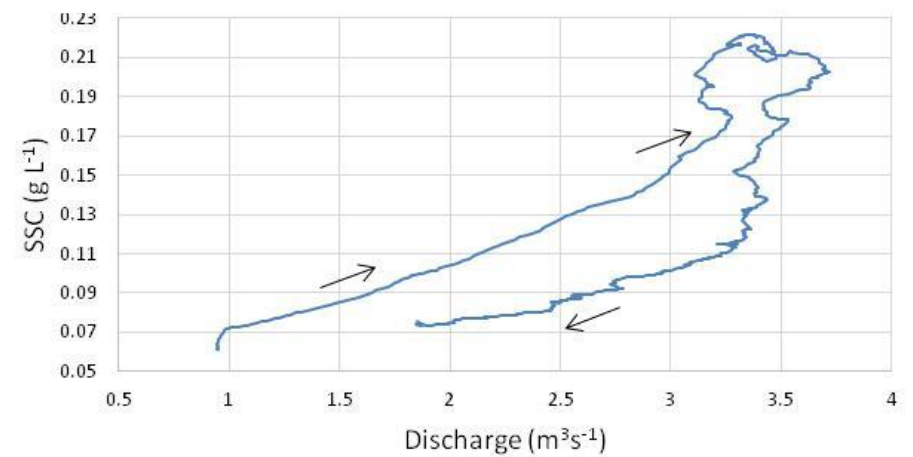
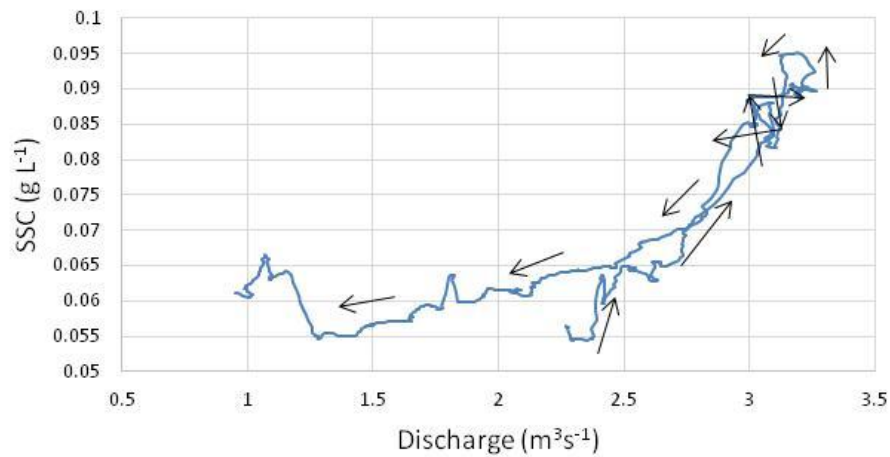
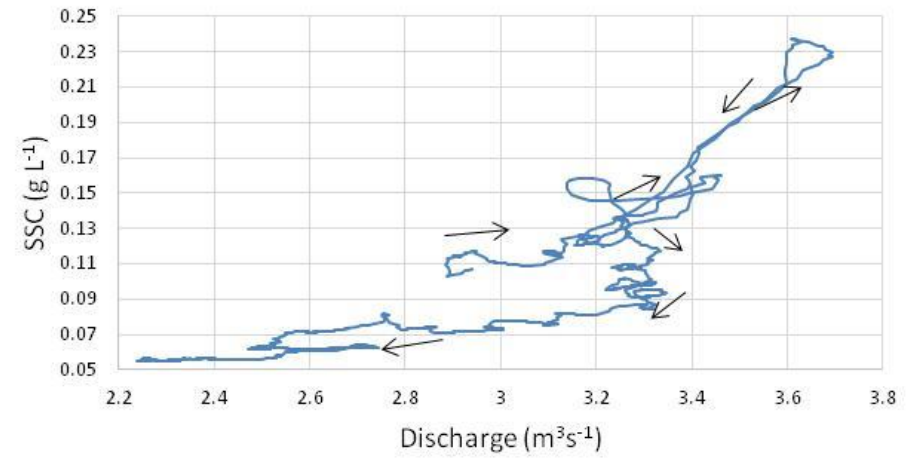
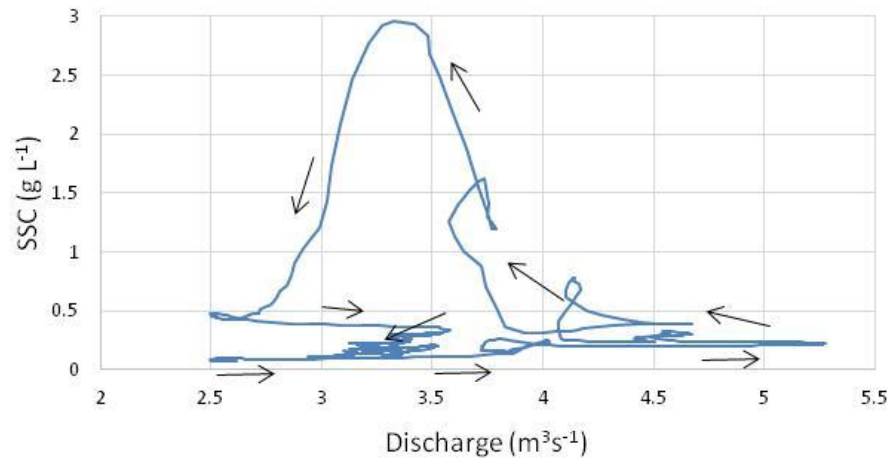


Figure 54 - Simple line graphs between smoothed discharge and suspended sediment concentration (SSC) series recorded at the South River site for each of the selected hydrological day sub-periods (DOY 207 - 210). Black arrows indicate the direction of hysteresis between the two variables.

## 6.5 Statistical Analysis

### 6.5.1 Cross Correlation

Cross correlation was undertaken to establish whether a relationship existed between two time series (cross correlation function - CCF) and potential lags and leads. Cross correlation was performed on discharge data from both sites, SSC from both sites, air temperature from all temperature sites, and water temperature from the South River site. Cross correlation of all of these allows for an understanding of phasing between each variable and sampling sites. Cross correlation was performed using the cross correlation function in Minitab statistical software, where discharge, SSC, air temperature, and water temperature time series were shifted  $\pm 350$  positions relative to variable 2 (Table 2). The highest cross correlation function indicated the dominant lead or lag between variable 1 and variable 2. All cross correlation functions were tested for statistical significance against cross correlation critical values and, all tests showed a statistical significance of 95%.

Cross correlation between air temperatures showed strong correlation functions and varying lag times. The Ablation site air temperature led against both the Upper North Tinytag site and the Lower North River site and the Lower North River air temperature site led against the Upper North Tinytag site air temperature. The smallest lag of 8 minutes and the largest cross correlation coefficient of 0.964 was experienced between the Lower North River site air temperature and the Upper North Tinytag site. The ablation air temperature - Lower North site air temperature had a lag of 32 minutes with the smallest cross correlation function of all the temperature correlations of 0.809. The largest lag of air temperatures was experienced between the Ablation site and the Upper North Tinytag site, with a lag of 56 minutes and a correlation coefficient of 0.895.

Cross correlation between discharges showed strong cross correlation functions and small lag times. There was zero lag between discharge at the Upper North River site and the Lower North River site, and the correlation coefficient was high at 0.945. The discharge at the Lower North River site experienced a lead time of 18 minutes (CCF 0.710) over the South River site. In comparison, the discharge at the Upper North River experienced a 25% increase in lead time at 24 minutes (CCF 0.856) over the South River site.

Cross correlation between air temperatures collected at the Upper North Tinytag site, Lower North site, and Ablation site all showed a strong correlation with water temperature recorded at the South River site, and all air temperature sites lead water temperature. The Upper North temperature - water temperature had a cross correlation coefficient of 0.897 and a lag of 6 minutes. In comparison, the air temperature recorded at both the Lower North site and Ablation site had a much bigger lead time. The Lower North air temperature had a lead time of 50 minutes (CFF 0.919) over water temperature, and the Ablation site air temperature had a lead time of 58 minutes over water temperature (CFF 0.800).

Air temperature recorded at the Lower North River site had an overall lead time of 112 minutes against the discharge of the Upper North site and an overall lead time of 118 minutes against the discharge of the Lower North site. Both cross correlations showed a strong correlation coefficient, with values of 0.724 and 0.700 respectively. The correlation between the Lower North air temperature and discharge at the South River site the temperature demonstrated that temperature led discharge by 254 minutes, however, the cross correlation function was much smaller in comparison to the other two sites with a value of 0.445.

A cross correlation was performed on air temperature and meltwater discharge because air temperature directly forces meltwater discharge. Air temperature recorded at the Upper North Tinytag led with a strong correlation against the discharge recorded at both the Upper North site and the Lower North Site, but the discharge recorded at the South River site led the air temperature with a much smaller cross correlation coefficient. The lag between the Upper North air temperature and the Lower North discharge was 144 minutes with a cross correlation coefficient of 0.652, and the lag between air temperature and the Upper North was 100 minutes with a cross correlation coefficient of 0.680. A lag of 112 minutes was experienced between the Upper North temperature and the South River discharge with a poor correlation function of 0.248.

The air temperature recorded at the Ablation site led the discharge recorded at all sites. The lag varied between each site, between the Lower North site it was 110 minutes, between the Upper North site the lag was 170 minutes, and between the South site, the lag was 194 minutes.

The cross correlation coefficient between the water temperature recorded at the South River site and the discharge of all sites were all high, ranging from 0.681 - 0.756. Water temperature led discharge at all sites with the biggest lag of 108 minutes taking place between the discharge at the South River site (CCF 0.681). In comparison, the lag between water temperature and the discharge at the Lower North site was 8 minutes smaller with a lag of 100 minutes, and the cross correlation coefficient was slightly larger at 0.707. The smallest lag experienced between water temperature and discharge occurred at the Upper North River site, the lag was 78 minutes, and compared to the other two sites showed the highest cross correlation coefficient of 0.756.

Water temperature was cross correlated against SSC because although the temperature may not directly force SSC like discharge does it still has the potential to cause indirect forcing of SSC and may act as a surrogate to air temperature. Cross correlation of water temperature against SSC recorded at all three sites showed large variations in both the lags and cross correlation functions. Water temperature led SSC at the Lower North River site by 18 minutes (CCF 0.656). Water temperature lagged behind SSC measured at the other two sites. At the South River site, the lag was small at 2 minutes with a strong correlation of 0.701, but at the Upper North site, the cross correlation was less than half of the other sites at only 0.300. The Upper North experienced a lag of 620 minutes which is the second highest lag out of all cross correlations performed in Table 2.

Cross correlation analysis between discharge and SSC was performed due to the overall potential discharge has to force the values of SSC. Analysis between discharge and SSC recorded at the same site shows a small cross correlation coefficient of less than 0.500. The Upper North site discharge led Upper North SSC by 418 minutes, there was zero lag experienced between the discharge and SSC recorded at the Lower north site, and between the discharge and SSC at the South site the SSC led by 56 minutes. There is a strong correlation between discharge recorded at the Upper North site and SSC recorded at the Lower North and South River site. The SSC leads the discharge at both sites, the Lower North site has a led time of 18 minutes (CCF 0.874), and the South site has a much larger lead time of 98 minutes (CCF 0.614). The cross correlation functions of all other discharge against SSC analysis were again all below 0.500. The discharge at the Lower North site led SSC values at the Upper North and South site. The Upper North site demonstrated a lag of 418 minutes,

whilst the South site demonstrated a much smaller lag of 18 minutes. Analysis between the discharge at the South site and SSC showed that discharge led SSC at the Upper North site by 200 minutes and that SSC at the Lower North site led discharge by 132 minutes.

Cross correlation between SSC between the Upper North and Lower North site, and between the Lower North and South site showed poor cross correlation functions of below 0.500. The Lower North site led the South site with a lag of 14 minutes, whilst the Upper North site lagged behind the Lower North site by a total of 306 minutes.

The majority of the cross correlation coefficient for temperature recorded at all three sites and SSC are below 0.500. The temperature recorded at the Lower North site leads the Lower North SSC by 64 minutes, and the SSC at the South site by 308 minutes. However, SSC at the Upper North site lags behind the temperature by 558 minutes. The temperature at the Upper North Tinytag site lagged behind the SSC recorded at both the Upper North site and the South site. The lag between the South site was 98 minutes, and the lag at the Upper North site was a much larger 560 minutes. The Upper North Tinytag temperature led the Lower North site by 134 minutes. SSC at the South and Lower North site lagged behind the temperature recorded at the ablation site by 440 minutes and 134 minutes. Conversely, SSC at the Upper North site led the temperature at the Ablation site by 498 minutes.

**Table 2 - Results of cross-correlation analysis performed on the discharge, SSC, water temperature, and air temperature. All CCF had critical values 0.052-0.062 and showed a statistical significance of 95%.**

Variable 1	Variable 2	CCF	Lag (Minutes)	Lag (Hours)
Discharge UN	Discharge LN	0.945	0	0.000
Discharge LN	Discharge S	0.710	18	0.300
Discharge UN	Discharge S	0.856	24	0.400
Discharge UN	SSC UN	0.218	418	6.967
Discharge UN	SSC LN	0.874	-18	-0.300
Discharge UN	SSC S	0.614	-98	-1.633
Discharge LN	SSC LN	0.241	0	0.000
Discharge LN	SSC S	0.170	18	0.300
Discharge LN	SSC UN	0.347	418	6.967
Discharge S	SSC S	0.187	-56	-0.933
Discharge S	SSC LN	0.183	-132	-2.200
Discharge S	SSC UN	0.403	200	3.333
SSC UN	SSC LN	0.187	-306	-5.100
SSC LN	SSC S	0.138	14	0.233
Air Temp UN	Air Temp LN	0.964	-8	-0.133

Air Temp Ablation	Air Temp LN	0.809	32	0.533
Air Temp Ablation	Air Temp UN	0.895	56	0.933
Air Temp LN	Discharge LN	0.700	118	1.967
Air Temp LN	SSC LN	0.567	64	1.067
Air Temp LN	SSC S	0.108	308	5.133
Air Temp LN	Discharge S	-0.445	254	4.233
Air Temp LN	Discharge UN	0.724	122	2.033
Air Temp LN	SSC UN	-0.303	-558	-9.300
Air Temp UN	SSC LN	0.561	80	1.333
Air Temp UN	Discharge LN	0.653	144	2.400
Air Temp UN	Discharge UN	0.680	100	1.667
Air Temp UN	SSC UN	-0.352	-560	-9.333
Air Temp UN	SSC S	0.086	-98	-1.633
Air Temp UN	Discharge S	0.248	112	1.867
Air Temp Ablation	SSC LN	0.343	134	2.233
Air Temp Ablation	Discharge LN	0.433	110	1.833
Air Temp Ablation	SSC S	0.119	440	7.333
Air Temp Ablation	Discharge S	0.238	194	3.233
Air Temp Ablation	Discharge UN	0.500	170	2.833
Air Temp Ablation	SSC UN	-0.417	-498	-8.300
Water Temp S	Discharge LN	0.707	100	1.667
Water Temp S	SSC LN	0.656	18	0.300
Water Temp S	Discharge UN	0.756	78	1.300
Water Temp S	SSC UN	-0.300	-620	-10.333
Water Temp S	SSC S	0.701	-2	-0.033
Water Temp S	Discharge S	0.681	108	1.800
Air temp UN	Water temp S	0.897	6	0.100
Air temp LN	Water Temp S	0.919	50	0.833
Air temp Ablation	Water Temp S	0.800	58	0.967

#### 6.5.1.1 Diurnal Discharge - Suspended Sediment Concentration

Cross correlation was performed on the hydrological diurnal discharge and SSC time series for the Upper North river site (DOY 195 - 199), Lower North River site (DOY 190 - 208), and the South River site (DOY 191 - 210) because meltwater discharge has the potential to cause direct forcing of the values of SSC. Cross correlation functions and lag times for diurnal discharge and SSC are presented in Table 3. All cross correlation functions were tested for statistical significance against cross correlation critical values and, all tests showed a statistical significance of 95%.

Diurnal discharge and SSC for the Upper North River site had a large range of lag times with varying values of cross correlation function throughout the period of measurement (DOY

195 - 199). During DOY 195 - 199, the largest lag was experienced on DOY 195 where discharge lagged SSC by 322 minutes, however, the smallest cross correlation function was the lowest at 0.407. DOY 196 had the highest cross correlation function at 0.717 and the discharge lagged SSC but with a much smaller lag of 12 minutes. Cross correlation between discharge and SSC for DOY 197 showed the second highest lag for the Upper North River with the stage being lagged by 250 minutes compared to SSC. The final two days of measurement for the Upper North River site (DOY 198 and 199) both had the same cross correlation and lag time. During these days there was zero lag between discharge and SSC and there was a correlation of 0.560. During this overall period at the Upper North River site, discharge lagged behind SSC by 117 minutes.

Cross correlation of diurnal stage and SSC time series for the South River site predominantly shows that discharge lags behind SSC by between 4 - 232 minutes with a moderately strong cross correlation function of above 0.500 for each diurnal lag (Table 3). Zero lag between discharge and SSC was experienced on DOY 191, 204, 209, and 210. During DOY 206 and 207 SSC lagged behind discharge. DOY 206 showed a lag of 46 minutes with a strong cross correlation function of 0.848, and DOY 207 showed the largest lag for the South River site at 252 minutes with a slightly smaller cross correlation function of 0.627. During this overall period at the South River site, discharge lagged behind SSC by 33 minutes.

Cross correlation of diurnal Discharge and SSC time series for the Lower North River site shows a more varied combination of lag and lead times compared to the South River site and Upper North River site. Zero lag between discharge and SSC was shown DOY 192, 196, 197, 198, and 208 with strong cross correlation functions ranging from 0.678 - 0.951. Discharge led SSC on DOY 190, 195, 204, 205, 207, and 208 with an average lag across those days of 226 minutes, a maximum lag of 406 minutes (DOY 204), and a minimum lag of 74 minutes (DOY 190). On the other hand, SSC led discharge on DOY 191, 193, 194, 199, 200, 201, 203, and 206. During this period the average lag time was 142 minutes, with a maximum lag of 254 minutes (DOY 201 and 203), and a minimum lag of 4 minutes (DOY 193). During this overall period at the Lower North River site, SSC lagged behind discharge by 21 minutes.

Cross correlation analysis of the selected Lower North River sub-periods (DOY 202 - 207) shows strong cross correlation functions of above 0.5 for all tests apart from DOY 202 B and 207 B. The first sections (A) of most sub-periods have a lag of zero between discharge and SSC apart from DOY 202 A which has a lag of 10 minutes, and DOY 204 A which has a lag of 6 minutes both in favour of SSC. The last sections (C) of most sub-periods also show zero lag between discharge and SSC with strong cross correlation functions. DOY 205 C is the only last section to show a lag, SSC leads discharge by 244 minutes. The middle sections (B) of the sub-periods showed a broad range in lag times and cross correlation functions. Discharge led SSC on DOY 202 B, 204 B, and 207 B, and SSC led discharge on DOY 203 B, 205 B, and 206 B. DOY 202 B experienced a lag of 108 minutes which is over 3.5 times smaller than the lag shown by cross correlation analysis of the whole hydrological period shown in Table 3. DOY 203 B experienced a lag of 4 minutes which is again much smaller than the lag shown in Table 3 with a difference in the lag of over 63 times. SSC led discharge by 102 minutes during DOY 205 B, however, during the whole hydrological day shown in Table 3 discharge led SSC by 296 minutes. DOY 206 B had a lag of 44 minutes which is 2 minutes bigger than the overall lag experienced in Table 3, and lastly, DOY 207 B had the same lag as in Table 3 at 6 minutes.

**Table 3 - Cross correlation analysis results for the Lower North River (DOY 190 - 208), Upper North River (DPY 195 - 199), and South River (191 - 210). Critical values for all sites showed the CCFs had a statistical significance of 95%. Critical values for each site ranged from 0.088 - 0.098 (Lower North River); 0.088 - 0.139 (Upper North River); 0.088 (South River).**

DOY	Variable 1	Variable 2	Lower North River			Upper North River			South River		
			CCF	Lag (minutes)	Lag (hours)	CCF	Lag (minutes)	Lag (hours)	CCF	Lag (minutes)	Lag (hours)
190	Discharge	SSC	0.664	74	1.23						
191	Discharge	SSC	0.611	-214	-3.57				0.680	0	0.00
192	Discharge	SSC	0.915	0	0.00				0.619	-12	-0.20
193	Discharge	SSC	0.907	-4	-0.07				0.687	-42	-0.70
194	Discharge	SSC	0.445	-200	-3.33				0.880	-18	-0.30
195	Discharge	SSC	0.431	368	6.13	0.407	-322	-5.37	0.702	0	0.00
196	Discharge	SSC	0.951	0	0.00	0.717	-12	-0.20	0.715	-8	-0.13
197	Discharge	SSC	0.907	0	0.00	0.482	-250	-4.17	0.767	-156	-2.60
198	Discharge	SSC	0.876	0	0.00	0.560	0	0.00	0.751	-130	-2.17
199	Discharge	SSC	0.864	-10	-0.17	0.560	0	0.00	0.595	-232	-3.87
200	Discharge	SSC	0.382	-158	-2.63				0.779	-52	-0.87
201	Discharge	SSC	0.516	-254	-4.23				0.747	-16	-0.27
202	Discharge	SSC	0.328	386	6.43				0.724	-62	-1.03
203	Discharge	SSC	0.516	-254	-4.23				0.693	-122	-2.03
204	Discharge	SSC	0.590	406	6.77				0.864	0	0.00
205	Discharge	SSC	0.676	296	4.93				0.797	-112	-1.87
206	Discharge	SSC	0.609	-42	-0.70				0.848	46	0.77
207	Discharge	SSC	0.538	6	0.10				0.627	252	4.20
208	Discharge	SSC	0.678	0	0.00				0.810	-4	-0.07
209	Discharge	SSC							0.784	0	0.00
210	Discharge	SSC							0.766	0	0.00

**Table 4 - Cross correlation analysis results for sub-period breakdowns (Figure 45, 46, 47). Critical values for the CCFs ranged from 0.098 to 0.220 and showed a statistical significance of 95%.**

DOY	Variable 1	Variable 2	CCF	Critical Value	Lag (minutes)	Lag (hours)
202 A	Discharge	SSC	0.792	0.139	-10	-0.17
202 B	Discharge	SSC	0.452	0.197	108	1.80
202 C	Discharge	SSC	0.939	0.113	0	0.00
203 A	Discharge	SSC	0.874	0.139	0	0.00
203 B	Discharge	SSC	0.724	0.197	-4	-0.07
203 C	Discharge	SSC	0.793	0.113	0	0.00
204 A	Discharge	SSC	0.918	0.113	-6	-0.10
204 B	Discharge	SSC	0.721	0.197	38	0.63
204 C	Discharge	SSC	0.827	0.139	0	0.00
205 A	Discharge	SSC	0.655	0.139	0	0.00
205 B	Discharge	SSC	0.752	0.197	-102	-1.70
205 C	Discharge	SSC	0.665	0.113	-244	-4.07
206 A	Discharge	SSC	0.902	0.139	0	0.00
206 B	Discharge	SSC	0.738	0.197	-44	-0.73
206 C	Discharge	SSC	0.956	0.113	0	0.00
207 A	Discharge	SSC	0.887	0.139	0	0.00
207 B	Discharge	SSC	0.361	0.220	6	0.10
207 C	Discharge	SSC	0.655	0.098	0	0.00

## 7 Discussion

This study set out to identify the fluvio-glacial characteristics of two contrasting alpine proglacial rivers and to evaluate short-term spatial and temporal patterns of sediment transfer within a progressively deglaciating catchment. This is important to understand under the current climate warming scenario which is predicted to continue well into the 21<sup>st</sup> Century because it is possible that the changes will have a consequential effect on fluvio-glacial sediment transport because of the importance of meltwater in mobilising and transferring sediments in glaciated regions (e.g. Huss *et al.*, 2014; Orwin & Smart, 2004a; Swift *et al.*, 2005b, 2006). The following section discusses the results from the two contrasting proglacial rivers and places the data within the wider scientific context.

### 7.1 Hydrology

Distinct diurnal hydrological cycles and the mean lag times between air temperature and proglacial discharge of the Feegletscher Nord (127 minutes) and Süd (186 minutes) demonstrate the meltwater connectivity of the glacier surface to the subglacial drainage system, and through the proglacial areas. These results showed that the Feegletscher Süd's

proglacial River was approximately 60 minutes slower to respond to the estimate of melt generation from the ablation stake and temperature sensors compared to the Feegletscher Nord's proglacial river. The lag times align with similar research performed on the Feegletscher Nord that has suggested lag times of between approximately -40 to +240 minutes (Smart, 2015). These lag times are partially influenced by the gravitational potential of meltwater which could be relatively high due to the overall steep topographic location of the Feegletscher. The high gravitational potential of meltwater at the Feegletscher, therefore, means that there are good conditions for englacial and subglacial conduit development caused by the high potential energy accessible for melt. The surface of the Feegletscher is characterised by being highly crevassed permitting for a more distributed input of supraglacial meltwater compared to other supraglacial drainage features (Flowers & Clarke, 2002). The lags experienced between air temperature and proglacial discharge did not show any significant increase or decline in trend over the period of measurement, which shows that minimal change to the removal of supraglacial snow pack or efficiency of the subglacial drainage system took place. As mentioned by previous studies (e.g. Nienow *et al.*, 1998), the lag times between air temperature and proglacial discharge may also signify the impact and overall development of the subglacial drainage system and meteorological drivers of glacier surface melt. These are commonly linked with possible sediment entrainment by meltwater at the basal ice to bed boundary, and further possible sediment entrainment in the proglacial entrainment stream. The entrainment of sediment within the drainage system of a proglacial stream is demonstrated in this study by the hysteretic patterns of the proglacial streams of the Feegletscher Nord and Süd.

The diurnal hydrological cycles from all sites did not demonstrate any major adjustments in form during the whole period of study, and this suggests that the drainage system of the Feegletscher did not experience any obvious development and that the decreases in albedo experienced that caused the exposure of more bare ice (Figures 26 - 28) had limited impacts to development. This aligns with previous research performed by Smart (2015) that found that the Feegletscher Nord experienced minimal drainage network development after DOY 180. The diurnal hydrological cycles (Figures 40-55) and lag times (Table 2 & 3) suggest that the Feegletscher already had an efficient drainage network at the beginning of the study period (DOY 190), and this concurs with studies performed on the Feegletscher Nord by

Collins (1979) and Smart (2015) who suggest that there was a lag of between -120 to +120 minutes (Collins, 1979) and -128 to +66 minutes (Smart, 2015). Collins (1979) concluded that the changes to the drainage network at the Feegletscher are quickly seen after early ablation occurs. This may be caused by conduits from previous years being conserved over the winter period instead of drainage pathways becoming fully closed by creep closure (e.g. Bartholomew *et al.*, 2012; Hewitt, 2013).

The average discharge at the North River increased by 63.89 % from the Upper North River site to the Lower North River site, with the Upper North site contributing 37.89 % and the Lower North River site contributing for 62.11 % of the total average discharge in the North River. The higher discharge at the Lower North River site is likely to arise from lateral stream contributions that come from both glacial but also non-glacial sources. No ground-penetrating radar or similar bathymetric type survey has been undertaken on the Feegletscher to establish which areas of the catchment drain through the North River and South River outlet. The average relative contribution from the discharge data is 76.58 % from the South outlet and 23.42 % from the North outlet, which might suggest a relative drainage distribution from each outlet but this is only an assumption, and due to a large number of interacting variables it is impossible to truly identify what areas of the hydrological system drain through each outlet without ground-penetrating surveys of the Feegletscher. The development and spatial contribution of the subglacial drainage network can particularly impact and modify the relationship between glacier meltwater discharge and SSC (e.g. Swift *et al.*, 2002, 2005a), and is a major control in the overall availability of sediment for mobilisation, and the rate of glacio-fluvial sediment evacuation (e.g. Hubbard *et al.*, 1995; Swift *et al.*, 2002, 2005a, 2005b).

## 7.2 Proglacial Suspended Sediment

The time series of proglacial SSC monitored at all sites showed strong diurnal hydrological driving of proglacial SSC at both the Feegletscher Nord and Süd. During the monitoring period, there was no significant increase or decrease in the mean SSC, suggesting that during the monitoring period there was no major change in the overall availability of sediment throughout the proglacial areas of the Feegletscher Nord and Süd. However, there was spatial and temporal variation between the Feegletscher Nord and Süd, but also

between each monitoring site, demonstrating that complex intra-basin spatial and temporal sediment dynamics exist.

Both of the monitoring sites along the proglacial stream of the Feegletscher Nord are subject to paraglacial rock avalanches, paraglacial debris flows, and slope modification which enabled the renewal of some sediments to the source area (Curry *et al.*, 2006, 2009; Cook *et al.*, 2013). However, in comparison to the Upper North River Site, the Lower North River site would be expected to exhibit enhanced non-glacial sediment loads because as the distance from the glacial terminus increases so does the extent of available sediment sources that can be exploited by a combination of subaerial or fluvial reworking (e.g. Gurnell, 1995; Orwin & Smart, 2004a). Also, compared to the Upper North River site, the Lower North River site should have reduced access to fine grained glaciogenic sediment at the proglacial stream margins and within the proglacial stream itself, reducing the amount of sediment for that is easily mobilised. This is because the area surrounding the Lower North River site is characterised by larger particle sized sediment deposits and consolidated lateral moraine material that require more hydraulic energy to mobilise compared to the Upper North River site that has a larger quantity of fine grained sediment that is more greatly accessible for reworking and remobilisation by fluvial mechanisms (Curry *et al.*, 2009; Cook *et al.*, 2013). The results reflect this as the Lower North site on the Feegletscher Nord's proglacial river on average showed a lower SSC and flux when discharge is factored in and indeed this aligns with some of the results Orwin and Smart (2004a) found from the Small River/ North Cirque Glacier (Canada) when they installed multiple turbidity sensors. They demonstrated significant differences in sediment transfer patterns and SSC between the upstream monitoring station and the downstream monitoring station with an average decrease in SSC of 45.69 % (Orwin & Smart, 2004a). Even though the Lower North River site experienced discharge and likely SSC contributions from lateral stream links which come from both glacial and non-glacial sources, the Lower North River only displayed an average SSF of 13.07 g/s compared to the 99.38 g/s at the Upper North site. This, therefore, demonstrates an average reduction in SSF of 86.31 g/s compared to the Upper North River, and even with additional sediment entrainment between the two sites, the results suggest that 86.85 % of entrained sediment was deposited within the proglacial channel before reaching the Lower North River site. The values of SSF will likely have a range of error

surrounding them that have not been calculated in this study. The errors will be caused by general instrumental error in the current discharge and SSC monitoring techniques, and uncertainty from the relationship between stage-discharge, and between discharge-SSC (Gurnell *et al.*, 1992; Hodgkins *et al.*, 2003).

The Feegletscher Süd's proglacial river had an average SSF of 49.18 g/s which is an average of 36.11 g/s (276.22 %) more than the Lower North river site and 50.20 g/s (50.52 %) less than the Upper North River site. When an average for the Feegletscher Nord's proglacial river is taken into consideration the Feegletscher Süd's proglacial river has a SSF that is 7.05 g/s (12.54 %) less, which is expected because the proglacial area of the Feegletscher Süd is predominantly characterised by bare bedrock and minimal proglacial glacio-fluvial sediment deposits compared to the Feegletscher Nord's proglacial area. The Feegletscher Süd's proglacial river experienced three major fluctuations on DOY 192, DOY 218, and DOY 232 in both discharge and SSC that demonstrated sudden deviation from the dominant and generally smooth diurnal discharge cycle and was unrelated to the precipitation events. These major fluctuations may indicate the sudden release of subglacially stored water in an outburst flood (e.g. Liestøl, 1977; Driedger & Fountain, 1989; Hagen, 1987; Walder & Driedger, 1995). Previous studies suggest that outburst floods most likely occur when the subglacial hydrological system is characterised by water-filled cavities (Gilbert *et al.*, 2012). However in this research, there is a lack of evidence to support this at the Feegletscher Süd, and more hydrological monitoring or ground penetrating radar/ bathymetric survey research would be needed to determine if such a hydrological characteristic is typically found at the Feegletscher.

The cross correlation analysis showed that at different sites there was a range of strengths in the relationship between discharge and SSC, however, overall the common relationship between these two variables was strong and mostly showed that an increase in discharge was followed by an increase in SSC. This concurs with research performed on SSC-discharge (e.g. Collins, 1979; Delaney *et al.*, 2018b; Perolo *et al.*, 2018). There was a large range of mean lags between SSC and proglacial discharge with lags of 418, 0, and -56 minutes at the Upper North, Lower North, and South River site which demonstrates the differences in strength of discharge controlling SSC, the range of sediment transfer capacities present and the availability of fine sediment at each monitoring site. Similarly, with the lag times

between air temperature and discharge, the lags between SSC and discharge did not show any significant increase or decline in trend throughout measurement but remained constant.

The mean zero lag between SSC and discharge at the Lower North River site for the whole monitoring period could indicate that SSC instantaneously reacted to discharge, and Smart (2015) suggested that a lag close to zero at a similar location within the Feegletscher Nord proglacial area was linked to this. However, the majority of the diurnal hysteretic loops presented for the Lower North River site (Figures 42 - 46) demonstrated equal amounts of both anti-clockwise and clockwise hysteresis. Therefore, the zero lag between SSC and discharge is produced from the positive and negative lags cancelling each other out (Table 3), and instead of instantaneous SSC forcing by discharge showed that a more complex range of sediment transport mechanisms was present at the Lower North River site. The occurrence of non-glacial sediment mobilisation processes present at the Lower North River site could be a likely cause of the complex SSC relationship with discharge. During days with enhanced glacier melting (DOY 202 - 207) the Lower North River showed a different hysteresis relationship which demonstrated a minimal increase in SSC until much later in the hydrological day in comparison to days with comparably lower glacier melting. This may signify exhaustion of closer and more commonly evacuated sediment sources and suggest a link with a sediment source that is easily mobilised and evacuated quickly before peak but was not available during regular meltwater discharge and/or a source that is situated further up-glacier (Mao *et al.*, 2014). These hysteresis patterns could also demonstrate changes in sediment storage between the monitoring stations of the Upper North River site and the Lower North River site, and similar suggestions were made by Orwin & Smart (2004a) between SSC monitoring sites at the Small River Glacier, Canada. There is no data from the Upper North River site during the period of (DOY 202 - 207) to add additional insight into how hydrological days, with enhanced glacier melting, impact the glacio-fluvial sedimentary response.

The Upper North River site demonstrated an overall anti-clockwise hysteretic relationship which suggests good availability and a lack of sediment exhaustion and therefore goes against the typical finding of most glaciers that have major diurnal fluctuations in SSC and discharge (e.g. Hodgkins, 1999; Irvine-Fynn *et al.*, 2005; Delaney *et al.*, 2018b; Perolo *et al.*,

2018). The majority of the current research on hysteretic loops related to sediment transfer has found that anti-clockwise hysteretic loops are caused by events that increase sediment supply after the hydrological maximum has been reached (e.g. Mao *et al.*, 2014). Anticlockwise hysteretic loops are known to be more numerous late in the ablation season and may indicate a possible distant contribution of sediment supply from glaciers and proglacial environments to meltwater (e.g. Lane *et al.*, 1996; Mao *et al.*, 2014; Misset *et al.*, 2019). These sources of sediment are suggested to be much further from the monitoring station than sediment sources active earlier in the ablation season (e.g. Lane *et al.*, 1996; Mao *et al.*, 2014; Misset *et al.*, 2019). However, the short-term nature of this study and because that the whole ablation season was not studied means that it cannot be determined if the anticlockwise hysteresis experienced at the Upper North River site was due to the timing of the monitoring within the ablation period.

Literature shows that increasing SSC, during decreasing water discharge, could be associated with sediment sources that are more easily accessible and available due to low stability (Baca, 2008). Also, newly exposed forefields from deglaciation are usually found to have unconsolidated sediment that is unstable, and highly available for reworking and remobilisation by fluvial mechanisms (e.g. Orwin & Smart, 2004a). This is demonstrated by the at both forefield sites of the North River. The Upper North River site used to be a lake that acted as a sink for glacial-fluvial sediment (Hampel, 2009), however, the area is now a braided proglacial source of unstable, unconsolidated fine sediment. In comparison to the Upper North River, the time since deglaciation of the Lower North site is less recent and as a result, more fine grained sediment has been reworked and remobilised. This means that there is less fine grained sediment at the Lower North River site. Therefore, the proglacial area situated near the Upper North River site is the most ideal location out of the two sites for stochastic deposition of fine sediments into the meltwater stream of the Feegletscher Nord via channel banks collapsing at the proglacial stream margins, or within the stream itself. Such events have been reported by various studies to result in increased SSC on the falling limb of a hysteresis loop (e.g. Sarma, 1986; Ashbridge, 1995; Russel *et al.*, 2001; Priesnitz & Schunke, 2002; Forbes & Lamoureux, 2005). Stochastic deposition of sediment into the Feegletscher Nord's proglacial stream can be seen through various fluctuations in sediment concentration that demonstrated sudden deviation from the dominant and

generally smooth diurnal SSC cycle, for example, on the falling limbs of DOY 196 and DOY 197. These deviations show a lack of association between peak values in discharge and SSC and could demonstrate that the experienced stochastic deposition of sediment is not connected with rises and falls in discharge values, but is caused only by the presence of the unstable and easily mobilised glaciogenic sediment (e.g. Richards & Moore, 2003; Orwin & Smart, 2004a).

Clockwise hysteretic patterns dominated at the proglacial river site of the Feegletscher Süd in which SSC peaked prior to water discharge and was higher during increasing discharges than decreasing discharges. This suggested the potential exhaustion of sediment and entrainment of channel sediments during rising flow. The overall clockwise hysteretic pattern experienced at the sampling site on the proglacial river of the Feegletscher Süd suggests that sediments are rapidly mobilised and exhausted before discharge reaches its maximum diurnal value. This reflects the majority of the current research on hysteretic loops related to sediment transfer that has found that clockwise hysteretic loops are associated with the existence of readily available sediments (e.g. Mao *et al.*, 2014). The diurnal exhaustion is likely to be caused by the fact that the Feegletscher Süd's upper proglacial area is not characterised by large quantities of glacio-fluvial sediment deposits but instead, a greater part of it is characterised by a clean bedrock forefield, and therefore it is unsurprising that there is a lower SS compared to the Upper North River site. However, the Feegletscher Süd's proglacial river flows through a region of the Little Ice Age moraine, and there is the capacity for enhanced sediment availability and entrainment from this section of the Feegletscher Süd's proglacial area. The fact that 76.58 % more discharge emanates from the South outlet compared to the North, and because the majority of the proglacial area is characterised by bare bedrock could suggest that some of the suspended sediment within the South river does not originate directly from the subglacial area of the Feegletscher Süd. In addition to entrainment from the Little Ice Age moraine, part of the suspended sediment entrained in the South river could be from the meltwater that is draining from the Northern lobe of the Feegletscher. However, without additional meltwater drainage research, this is impossible to confirm. These characteristics align with literature that suggests that clockwise hysteresis have also been linked to the activation of sediment sources in the lower area of the catchment due to mechanisms, such as, bank

erosion near the proglacial monitoring station (Mao *et al.*, 2014). It is therefore clear, that the availability of fine forefield sediment and the interaction between sediment availability and glacio-fluvial mechanisms of sediment transport are major controlling factors on the temporal and spatial differences in SSC observed between the proglacial study sites of the two rivers.

Without a rain gauge situated at each monitoring location, it is difficult to assess the strength of associations between rainfall and SSC. The Lower North, Upper North, and South River site all indicated that the evacuation of suspended sediments was high during a precipitation led day. However, the day that followed showed a clockwise hysteretic loop with reduced quantities of sediment evacuation, with the Lower North and South River site showing a larger reduction in the evacuated sediment compared to the Upper North River site. The reduction in evacuated sediment is because the surfaces surrounding the Lower North and South monitoring stations have reduced fine glaciofluvial material in comparison to the Upper North River site, and this means that the enhanced evacuation of sediment caused by the precipitation limited the supply of fine material and caused faster exhaustion of sediment on the day after precipitation. However, after the precipitation event on DOY 202, the Lower North River site had higher than average quantities of SSC on the following day but still showed a clockwise hysteresis relationship. The higher than average sediment evacuation on DOY 203 may signify a link with a sediment source that was not available during regular meltwater discharge, and the contributions most likely came from both glacial but also non-glacial sources from areas in the catchment where the precipitation type was rainfall and not snowfall (e.g. Mao *et al.*, 2014). Compared to the Upper North River site, the lower quantities of fine sediment, the increased sediment stability, and increased age since deglaciation at the Lower North and South River sites may result in a weaker relationship between rainfall and SSC and means that these sites need higher intensity and/or duration of rainfall to mobilise sediment. Orwin and Smart (2004b) suggested that sections of a proglacial area that have been deglaciated for longer periods are more likely to have a lesser response in sediment transfer caused by rainfall compared to proglacial areas that have more recently deglaciated. The overall patterns between rainfall and SSC have similarities with what Smart (2015) found within the proglacial area of Feegletscher Nord, and suggest that the sedimentary and geomorphological characteristics

of Feegletscher Nord and Süd are the main factors that contribute to patterns between rainfall and SSC.

The differences in patterns of glacio-fluvial sedimentation between the sites support the current literature that shows that after deglaciation occurs, proglacial SSC is likely to be high (e.g. Cossart & Fort, 2008) but then reduce as surface and slope sediments become less available, more stable, and consequently less prone to reworking and remobilisation (e.g. Orwin & Smart, 2004a). Surface and slope sediments are likely to stabilise because of the eluviation of fine sediment and consequent armouring of surface layers due to mechanisms such as overland flow and enhanced by progressive vegetation colonisation (Porter *et al.*, 2018). The presence of vegetation increases sediment cohesion, shear strength, rainfall interception, and infiltration, and consequently, surface runoff and sediment mobilisation are reduced (Klaar *et al.*, 2015). The process of stabilisation can cause proglacial forefield surfaces to no longer function as a major source of sediment and can occur within decades of deglaciation (Orwin and Smart, 2004b). Stabilisation of sediment is demonstrated between the Upper North River and Lower North River site and shows that a possibility for variations in hysteresis experienced at the different sites along the Feegletscher Nord's proglacial stream reflects the overall availability of unstable fine glaciogenic sediment for reworking and remobilisation varies depending on the site and reduces with time since glacier retreat. Therefore, in comparison to the Feegletscher Süd, the levels of SSC and SSF experienced at the Feegletscher Nord can be increased by the existence of proglacial deposits related to retreat.

Overall, it is clear that the combined evidence from all sites indicates that all sites show complex patterns of glacio-fluvial sedimentation that varies spatially and temporally. The differences identified between sites were likely due to the variations in fine grained glaciogenic sediment availability within the proglacial channels, variations in the meltwater and sediment input from the Feegletscher, and differences in geomorphological histories. The results from the Feegletscher Nord and Süd are supported by evidence from previous studies that display the proglacial controls on SSC patterns (e.g. Smart, 2015; Mao & Carrillo, 2016; Delaney *et al.*, 2018a). This study has shown that identifying spatial and temporal patterns of glacio-fluvial sedimentation, even from a small glaciated catchment, is difficult but additional complexity is added when a glaciated catchment with two

geomorphologically contrasting proglacial zones is studied. The differences in sediment availability and sediment supply to the two sites within the proglacial area of the Feegletscher Nord showed that a major control on the interpretation of SSC and discharge results is the location of the monitoring stations within the proglacial forefield. As suggest by Orwin and Smart (2004a), the location and number of monitoring stations will depend on the aim of the research, and only one monitoring station is needed to establish the sediment transfer from a glaciated catchment. However, multiple monitoring stations across the whole extent of the proglacial area are required to gain a full understanding of sediment transfer relationships within the catchment and enable data extrapolation to suggest future glacio-fluvial sedimentary responses to progressive alpine retreat and deglaciation (Orwin & Smart, 2004a). The spatial and temporal differences between the Feegletscher Nord and Süd make it clear that multiple monitoring stations are especially important when multiple proglacial zones are compared, particularly if the proglacial zones have contrasting geomorphological and or paraglacial history.

### 7.3 Future Deglaciation

Temperate alpine glaciers are particularly sensitive to climate change (Huss *et al.*, 2010), and as deglaciation continues under the current climate projections for Switzerland (CH2018, 2018), the overall sediment delivery within a deglaciating basin is likely to peak immediately following deglaciation, followed by slow, uni-directional decline as surface sediments stabilise (e.g. Ballantyne, 2002a; Porter *et al.*, 2018). Centuries after deglaciation has occurred the quantity of glaciogenic sediment reaches its maximum value during the paraglacial period that has been described by various studies (e.g. Church & Ryder, 1972; Mercier, 2008; Mercier & Étienne, 2008). As climate warming continues to increase and increase the rapidity of overall ice retreat and thinning, the duration of the ablation season of glaciers is set to increase with an earlier melting of accumulated snow over in the ablation seasons and a short term increase in the magnitude of proglacial meltwater discharge is forecast (Finger *et al.*, 2012; Mao *et al.*, 2014). The likelihood of longer and warmer glacier ablation seasons will result in enhancing the geomorphological activity, sediment transfer within deglaciating catchments, and the overall delivery of sediment to the proglacial river, however, as the glacier volume reduces over time there will be a reduction in the magnitude of proglacial meltwater discharge which could consequently

reduce the transportation of sediment (e.g. Barnett *et al.*, 2005; Farinotti *et al.*, 2009). The overall availability of sediment for mobilisation is uncertain, as sediment may either become stored within the proglacial forefield, transferred down-catchment via the proglacial stream, or conditioned to become consolidated, vegetated, stabilised, and immobile. Exhaustion of the available sediment supply will occur unless large amounts of sediments are stored within the proglacial catchment. Stochastic delivery of unstable, unconsolidated, and easily mobilised glaciogenic sediment into proglacial streams that are not related to rises and falls in meltwater discharge but are caused by mechanisms such as channel bank collapse initially increase with progressive deglaciation. The stochastic delivery of sediment will initially increase with deglaciation as the proglacial area increases in size and the proglacial stream lengthens, however, stochastic sediment delivery will reduce as vegetation stabilises sediment, the availability of sediment reduces and the magnitude of meltwater discharge reduces. Studies performed within Arctic glaciated catchments showed this to be a possibility due to likely increases in geomorphological paraglacial activity and the overall availability of glaciogenic sediment (e.g. Mercier, 2000; Porter *et al.*, 2010). Therefore, further deglaciation will result in additional variations of sediment availability and supply, and the mechanisms of sediment remobilisation, reworking, and transportation within deglaciating catchments that could be exposed by a transformation in the principal daily hysteretic pattern. Long term studies are required in deglaciating basins to fully determine the subsequence response to hydrological climatic changes (Mao *et al.*, 2014).

#### 7.4 Future Research

Through the performance of this research additional areas for future research to improve and provide further insight into spatial and temporal patterns of glacio-fluvial sedimentation at the Feegletscher and other retreating Alpine glaciers have come to light. In order to get a full understanding of catchment-wide glacio-fluvial sedimentation it is evident that a fully integrated study is needed that incorporates meteorological inputs, in particular, precipitation and glacier surface radiation, as well as inputs, throughputs, and outputs of glacier meltwater and sediment.

In order to get accurate controls and characteristics of meltwater throughput within the glacial hydrological network, it is important to further examine meltwater storage and assess development throughout the ablation season. This will further enable the assessment

of subglacial sediment availability, entrainment, and evacuation, and can be used during the creation of glacier runoff models (e.g. Jansson *et al.*, 2003). The determination of meltwater throughput is especially important given the predicted changes to climate and the sensitivity of temperate alpine glaciers to these changes (Huss *et al.*, 2010). Increased ablation rates during deglaciation have the ability to increase meltwater storage and release through glaciers.

A large portion of suspended sediment originates subglacially, an enhanced understanding of sedimentation in Feegletscher's catchment requires more detailed characterisation of subglacial erosion and sub- and englacial hydrological features. Ground-penetrating radar or similar bathymetric type survey would be a useful technique that would enable ice volume, meltwater water storage and transfer within the hydrological network, the hydrological networks themselves to be assessed (e.g. Urbini & Baskaradas, 2010; Urbini *et al.*, 2017).

As discussed in a previous section, a key control on the interpretation of meltwater discharge and SSC is the location of the monitoring stations within the proglacial forefield. However, the relative importance of multiple monitoring stations becomes even greater when geomorphologically contrasting proglacial zones are studied and compared. The geomorphological history of each proglacial zone needs to be taken into consideration when the locations of monitoring stations are chosen to get a full understanding of sediment transfer. For example, to get a better understanding of sediment transport within the proglacial area of the Feegletscher Süd a minimum of three monitoring station should be used, with one located near to the glacier terminus, another located at the end of the bare bedrock section, and another at the end of the Little Ice Age moraine. In addition, to get a full understanding of glacio-fluvial sedimentation within a catchment it is important that a long term study is undertaken, as glacio-fluvial sedimentation can be sensitive to precipitation (e.g. Iida *et al.*, 2012), the climate during the ablation season (e.g. Gao & Josefson, 2012), and high magnitude events (e.g. Schiefer *et al.*, 2010). Long term studies are especially important to predict glacio-fluvial sedimentation responses to future glacier retreat.

## 8 Conclusion

Investigation of the fluvio-glacial characteristics and patterns of sediment transfer showed that there was variability between the two study sites along the Feegletscher Nord's proglacial stream, and between the Feegletscher Nord's and Süd's proglacial stream. However, the study demonstrated that during the monitoring period there was no major adjustment to the subglacial hydrological system or sediment transfer patterns. The Feegletscher Süd's proglacial river responded approximately 60 minutes slower to estimated melt compared to the Feegletscher Nord's proglacial river. Discharge data revealed that the relative drainage distribution from each outlet is estimated at 76.58 % from the South outlet and 23.42 % from the North outlet, with the Feegletscher Nord's proglacial river showing a discharge split of 37.89 % at the Upper North site and 62.11 % at the Lower North site. The differences in discharge between the two sites on the Feegletscher Nord's proglacial river have been attributed to lateral stream contributions from both glacial and non-glacial sources.

During the monitoring period, relative SSF between each proglacial river was 53.34 % for the Feegletscher Nord and 46.66 % from the Feegletscher Süd. The Feegletscher Nord showed that 86.85 % of entrained sediment was deposited within the proglacial channel between the Upper North site the Lower North River site. Clockwise and anti-clockwise hysteresis was observed at all monitoring sites, with the Feegletscher Süd showing an overall clockwise hysteresis, the upper monitoring site on the Feegletscher Nord showing anti-clockwise hysteresis, and the lower monitoring site on the Feegletscher Nord showing equal amounts of clockwise and anti-clockwise. The differences in observed hysteresis between the three locations is attributed to sediment exhaustion, and the overall availability and stability of fine grained sediment within each proglacial area which is controlled by variations in sedimentary and geomorphological characteristics.

To the best of this investigation's knowledge, this is the first study to identify short-term intra-basin spatial and temporal patterns of glacio-fluvial sedimentation of two geomorphologically contrasting proglacial zones. The study has made it clear that even within a relatively small catchment there are a range of spatial and temporal patterns of glacio-fluvial sedimentation, and a major control on determining these patterns is the location and quantity of the monitoring stations within the proglacial forefield. The added

complexity of studying geomorphologically contrasting proglacial zones shows how important it is to consider the geomorphological history of the proglacial zone when identifying the location and quantity of monitoring stations.

Climate change is predicted to impact future glacio-fluvial sedimentation (e.g. Bogen, 2008; Delaney & Adhikari, 2020). Progressive retreat and deglaciation is likely to increase paraglacial activity which is expected to increase suspended SSC and overall sediment fluxes within the Feegletscher's catchment. However, as progressive deglaciation continues, and the overall ice volume of the Feegletscher Nord and Süd reduces there will likely be a decrease in subglacial erosion, but a continuation of sediment removal and forefield sediment stabilisation. Enhanced stability and transportation of the forefield glaciogenic sediments may lead to exhaustion of sediment within deglaciating catchment environments after more than 2.3 ka (Ballantyne, 2002a). This study only assessed short term patterns of glacio-fluvial sedimentation, however, long-term fully integrated studies are required to get a full understanding on the fluvio-glacial characteristics, and the spatial and temporal patterns of sediment transfer within a glaciated catchment. A fully integrated catchment-wide study needs to encompass meteorological inputs to catchment, as well as inflow, through-flow, and outflow of glacier meltwater and sediment. This will enable data to be extrapolated and suggest future changes to SSC and fluxes, sediment transportation mechanism, and to acquire a full understanding of the impacts caused by future deglaciation.

### Reference List

Alcamo, J., Flörke, M., & Märker, M. (2007). Future long-term changes in global water resources driven by socio-economic and climatic changes. *Hydrological Sciences Journal*, 52(2), 247-275.

Allen, J. R. L. (1982). *Sedimentary Structures: Their Character and Physical Basis*. Developments in Sedimentology, Elsevier, Amsterdam.

Allen, J. R. L. (1985). *Principles of Physical Sedimentology*. Allen and Unwin, London.

Alley, R. B., Blankenship, D. D., Bentley, C. R. & Rooney, S. T. (1987). Till beneath Ice Stream B 3. Till deformation: evidence and implications. *Journal of Geophysical Research*, 92, 8921-8929.

Alley, R. B. (1992). How can low-pressure channels and deforming tills coexist subglacially? *Journal of Glaciology*, 38(128), 200-207.

Alley, R. B., Cuffey, K. M., Evenson, E. B., Strasser, J. C., Lawson, D. E., & Larson, G. J. (1997). How glaciers entrain and transport basal sediment: physical constraints. *Quaternary Science Reviews*, 16(9), 1017-1038.

Alley, R. B. (2000). Continuity comes first: recent progress in understanding subglacial deformation. In Maltman, A. J., Hubbard, B. and Hambrey, M. J. (eds), *Deformation of Glacial Materials*. Geological Society, London, Special Publication, 176, 171-9.

Anderson, S. P., Fernald, K. T., Anderson, R. L., & Humphrey, N. F. (1999). Physical and chemical characterization of a spring flood event, Bench Glacier, Alaska, USA: evidence for water storage. *Journal of Glaciology*, 45(150), 177-189.

Andrews, L. C., Hoffman, M. J., Neumann, T. A., Catania, G. A., Lüthi, M. P., Hawley, R. L., Schild, K. M., Ryser, C., Morriss, B. F., & Los Alamos National Lab. (LANL), Los Alamos, NM (United States). (2018). Seasonal evolution of the subglacial hydrologic system modified by supraglacial lake drainage in western greenland. *Journal of Geophysical Research. Earth Surface*, 123(6), 1479-1496.

Aschwanden, A. (2016). Thermodynamics of Glaciers. *University of Alaska Fairbanks, USA*.

Ashworth, P. J. & Ferguson, R. I. (1986). Interrelationships of channel processes, changes and sediments in a proglacial river. *Geografiska Annaler*, 68A, 361-71.

Bača, P. (2008). Hysteresis effect in suspended sediment concentration in the Rybárik basin, Slovakia. *Hydrological Science Journal*, 53, 224-235.

Ballantyne, C. K. (2002a). A general model of paraglacial landscape response. *The Holocene*, 12(3), 371-376.

- Ballantyne, C. K. (2002b). Paraglacial geomorphology. *Quaternary Science Reviews*, 21(18), 1935-2017.
- Barnett, T. P., Adam, J. C. & Lettenmeier, D. P. (2005). Potential impacts of a warming climate on water availability in snow dominated regions. *Nature*, 438, 303-309.
- Bartholomew, I., Nienow, P., Mair, D., Hubbard, A., King, M. A., & Sole, A. (2010). Seasonal evolution of subglacial drainage and acceleration in a Greenland outlet glacier. *Nature Geoscience*, 3(6), 408-411.
- Bartholomew, I., Nienow, P., Sole, A., Mair, D., Cowton, T., & King, M. A. (2012). Short-term variability in Greenland Ice Sheet motion forced by time-varying meltwater drainage: Implications for the relationship between subglacial drainage system behaviour and ice velocity. *Journal of Geophysical Research Atmospheres*, 117, 1-17.
- Bauder, A., Funk, M., & Huss, M. (2007). Ice-volume changes of selected glaciers in the Swiss Alps since the end of the 19th century. *Annals of Glaciology*, 46(1), 145-149.
- Beaud, F., Venditti, J. G., Flowers, G. E., & Koppes, M. (2018). Excavation of subglacial bedrock channels by seasonal meltwater flow. *Earth Surface Processes and Landforms*, 43(9), 1960-1972.
- Benn, D., & Evans, D. J. (2010). *Glaciers and glaciation* (2nd ed.). London: Hodder Education.
- Bircher W. 1982. Zur Gletscher- und Klimageschichte des Saastales. Glazialmorphologische und dendroklimatologische Untersuchungen. *Physische Geographie*, 9, Geographisches Institut der Universität: Zürich.
- Björnsson, H., Pálsson, F., Sigurðsson, O., & Flowers, G. E. (2003). Surges of glaciers in Iceland. *Annals of Glaciology*, 36(1), 82-90.
- Blatter, H., & Hutter, K. (1991). Polythermal conditions in Arctic glaciers, *J. Glaciol.*, 37(126), 261-269.
- Bogen, J. (1995). Sediment transport and deposition in mountain rivers. Sediment and water quality in river catchments, edited by I. D. L. Foster, A. M. Gurnell and B. W. Webb. John Wiley & Sons, Chichester, 437-451.

- Bogen, J. (1996). Erosion rates and sediment yields of glaciers. *Annals of Glaciology*, 22, 48-52.
- Bogen, J., & Bønsnes, T. E. (2003). Erosion and sediment transport in High Arctic rivers, Svalbard. *Polar Research*, 22(2), 175-189.
- Bogen J. 2008. The impact of climate change on glacial sediment delivery to rivers. In *Sediment Dynamics in Changing Environments*, J Schmidt et al. (eds). IAHS Publication 325. IAHS Press: Wallingford; 432– 439.
- Bond, T. C., & Bergstrom. (2006). Light absorption by carbonaceous particles: An investigative review. *Aerosol Sci. Technology*, 40, 27-67.
- Boulton, G. S. (1979). Processes of glacier erosion on different substrata. *Journal of glaciology*, 23, 15-38.
- Boulton, G. S. & Eyles, N. (1979). Sedimentation by valley glaciers: a model and genetic classification. In Schluchter, C. (ed.), *Moraines and Varves*. Balkema, Rotterdam, 11-23.
- Boulton, G. S. (1982). Processes and patterns of glacial erosion. In: Coates D. R. (eds) *Glacial Geomorphology*. Springer, Dordrecht.
- Boulton, G. S., & Hindmarsh, R. C. A. (1987). Sediment deformation beneath glaciers: rheology and geological consequences. *Journal of Geophysical Research: Solid Earth (1978–2012)*, 92(B9), 9059-9082.
- Bousquet, R., Goffé, B., Vidal, O., Oberhänsli, R., & Patriat, M. (2002). The tectonometamorphic history of the Valaisan domain from the Western to the Central Alps: New constraints on the evolution of the Alps. *Geological Society of America Bulletin*, 114(2), 207-225.
- Brown, G. H., Tranter, M. & Sharp, M. J. (1996). Experimental investigations of the weathering of suspended sediment by Alpine glacial meltwaters. *Hydrological Processes*, 10, 579-597.
- Buoncristiani, J.-F. & Campy, M. (2001). Late Pleistocene Detrital Sediment Yield of the Jura Glacier, France. *Quaternary Research*, 56, 51-61.

Carrivick, J. L., Geilhausen, M., Warburton, J., Dickson, N. E., Carver, S. J., Evans, A. J., & Brown, L. E. (2013). Contemporary geomorphological activity throughout the proglacial area of an alpine catchment. *Geomorphology*, 188, 83-95.

Carrivick, J. L., & Tweed, F. S. (2013). Proglacial lakes: character, behaviour and geological importance. *Quaternary Science Reviews*, 78, 34-52.

Carrivick, J. L., & Heckmann, T. (2017). Short-term geomorphological evolution of proglacial systems. *Geomorphology*, 287, 3–28.

Cess, R. D., Potter, G. L., Zhang, M. H., Blanchet, J.P., Chalita, S., *et al.* (1991). Interpretation of snow-climate feedback as produced by 17 general-circulation models. *Science*, 253, 888 – 892.

Church, M., & Ryder, J. M. (1972). Paraglacial sedimentation: a consideration of fluvial processes conditioned by glaciation. *Geological Society of America Bulletin*, 83(10), 3059-3072.

Chy'lek, P., Ramaswamy, V., & Srivastava, V. (1983). Albedo of soot-contaminated snow. *Journal of Geophysical Research*, 88, 837 – 843.

CH2018. (2018). Swiss Climate Change Scenarios CH2018. C2SM, MeteoSwiss, ETH, NCCR Climate, and OcCC. Zurich, Switzerland, ISBN: 978-3-952031-3-3.

Clarke, G. K. (1987). Subglacial till: a physical framework for its properties and processes. *Journal of Geophysical Research: Solid Earth (1978–2012)*, 92(B9), 9023-9036.

Cofaigh, C. Ó., Evans, J., Dowdeswell, J. A., & Larter, R. D. (2007). Till characteristics, genesis and transport beneath antarctic paleo-ice streams. *Journal of Geophysical Research - Earth Surface*, 112(F3), 1-16.

Colgan, W., Rajaram, H., Anderson, R., Steffen, K., Phillips, T., Joughin, I., Jay Zwally, H., & Abdalati, W. (2011). The annual glaciohydrology cycle in the ablation zone of the greenland ice sheet: Part 1. hydrology model. *Journal of Glaciology*, 57(204), 697-709.

Collins, D. N. (1979). Meltwater characteristics as indicators of the hydrology of Alpine glaciers. Doctoral thesis, University of Nottingham, Nottingham.

Collins, D. N. (1979). Hydrochemistry of meltwaters draining from an alpine glacier. *Arctic and Alpine Research*, 11(3), 307-324.

Collins, D. N. (1979). Quantitative determination of the subglacial hydrology of two Alpine glaciers. *Journal of Glaciology*, 23, 347-362.

Collins, D. N. (1979). Sediment concentration in melt waters as an indicator of erosion processes beneath an Alpine glacier. *Journal of Glaciology*, 23, 247-257.

Collins, D. N. (1989). Hydrometeorological Conditions, Mass Balance and Runoff from Alpine Glaciers. In: Oerlemans, J. (ed.) Glacier fluctuations and climatic change. *Glaciology and Quaternary Geology*, vol 6. Springer, Dordrecht, pp. 235-260.

Collins, D. N. (1990). Seasonal and annual variations of suspended sediment transport in meltwaters draining from an Alpine glacier. *Hydrology in Mountainous Regions I: Hydrological Measurements; the Water Cycle*, 439-446.

Collins, D. N. (1995). Dissolution kinetics, transit times through subglacial hydrological pathways and diurnal variations of solute content of meltwater drainage from an alpine glacier. *Hydrological Processes*, 9, 897-910.

Collins, D. N. (1998). Suspended sediment flux in meltwaters draining from Batura glacier as an indicator of the rate of glacial erosion in the Karakoram mountains. *Journal of Quaternary Science*, 13(6), 1-10.

Collins, D. N. (2008). Climatic warming, glacier recession and runoff from Alpine basins after the Little Ice Age maximum. *Annals of Glaciology*, 48(1), 119-124.

Cook, S. J., Porter, P. R., & Bendall, C. A. (2013). Geomorphological consequences of a glacier advance across a paraglacial rock avalanche deposit. *Geomorphology*, 189, 109-120.

Cossart, E., & Fort, M. (2008). Sediment release and storage in early deglaciated areas: Towards an application of the exhaustion model from the case of massif des écrivains (french alps) since the little ice age. *Norsk Geografisk Tidsskrift*, 62(2), 115-131.

Covington, M. D., Banwell, A. F., Gulley, J., Saar, M. O., Willis, I., & Wicks, C. M. (2012). Quantifying the effects of glacier conduit geometry and recharge on proglacial hydrograph form. *Journal of Hydrology*, 414, 59-71.

Curry, A. M., Cleasby, V. & Zukowskyj, P. (2006). Paraglacial response of steep, sediment-mantled slopes to post-'Little Ice Age' glacier recession in the central Swiss Alps. *Journal of Quaternary Science*, 21, 211-225.

Curry, A. M., Sands, T. B., & Porter, P. R. (2009). Geotechnical controls on a steep lateral moraine undergoing paraglacial slope adjustment. *Geological Society, London, Special Publications*, 320(1), 181-197.

Delaney, I., Bauder, A., Huss, M., & Weidmann, Y. (2018a). Proglacial erosion rates and processes in a glacierized catchment in the swiss alps. *Earth Surface Processes and Landforms*, 43(4), 765-778.

Delaney, I., Bauder, A., Werder, M. A., & Farinotti, D. (2018b). Regional and annual variability in subglacial sediment transport by water for two glaciers in the swiss alps. *Frontiers in Earth Science*, 6, 1-17.

Delaney, I., & Adhikari, S. (2020). Increased subglacial sediment discharge in a warming climate: Consideration of ice dynamics, glacial erosion, and fluvial sediment transport. *Geophysical Research Letters*, 47(7), 1-11.

Driedger, C. L., & Fountain, A. G. (1989). Glacier outburst floods at Mount Rainier, Washington State, USA. *Annals of Glaciology*, 13, 51-55.

Etzelmüller, B., Ødegård, R. S., Vatne, G., Mysterud, R. S., Tønning, T., & Sollid, J. L. (2000). Glacier characteristics and sediment transfer system of Longyearbreen and Larsbreen, western Spitsbergen. *Norsk Geografisk Tidsskrift*, 54(4), 157- 168.

Evans, M. (1997). Temporal and spatial representativeness of alpine sediment yields: Cascade Mountains, British Columbia. *Earth Surface Processes and Landforms*, 22(3), 287-295.

Evans, D. J. A., Phillips, E. R., Hiemstra, J. F., & Auton, C. A. (2006). Subglacial till: formation, sedimentary characteristics and classification. *Earth-Science Reviews*, 78(1), 115-176.

Farinotti, D., Huss, M., Bauder, A., & Funk, M. (2009). An estimate of the glacier ice volume in the Swiss Alps. *Global and Planetary Change*, 68(3), 225-231.

Farinotti, D. (2010). Simple methods for inferring glacier ice-thickness and snow accumulation distribution. Doctoral thesis, *Eidgenössische Technische Hochschule (ETH) Zürich*.

Farinotti, D., Usselman, S., Huss, M., Bauder, A., & Funk, M. (2012). Runoff evolution in the Swiss Alps: projections for selected high-alpine catchments based on ENSEMBLES scenarios. *Hydrological Processes*, 26(13), 1909-1924.

Fausto, R. S., Mernild, S. H., Hasholt, B., Ahlstrøm, A. P., & Knudsen, N. T. (2012). Modeling suspended sediment concentration and transport, mittivakkat glacier, southeast greenland. *Arctic, Antarctic, and Alpine Research*, 44(3), 306-318.

Federal Office of Meteorology and Climatology MeteoSwiss (FOMCMS). (2018). the Climate of Switzerland. *Federal Office: MeoteoSwiss*. Retrieved April, 4, 2018, from <http://www.meteoswiss.admin.ch/home/climate/the-climate-of-switzerland.html>.

Fenn, C. R., Gurnell, A. M., & Beecroft, I. R. (1985). An evaluation of the use of suspended sediment rating curves for the prediction of suspended sediment concentration in a proglacial stream. *Geografiska Annaler. Series A. Physical Geography*, 71-82.

Fenn, C. R. (1987). Sediment transfer processes in Alpine glacier basins. *Glacio-Fluvial Sediment Transfer: An Alpine Perspective*. John Wiley and Sons, New York. 1987. p 59-85.

Fenn, C. R. (1989). Quantifying the errors involved in transferring suspended sediment rating equations across ablation seasons. *Annals of Glaciology*, 13, 64-68.

Fenn, C. R., & Gomez, B. (1989). Particle size analysis of the sediment suspended in a proglacial stream: Glacier de Tsidjiore Nouve, Switzerland. *Hydrological Processes*, 3(2), 123-135.

Finger, D., Heinrich, G., Gobiet, A., & Bauder, A. (2012). Projections of future water resources and their uncertainty in a glacierized catchment in the Swiss Alps and the subsequent effects on hydropower production during the 21st century. *Water Resources Research*, 48, 1-20.

Fitzsimons, S. J., & Veit, H. (2001). Geology and geomorphology of the European Alps and the Southern Alps of New Zealand: A comparison. *Mountain Research and Development*, 21(4), 340-349.

Flowers, G. E. & Clarke, G. K. C. (2000). An integrated modelling approach to understanding subglacial hydraulic release events. *Annals of Glaciology*, 31, 222-8.

Flowers, G. E., & Clarke, G. K. (2002). A multicomponent coupled model of glacier hydrology 2. Application to Trapridge Glacier, Yukon, Canada. *Journal of Geophysical Research: Solid Earth* (1978–2012), 107(B11), ECV-10.

Flowers, G. E. (2008). Subglacial modulation of the hydrograph from glacierized basins. *Hydrological Processes*, 22(19), 3903-3918.

Forbes, A. C., & Lamoureux, S. F. (2005). Climatic controls on streamflow and suspended sediment transport in three large middle arctic catchments, Boothia Peninsula, Nunavut, Canada. *Arctic, Antarctic, and Alpine Research*, 37(3), 304-315.

Fountain, A. G. & Walder, J. S. (1998). Water flow through temperate glaciers. *Reviews of Geophysics*, 36 (3), 299-328.

Fountain, A. G., Jacobel, R. W., Schlichting, R., & Jansson, P. (2005). Fractures as the main pathways of water flow in temperate glaciers. *Nature*, 433(7026), 618-621.

Fowler, A. C., & Larson, D. A. (1978). On the flow of polythermal glaciers: I. Model and preliminary analysis, *Proc. R. Soc. London, Ser. A*, 363, 217–242.

Fugazza, D. (2019). All eyes on glaciers: Remote sensing of the cryosphere. Università degli Studi di Milano. [https://doi.org/10.13130/fugazza-davide\\_phd2019-02-0](https://doi.org/10.13130/fugazza-davide_phd2019-02-0).

Gao, W., Gao, S., Li, Z., Lu, X., Zhang, M., & Wang, S. (2013). Suspended sediment and total dissolved solid yield patterns at the headwaters of Urumqi River, northwestern China:

a comparison between glacial and non-glacial catchments. *Hydrological Processes*, 28, 5034–5047.

Geilhausen, M., Morche, D., Otto, J. C., Schrott, L. (2013). Sediment discharge from the proglacial zone of a retreating Alpine glacier. *Zeitschrift für Geomorphologie*, 57 (3), 29-53.

Gilbert, A., Vincent, C., Wagnon, P., Thibert, E., & Rabatel, A. (2012). The influence of snow cover thickness on the thermal regime of tête rousse glacier (mont blanc range, 3200 m a.s.l.): Consequences for outburst flood hazards and glacier response to climate change. *Journal of Geophysical Research: Earth Surface*, 117(F4), 1-17.

Gimbert, F., Tsai, V. C., Amundson, J. M., Bartholomaeus, T. C., & Walter, J. I. (2016). Subseasonal changes observed in subglacial channel pressure, size, and sediment transport. *Geophysical Research Letters*, 43(8), 3786-3794.

Gindraux, S., Boesch, R., & Farinotti, D. (2017). Accuracy assessment of digital surface models from unmanned aerial vehicles' imagery on glaciers. *Remote Sensing*, 9(2), 186.

Gao, P., & Josefson, M. (2012). Event-based suspended sediment dynamics in a central new york watershed. *Geomorphology*, 139, 425-437.

Grove, J.M. (2004). Little ice ages: ancient and modern. 2nd edition. Routledge, London and New York, 2 vols. <http://doi.org/10.4324/9780203770245>.

Guillon, H., Mugnier, J., & Buoncristiani, J. (2018). Proglacial sediment dynamics from daily to seasonal scales in a glaciated alpine catchment (bossons glacier, mont blanc massif, france). *Earth Surface Processes and Landforms*, 43(7), 1478-1495.

Gulley, J. D., Benn, D. I., Screaton, E., & Martin, J. (2009). Mechanisms of englacial conduit formation and their implications for subglacial recharge. *Quaternary Science Reviews*, 28(19), 1984-1999.

Gulley, J. D., Walthard, P., Martin, J., Banwell, A. F., Benn, D. I., & Catania, G. (2012a). Conduit roughness and dye-trace breakthrough curves: why slow velocity and high dispersivity may not reflect flow in distributed systems. *Journal of Glaciology*, 58(211), 915-925.

Gulley, J. D., Grabiec, M., Martin, J. B., Jania, J., Catania, G., & Glowacki, P. (2012b). The effect of discrete recharge by moulins and heterogeneity in flow-path efficiency at glacier beds on subglacial hydrology. *Journal of Glaciology*, 58(211), 926-940.

Gurnell, A. M. (1982). The dynamics of suspended sediment concentration in an Alpine proglacial stream network. *Hydrological Aspects of Alpine and High Mountain Areas*, 319-330.

Gurnell, A. M., & Fenn, C. R. (1984). Box-Jenkins transfer function models applied to suspended sediment concentration-discharge relationships in a proglacial stream. *Arctic and Alpine Research*, 16(1), 93-106.

Gurnell, A. M. (1987). *Glacio-Fluvial Sediment Transfer: An Alpine Perspective*. Chichester: Wiley.

Gurnell, A. M., & Warburton, J. (1990). The significance of suspended sediment pulses for estimating suspended sediment load and identifying suspended sediment sources in Alpine glacier basins. *Hydrology of Mountainous Regions*, 1, 463- 470.

Gurnell, A. M., Clark, M. J., Hill, C. T., Greenhalgh, J., Bogen, J., Walling, D. E., & Day, T. (1992). Reliability and representativeness of a suspended sediment concentration monitoring programme for a remote alpine proglacial river. In *Erosion and Sediment Transport Monitoring in River Basins, Proceedings of the Oslo Symposium*, 24, p28. Wallingford, Oxfordshire, UK: IAHS Press.

Gurnell, A. M. (1995). *Sediment yield from alpine glacier basins*. Chichester: Wiley.

Haas, F., Heckmann, T., Wichmann, V., & Becht, M. (2011). Quantification and modeling of fluvial bedload discharge from hillslope channels in two alpine catchments (Bavarian Alps, Germany). *Zeitschrift für Geomorphologie*, 55 (3), 147-168.

Haerberli, W., & Beniston, M. (1998). Climate change and its impacts on glaciers and permafrost in the Alps. *Ambio*, 258-265.

Hagen, J. O. (1987). Glacier surge at Usherbreen, Svalbard. *Polar Research*, 5 (2), 239-252

Haldorsen, S. (1981). Grain-size distribution of subglacial till and its relation to glacial crushing and abrasion. *Boreas*, 10(1), 91-105.

Hallet, B., Hunter, L., & Bogen, J. (1996). Rates of erosion and sediment evacuation by glaciers: A review of field data and their implications. *Global and Planetary Change*, 12(1), 213-235.

Hambrey, M. J., Huddart, D., Bennett, M. R., & Glasser, N. F. (1997). Genesis of 'hummocky moraines' by thrusting in glacier ice: evidence from Svalbard and Britain. *Journal of the Geological Society*, 154(4), 623-632.

Hambrey, M. J., Bennett, M. R., Dowdeswell, J. A., Glasser, N. F., & Huddart, D. (1999). Debris entrainment and transfer in polythermal valley glaciers. *Journal of Glaciology*, 45(149), 69-86.

Hammer, K. M., & Smith, N. D. (1983). Sediment production and transport in a proglacial stream: Hilda Glacier, Alberta, Canada. *Boreas*, 12(2), 91-106.

Hamshaw, S. D., Dewoolkar, M. M., Schroth, A. W., Wemple, B. C., & Rizzo, D. M. (2018). A new Machine-Learning approach for classifying hysteresis in Suspended-Sediment discharge relationships using High-Frequency monitoring data. *Water Resources Research*, 54(6), 4040-4058.

Hannah, D. M., & Gurnell, A. M. (2001). A conceptual, linear reservoir runoff model to investigate melt season changes in cirque glacier hydrology. *Journal of Hydrology*, 246(1), 123-141.

Haritashya, U. K., Singh, P., Kumar, N., & Gupta, R. P. (2006). Suspended sediment from the Gangotri Glacier: Quantification, variability and associations with discharge and air temperature. *Journal of Hydrology*, 321(1), 116-130.

Hasnain, S. I. (1996). Factors controlling suspended sediment transport in Himalayan glacier meltwaters. *Journal of hydrology*, 181(1), 49-62.

Hasnain, S. I. (1999). Runoff characteristics of a glacierised catchment, Garhwal Himalaya, India. *Hydrological Sciences*, 44, 847-54.

Hasnain, S. I. & Thayyen, R. J. (1999). Discharge and suspended sediment concentration of meltwaters draining from the Dokriani glacier, Garhwal Himalaya, India. *Journal of Hydrology*, 218, 191-8.

Hewitt, I. J. (2013). Seasonal changes in ice sheet motion due to melt water lubrication. *Earth Planetary Science Letters*, 371–372, 16–25.

Hock, R & Hooke, R. (1993). Evolution of the internal drainage system in the lower part of the ablation area of Storglaciären, Sweden. *Geological Society of America Bulletin*, 105, 537-546.

Hock, R., & Jansson, P. (2005). Modeling glacier hydrology. Wiley: *Encyclopedia of hydrological sciences*.

Hodgkins, R. (1999). Controls on suspended-sediment transfer at a High-Arctic glacier, determined from statistical modelling. *Earth Surface Processes and Landforms*, 24(1), 1-21.

Hodgkins, R., Cooper, R., Wadham, J., & Tranter, M. (2003). Suspended sediment fluxes in a high-Arctic glacierised catchment: implications for fluvial sediment storage. *Sedimentary Geology*, 162(1), 105-117.

Hodson, A. J., Tranter, M., Dowdeswell, J. A., Gurnell, A. M. & Hagen, J. O. (1997). Glacier thermal regime and suspended sediment yield: a comparison of two high arctic glaciers. *Annals of Glaciology*, 24, 32-7.

Hodson, A., Gurnell, A., Tranter, M., Bogen, J., Hagen, J. O., & Clark, M. (1998). Suspended sediment yield and transfer processes in a small High-Arctic glacier basin, Svalbard. *Hydrological Processes*, 12(1), 73-86.

Hodson, A. J., & Ferguson, R. I. (1999). Fluvial suspended sediment transport from cold and warm-based glaciers in Svalbard. *Earth Surface Processes and Landforms*, 24(11), 957-974.

Hoffman, M., & Price, S. (2014). Feedbacks between coupled subglacial hydrology and glacier dynamics. *Journal of Geophysical Research. Earth Surface*, 119(3), 414-436.

Hooke, R. L. (1984). On the role of mechanical energy in maintaining subglacial water conduits at atmospheric pressure. *Journal of Glaciology*, 30(105), 180-187.

Hooke, R. Le B., Laumann, T. & Kohler, J. (1990). Subglacial water pressures and the shape of subglacial conduits. *Journal of Glaciology*, 36, 67-71.

Hooke, R. Le B. & Elverhøi, E. (1996). Sediment flux from a fjord during glacial periods, Isfjorden, Spitsbergen. *Global and Planetary Change*, 12, 237-49.

Hubbard, B. & Sharp, M. J. (1993). Weertman regelation, multiple refreezing effects and the isotopic evolution of the basal ice layer. *Journal of Glaciology*, 39, 275-91.

Hubbard, B. P., Sharp, M. J., Willis, I. C., Nielsen, M. T., & Smart, C. C. (1995). Borehole water-level variations and the structure of the subglacial hydrological system of Haut Glacier d'Arolla, Valais, Switzerland. *Journal of Glaciology*, 41(139), 572-583.

Hubbard, B., & Nienow, P. (1997). Alpine subglacial hydrology. *Quaternary Science Reviews*, 16(9), 939-955.

Huss, M., Zemp, M., Joerg, P. C., & Salzmann, N. (2014). High uncertainty in 21st century runoff projections from glacierized basins. *Journal of Hydrology*, 510, 35-48.

Iida, T., Kajihara, A., Okubo, H., & Okajima, K. (2012). Effect of seasonal snow cover on suspended sediment runoff in a mountainous catchment. *Journal of Hydrology*, 428-429, 116-128.

Irvine-Fynn, T. D. L., Moorman, B. J., Willis, I. C., Sjogren, D. B., Hodson, A. J., Mumford, P. N., & Williams, J. L. M. (2005). Geocryological processes linked to High Arctic proglacial stream suspended sediment dynamics: examples from Bylot Island, Nunavut, and Spitsbergen, Svalbard. *Hydrological Processes*, 19(1), 115-135.

Irvine-Fynn, T. D. L., Hodson, A. J., Moorman, B. J., Vatne, G., & Hubbard, A. L. (2011). polythermal glacier hydrology: A review. *Reviews of Geophysics*, 49(4), 1-37.

Ivy-Ochs, S., Kerschner, H., Reuther, A., Preusser, F., Heine, K., et al. (2008). Chronology of the last glacial cycle in the European Alps. *Journal of Quaternary Science*, 23(6-7), 559-573.

Iverson, N. R., Hanson, B., Hooke, R. L., & Jansson, P. (1995). Flow mechanism of glaciers on soft beds. *Science*, 267(5194), 80.

Iverson, N. R., Helanow, C., & Zoet, L. K. (2019). Debris-bed friction during glacier sliding with ice–bed separation. *Annals of Glaciology*, 60(80), 30-36.

Jansson, P., Hock, R., & Schneider, T. (2003). The concept of glacier storage: a review. *Journal of Hydrology*, 282(1), 116-129.

Joerin, U. E., Stocker, T. F., & Schlüchter, C. (2006). Multicentury glacier fluctuations in the swiss alps during the holocene. *The Holocene*, 16(5), 697-704.

Joshi, R., Kumar, K., & Adhikari, V. P. S. (2016). Modelling suspended sediment concentration using artificial neural networks for gangotri glacier. *Hydrological Processes*, 30(9), 1354-1366.

Jouvet, G., Weidmann, Y., Seguinot, J., Funk, M., Abe, T., Sakakibara, D., . . . Sugiyama, S. (2017). Initiation of a major calving event on the bowdoin glacier captured by UAV photogrammetry. *The Cryosphere*, 11(2), 911-921.

Juen, I., Kaser, G. & Georges, C. (2007). Modelling observed and future runoff from a glacierised tropical catchment (Cordillera Blanca, Peru). *Global and Planetary Change*, 50, 37-48.

Kamb, B. (1987). Glacier surge mechanism based on linked cavity configuration of the basal water conduit system. *Journal of Geophysical Research*, 92(B9), 9083- 9100.

Kaser, G., Großhauser, M., Marzeion, B., & Barry, R. G. (2010). Contribution potential of glaciers to water availability in different climate regimes. *Proceedings of the National Academy of Sciences of the United States of America*, 107(47), 20223-20227.

King, E. C., Smith, A. M., Murray, T., & Stuart, G. W. (2008). Glacier-bed characteristics of midtre lovénbreen, svalbard, from high-resolution seismic and radar surveying. *Journal of Glaciology*, 54(184), 145-156.

Kirkbride, M. P. (1995). Processes of glacial transportation. In Menzies, J. (ed.), *Modern and past glacial environments*. Butterworth-Heinemann, Oxford, 147-69.

Klaar, M. J., Kidd, C., Malone, E., Bartlett, R., Pinay, G., Chapin, F. S., & Milner, A. (2015). Vegetation succession in deglaciated landscapes: Implications for sediment and landscape stability. *Earth Surface Processes and Landforms*, 40(8), 1088-1100.

Klok, E. J., Greuell, W., & Oerlemans, J. (2003). Temporal and spatial variation of the surface albedo of Morteratschgletscher, Switzerland, as derived from 12 Landsat images. *Journal of Glaciology*, 49, 491 – 502.

Klok, E. J., Greuell, W., & Oerlemans, J. (2004). Modelled climate sensitivity of the mass balance of Morteratschgletscher and its dependence on albedo parameterization. *International Journal of Climatology*, 24, 231 – 245.

Knudsen, N. T., Yde, J. C., & Gasser, G. (2007). Suspended sediment transport in glacial meltwater during the initial quiescent phase after a major surge event at Kuannersuit Glacier, Greenland. *Geografisk Tidsskrift-Danish Journal of Geography*, 107(1), 1-7.

Kühni, A., & Pfiffner, O. A. (2001). The relief of the Swiss Alps and adjacent areas and its relation to lithology and structure: topographic analysis from a 250-m DEM. *Geomorphology*, 41(4), 285-307.

Lappegard, G., Kohler, J., Jackson, M., & Hagen, J. O. (2006). Characteristics of subglacial drainage systems deduced from load-cell measurements. *Journal of Glaciology*, 52(176), 137-148.

Lane, S. N., Bakker, M., Gabbud, C., Micheletti, N., & Saugy, J. (2017). Sediment export, transient landscape response and catchment-scale connectivity following rapid climate warming and alpine glacier recession. *Geomorphology*, 277, 210-227.

Leggat, M. S., Owens, P. N., Stott, T. A., Forrester, B. J., Déry, S. J., & Menounos, B. (2015). Hydro-meteorological drivers and sources of suspended sediment flux in the proglacial zone of the retreating Castle Creek glacier, Cariboo Mountains, British Columbia, Canada. *Earth Surface Processes and Landforms*, 40, 1542-1559.

Liestøl, O. (1977). Stetvatnet, a glacier dammed lake in the Kongsfjorden area, Spitsbergen. *Norsk Polarinstitutt Årbok 1975*, 31–35.

Lliboutry, L. (1979). Local friction laws for glaciers: a critical review and new openings. *Journal of Glaciology*, 23, 67-95.

Lønne, I., & Lyså, A. (2005). Deglaciation dynamics following the Little Ice Age on Svalbard: Implications for shaping of landscapes at high latitudes. *Geomorphology*, 72(1), 300-319.

Liu, Q., Liu, S., & Cao, W. (2018). Seasonal variation of drainage system in the lower ablation area of a monsoonal temperate debris-covered glacier in mt. Gongga, south-eastern Tibet. *Water*, 10(8), 1050.

Lovell, H., Fleming, E. J., Benn, D. I., Hubbard, B., Lukas, S., & Naegeli, K. (2015). Former dynamic behaviour of a cold-based valley glacier on Svalbard revealed by basal ice and structural glaciology investigations. *Journal of Glaciology*, 61(226), 309-328.

Lukas, S., Nicholson, L. I., Ross, F. H., & Humlum, O. (2005). Formation, meltout processes and landscape alteration of high-Arctic ice-cored moraines— Examples from Nordenskiöld Land, central Spitsbergen. *Polar Geography*, 29(3), 157-187.

Mao, L., Dell'Agnese, A., Huincahe, C., Penna, D., Engel, M., Niedrist, G., & Comiti, F. (2014). Bedload hysteresis in a glacier-fed mountain river. *Earth Surface Processes and Landforms*, 39(7), 964-976.

Mao, L., & Carrillo, R. (2016). Temporal dynamics of suspended sediment transport in a glacierized Andean basin. *Geomorphology*, 287, 116–125.

Mair, D., Willis, I., Fischer, U. H., Hubbard, B., Nienow, P., & Hubbard, A. (2003). Hydrological controls on patterns of surface, internal and basal motion during three "spring events": Haut Glacier d'Arolla, Switzerland. *Journal of Glaciology*, 49(167), 555-567.

Maizels, J. K. (1979). Proglacial aggradation and changes in braided channel patterns during a period of glacier advance: an Alpine example. *Geografiska Annaler. Series A. Physical Geography*, 61(1-2), 87-101.

Male, D. H., & Granger, R. J. (1981). Snow surface energy exchange. *Water Resource Research*, 17, 609 – 627.

McGuire, B. (2010). Potential for a hazardous geospheric response to projected future climate changes. *Philosophical Transactions of the Royal Society of London. Series A: Mathematical, Physical, and Engineering Sciences*, 368(1919), 2317-2345.

Meierbachtol, T., Harper, J., & Humphrey, N. (2013). Basal drainage system response to increasing surface melt on the greenland ice sheet. *Science (American Association for the Advancement of Science)*, 341(6147), 777-779.

Menzies, J., & Meer, J. (2017). *Past Glacial Environments* (2nd ed.). Elsevier.

Mercier, D. (2000). From glacial to paraglacial: the metamorphosis of polar landscapes in Svalbard. *Annales de Géographie*. 109(616), 580-596.

Mercier, D. (2008). Paraglacial and paraperiglacial landsystems: concepts, temporal scales and spatial distribution. *Géomorphologie : relief, processus, environnement*, 14(4), 223-233.

Mercier, D., & Étienne, S. (2008). Paraglacial geomorphology: processes and paraglacial context. *Geomorphology*, 95, 1-102.

Miller, O., Solomon, D. K., Miège, C., Koenig, L., Forster, R., Schmerr, N., Ligtenberg, S. R. M., Legchenko, A., Voss, C. I., Montgomery, L., & McConnell, J. R. (2020). Hydrology of a perennial firn aquifer in southeast greenland: An overview driven by field data. *Water Resources Research*, 56(8),1-23.

Misset, C., Recking, A., Legout, C., Poiriel, A., Cazilhac, M., Esteves, M., & Bertrand, M. (2019). An attempt to link suspended load hysteresis patterns and sediment sources configuration in alpine catchments. *Journal of Hydrology (Amsterdam)*, 576, 72-84.

Nanni, U., Gimbert, F., Vincent, C., Graff, D., Walter, F., Piard, L., & Moreau, L. (2020). Quantification of seasonal and diurnal dynamics of subglacial channels using seismic observations on an alpine glacier. *The Cryosphere*, 14(5), 1475.

Neshyba, S. P., Grenfell, T. C., & Warren, S. G. (2003). Representation of a nonspherical ice particle by a collection of independent spheres for scattering and absorption of radiation: 2. Hexagonal columns and plates. *Journal of Geophysical Research*, 108 (D15), 4448.

Nienow, P., Sharp, M., & Willis, I. (1998). Seasonal changes in the morphology of the subglacial drainage system, Haut Glacier d'Arolla, Switzerland. *Earth Surface Processes and Landforms*, 23(9), 825-843.

Nye, J. F. (1976). Water flow in glaciers; jokulhlaups, tunnels and veins. *Journal of Glaciology*, 17, 181-207.

Oberli, S. (2019). Before/after comparison of Fee glacier (Valais alps). Retrieved October, 11, 2019, from SwissGlaciers.org.

Orwin, J. F., & Smart, C. C. (2004a). Short-term spatial and temporal patterns of suspended sediment transfer in proglacial channels, Small River Glacier, Canada. *Hydrological Processes*, 18(9), 1521-1542.

Orwin, J. F., & Smart, C. C. (2004b). The evidence for paraglacial sedimentation and its temporal scale in the deglaciating basin of Small River Glacier, Canada. *Geomorphology*, 58(1), 175-202.

Østrem, G. (1975). Sediment transport in glacial meltwater streams. In Jopling, A. V. & MacDonald, B. C. (eds), *Glaciofluvial and Glaciolacustrine Sedimentation*. SEPM Special Publication, 23, 101-22.

Otto, J., Schrott, L., Jaboyedoff, M., & Dikau, R. (2009). Quantifying sediment storage in a high alpine valley (turtmantal, switzerland). *Earth Surface Processes and Landforms*, 34(13), 1726-1742.

Paterson, W. S. B. (2016). *The physics of glaciers* (3rd ed.). Saint Louis: Elsevier Science.

Pearce, J. T., Pazzaglia, F. J., Evenson, E. B., Lawson, D. E., Alley, R. B., Germanoski, D. & Denner, J. D. (2003). Bedload component of glacially discharged sediments: Insights from the Matanuska Glacier, Alaska. *Geology*, 31, 7-10.

Pedersen, C. A., & Winther, J. G. (2005). Intercomparison and validation of snow albedo parameterization schemes in climate models, *Climate Dynamics*, 25, 351 – 362.

Perolo, P., Bakker, M., Gabbud, C., Moradi, G., Rennie, C., & Lane, S. N. (2018). Subglacial sediment production and snout marginal ice uplift during the late ablation season of a temperate valley glacier. *Earth Surface Processes and Landforms*, 44(5), 1117-1136.

Perovich, D. K., Grenfell, T. C., Light, B., & Hobbs, P. V. (2002). Seasonal evolution of the albedo of multiyear Arctic sea ice. *Journal of Geophysical Research*, 107(C10), 8044.

Pettersson, R., Jansson P., & Blatter, H. (2004). Spatial variability in water content at the cold-temperate transition surface of the polythermal Storglaciären, Sweden, *Journal of Geophysical Research*, 109(F2), 1-12.

Porter, P. R., Vatne, G., Ng, F., & Irvine-Fynn, T. D. (2010). Ice-marginal sediment delivery to the surface of a high-Arctic glacier: Austre Brøggerbreen, Svalbard. *Geografiska Annaler: Series A, Physical Geography*, 92(4), 437-449.

Porter, P.R. & Smart, Martin & Irvine-Fynn, Tristram. (2018). Glacial Sediment Stores and Their Reworking: Landform and Sediment Dynamics In: Heckmann T., Morche D. (eds) *Geomorphology of proglacial systems: Landform and sediment dynamics in recently deglaciated alpine landscapes*. Springer, Cham, 157-176.

Priesnitz, K., & Schunke, E. (2002). The fluvial morphodynamics of two small permafrost drainage basins, richardson mountains, northwestern canada. *Permafrost and Periglacial Processes*, 13(3), 207-217.

Rempel, A. W. (2008). A theory for ice-till interactions and sediment entrainment beneath glaciers. *Journal of Geophysical Research - Earth Surface*, 113(F1), 1-20.

Richards, G., & Moore, R. D. (2003). Suspended sediment dynamics in a steep, glacierfed mountain stream, Place Creek, Canada. *Hydrological Processes*, 17(9), 1733-1753.

Riihimaki, C. A., MacGregor, K. R., Anderson, R. S., Anderson, S. P., & Loso, M. G. (2005). Sediment evacuation and glacial erosion rates at a small alpine glacier. *Journal of Geophysical Research - Earth Surface*, 110(F3), 1-17.

Riley, N. W. (1982). Rock wear by sliding ice. *unpublished PhD Thesis*, University of Newcastle upon Tyne, 145.

Röthlisberger, H. (1972). Water pressure in intra- and subglacial channels. *Journal of Glaciology*, 11, 177-203.

Röthlisberger, H. & Lang, H. (1987). Glacial hydrology. In Gurnell, A. M. & Clark, M. J. (eds), *Glacio-fluvial Sediment Transfer*. Wiley, New York, 207-84.

Schiefer, E., Hassan, M. A., Menounos, B., Pelpola, C. P., & Slaymaker, O. (2010). Interdecadal patterns of total sediment yield from a montane catchment, southern coast mountains, british columbia, canada. *Geomorphology*, 118(1), 207-212.

Schmid, S. M., Pfiffner, O. A., Froitzheim, N., Schönborn, G. & Kissling, E. (1996). Geophysical – geological transect and tectonic evolution of the Swiss – Italian Alps. *Tectonics*, 15(5), 1036-1064.

Schoof, C. 2004. The effect of cavitation on glacier sliding. *Proc. R. Soc. London, Ser.A*, 461(2055), 609–627.

Schrott, L., Hufschmidt, G., Hankammer, M., Hoffmann, T., & Dikau, R. (2003). Spatial distribution of sediment storage types and quantification of valley fill deposits in an alpine basin, reintal, bavarian alps, germany. *Geomorphology*, 55(1), 45-63.

Sharp, M. J., Gemmell, J. C. & Tison, J. -L. (1989). Structure and stability of the former subglacial drainage system of the Glacier de Tsanfleuron, Switzerland. *Earth Surface Processes and Landforms*, 14, 119-34.

Sharp, M., Richards, K., Willis, I., Arnold, N., Nienow, P., Lawson, W., & Tison, J. L. (1993). Geometry, bed topography and drainage system structure of the Haut Glacier d'Arolla, Switzerland. *Earth Surface Processes and Landforms*, 18(6), 557-571.

Sharp, M., Richards, K. S., & Tranter, M. (Eds.). (1998). *Glacier hydrology and hydrochemistry*. Wiley.

Smart, M. J. (2015). *Deglaciation dynamics of the feegletscher nord, Switzerland: implications for glacio-fluvial sediment transfer*. Unpublished doctoral dissertation, University of Hertfordshire, Hatfield.

Sold, L., Huss, M., Machguth, H., Joerg, P.C., Vieli, G.L., Linsbauer, A., *et al.* (2016). Mass balance re-analysis of Findelengletscher, Switzerland; benefits of extensive snow accumulation measurements. *Frontiers in Earth Science*, 4 (18), 1-16.

Souchez, R., & Lorrain, R. (1987). The subglacial sediment system. In Gurnell, A. M., & Clark, M. J., *Glacio-Fluvial Sediment Transfer: An Alpine Perspective*. Chichester: Wiley, 179-184.

Srivastava, D., Kumar, A., Verma, A., & Swaroop, S. (2014). Characterization of suspended sediment in meltwater from glaciers of garhwal himalaya. *Hydrological Processes*, 28(3), 969-979.

Stott, T., & Mount, N. (2007). Alpine proglacial suspended sediment dynamics in warm and cool ablation seasons: Implications for global warming. *Journal of Hydrology*, 332(3), 259-270.

Stroeve, J., Nolin., A. & Steffen., K. (1997). Comparison of AVHRR-derived and in situ surface albedo over the Greenland Ice Sheet. *Remote Sensing of Environment*, 62, 262 – 276.

Swift, D. A., Nienow, P. W., Spedding, N., & Hoey, T. B. (2002). Geomorphic implications of subglacial drainage configuration: rates of basal sediment evacuation controlled by seasonal drainage system evolution. *Sedimentary Geology*, 149(1), 5-19.

Swift, D. A., Nienow, P. W., Hoey, T. B., & Mair, D. W. (2005a). Seasonal evolution of runoff from Haut Glacier d'Arolla, Switzerland and implications for glacial geomorphic processes. *Journal of hydrology*, 309(1), 133-148.

Swift, D. A., Nienow, P. W., & Hoey, T. B. (2005b). Basal sediment evacuation by subglacial meltwater: suspended sediment transport from Haut Glacier d'Arolla, Switzerland. *Earth Surface Processes and Landforms*, 30(7), 867-883.

Swift, D. A. (2006). Haut Glacier d'Arolla, Switzerland: hydrological controls on subglacial sediment evacuation and glacial erosional capacity. In Knight, P. G. (ed.), *Glacier Science and Environmental Change*. Blackwell, Oxford, 23-5.

Tananaev, N.I. (2015). Hysteresis effects of suspended sediment transport in relation to geomorphic conditions and dominant sediment sources in medium and large rivers of the Russian Arctic. *Hydrology Research*, 46 (2), 232-243.

Thomas, D. S. G. & Goudie, A. S. (2000). *The Dictionary of Physical Geography* (3rd ed.). Malden, Mass: Blackwell Publishers.

Urbini, S., & Baskaradas, J. A. (2010). GPR as an effective tool for safety and glacier characterization: experiences and future development. In *Ground Penetrating Radar (GPR), 2010 13th International Conference on* (pp. 1-6).

Uhlmann, M., Korup, O., Huggel, C., Fischer, L., & Kargel, J. S. (2013). Supra-glacial deposition and flux of catastrophic rock-slope failure debris, south-central alaska: supra-glacial deposition and sediment flux, alaska. *Earth Surface Processes and Landforms*, 38(7), 675-682.

Urbini, S., Zirizzotti, A., Baskaradas, J., Tabacco, I., Cafarella, L., Senese, A., Smiraglia, C., & Diolaiuti, G. (2017). Airborne radio echo sounding (RES) measures on alpine glaciers to evaluate ice thickness and bedrock geometry: Preliminary results from pilot tests performed in the ortles cevedale group (italian alps). *Annals of Geophysics*, 60(2), 1-12.

Vernon, A. (2008). Thermochronological approach to the late Neogene exhumation of the European Alps. *Applied geology*. Université Joseph-Fourier - Grenoble I; Edinburgh University, 2008. English.

Walder, J. S. & Fowler, A. (1994). Channelized subglacial drainage over a deformable bed. *Journal of Glaciology*, 40(134). 3-15.

Walder, J.S., & Driedger, C.L. (1995). Frequent outburst floods from South Tahoma Glacier, Mount Rainier, USA: relation to debris flows, meteorological origin, and implications for subglacial hydrology. *Journal of Glaciology*, 41 (137), 1-10.

Warburton, J. (1990). An alpine proglacial fluvial sediment budget. *Geografiska Annaler. Series A. Physical Geography*, 72(3-4), 261-272.

Warburton, J. (2007). Sediment budgets and rates of sediment transfer across cold environments in Europe: a commentary. *Geografiska Annaler: Series A, Physical Geography*, 89(1), 95-101.

Warren, S. G., & Wiscombe, W. J. (1980). A model for the spectral albedo of snow. II: Snow containing atmospheric aerosols. *Journal of Atmospheric Science*, 37, 2734 – 2745.

Warren, S. G. (1982). Optical properties of snow, *Reviews of Geophysics*, 20, 67 – 89.

Warren, S. G., & Clarke, A. D. (1990). Soot in the atmosphere and snow surface of Antarctica. *Journal of Geophysical Research*, 95, 1811-1816.

Weertman, J. (1964). The theory of glacier sliding. *Journal of Glaciology*, 5, 287-303.

Zemp, M., Haeberli, W., Hoelzle, M., & Paul, F. (2006). Alpine glaciers to disappear within decades? *Geophysical Research Letters*, 33(13).

Zuecco, G., Penna, D., Borga, M., & Meerveld, H. J. (2016). A versatile index to characterize hysteresis between hydrological variables at the runoff event timescale. *Hydrological Processes*, 30(9), 1449-1466.

Zuo, Z., & Oerlemans, J. (1996). Modelling albedo and specific balance of the Greenland Ice Sheet: Calculations for the Sondre Stromfjord transect. *Journal of Glaciology*, 42, 305 – 317.

## Appendix

### Appendix A - Detailed overview of hysteresis loops for the Upper North River Site.

Site	DOY	Hydrological Day	Max Q (m <sup>3</sup> s <sup>-1</sup> )	Max Q time	Max SSC (g l <sup>-1</sup> )	Max SSC time	Hysteresis	Precipitation (mm)
Upper North	195	Recording started at 195.68 (16:24 PM) - 196.18 (04:16 AM)	1.110	195.96 (23:00 PM)	0.355	195.85 (20:24 PM)	Anticlockwise	13.87 195.76 (18:16 PM) - 196.31 (8:10 AM)
	196	196.18 (04:16 AM) - 197.33 (07:52 AM)	0.963	196.22 (05:22 AM)	0.168	196.26 (06:08 AM)	Clockwise	10.45
	197	197.33 (07:52 AM) - 198.32 (07:36 AM)	0.982	197.68 (16:26 PM)	0.124	197.52 (12:22 PM)	Clockwise	
	198	198.32 (07:36 AM) - 199.34 (08:12 AM)	1.172	198.63 (15:10 PM)	0.118	199.11 (02:42 AM)	Anticlockwise	
	199	199.34 (08:12 AM) - Recording ended at 199.68 (17:30 PM)	1.205	199.62 (14:50 PM)	0.092	199.56 (13:32 PM)	Clockwise	

## Appendix B - Detailed overview of hysteresis loops for the Lower North River site.

Site	DOY	Hydrological Day	Max Q (m <sup>3</sup> s <sup>-1</sup> )	Max Q time	Max SSC (g l <sup>-1</sup> )	Max SSC time	Hysteresis	Precipitation (mm)
Lower North	190	Recording started at 190.68 (16:18 PM) - 191.31 (07:28 AM)	1.284	190.69 (16:28 PM)	0.125	190.93 (22:14 PM)	-	
	191	191.31 (07:28 AM) - 192.32 (07:34 AM)	2.100	191.65 (15:32 PM)	0.115	191.45 (10:52 AM)	Clockwise	
	192	192.32 (07:34 AM) - 193.32 (07:44 AM)	1.202	192.57 (13:42 PM)	0.082	192.58 (13:56 PM)		
	193	193.32 (07:44 AM) - 194.32 (07:34 AM)	1.250	193.53 (12:44 PM)	0.117	193.53 (12:42 PM)		
	194	194.32 (07:34 AM) - 195.32 (07:34 AM)	1.870	194.67 (16:04 PM)	0.131	194.51 (12:20 PM)	Anticlockwise	
	195	195.32 (07:34 AM) - 196.17 (04:00 AM)	1.770  1.750	195.60 (14:30 PM)  195:96 (23:02 PM)	0.0935  0.863  0.109	195.48 (11:26 AM)  195.88 (21:04 PM)  195.99 (23:48 PM)		12.86 195.76 (18.16 PM)
	196	196.17 (04:00 AM) - 197.34 (08:06 AM)	0.986	196.23 (05:32 AM)	0.069	196.24 (05:48 AM)	Anticlockwise	11.27 196.17 (04:00 AM) - 196.34 (08:10 AM).
	197	197.34 (08:06 AM) - 198.31 (07:24 AM)	0.877	197.67 (16:04	0.088	197.61 (14:32 PM)	Clockwise	

			PM)				
198	198.31 (07:24 AM) - 199.35 (08:20 AM)	1.273	198.63 (15:10 PM)	0.128	198.52 (12:35 PM)	Clockwise	
199	199.35 (08:20 AM) - 200.31 (07:28 AM)	1.359	199.63 (15:02 PM)	0.109	199.58 (14:00 PM)	Clockwise	
200	199.35 (08:20 AM) - 201.31 (07:24 AM)	1.964	200.61 (14:38 PM)	0.117	200.52 (12:22 PM)	Clockwise	
201	201.31 (07:24 AM) - 202.29 (06:52 AM)	2.048	201.57 (13:34 PM)	0.103	201.42 (10:02 AM)	Clockwise	0.402 201.73 (17:30 PM) - 201.74 (17:48 PM)
202	202.29 (06:52 AM) - 203.31 (07:32 AM)	2.441	202.62 (14:50 PM)	1.983	202.58 (13:54 PM)	Clockwise	1.608 202.16 (03:54 AM) - 202.23 (05:28 AM)
203	203.31 (06:46 AM) - 204.28 (06:46 AM)	2.650	203.60 (14:20 PM)	0.251	203.63 (15:00 PM)	Clockwise	
204	204.28 (06:46 AM) - 205.29 (07:04 AM)	2.499	204.62 (14:48 PM)	0.378	204.65 (15:38 PM)	Clockwise	
205	205.29 (07:04 AM) - 206.31 (07:22 AM)	3.090	205.62 (14:50 PM)	0.774	205.53 (12:40 PM)	Clockwise	
206	206.31 (07:42 AM) - 207.32 (07:42 AM)	3.658	206.60 (14:26 PM)	0.918	206.58 (13:48 PM)	Clockwise	3.015. 206.65 (15:34 PM) 0.201. 207.00 (23:58 AM) - 207.01 (00:20 AM) 2.814
207	207.32 (07:42 AM) - 208.34 (08:10 AM)	3.781	207.68 (16:14 PM)	1.676	207.68 (16:24 PM)	Clockwise and Anticlockwise	

## Appendix C - Detailed overview of hysteresis loops for the South River site.

Site	DOY	Hydrological Day	Max Q (m <sup>3</sup> s <sup>-1</sup> )	Max Q time	Max SSC (g l <sup>-1</sup> )	Max SSC time	Hysteresis	Precipitation (mm)
South	191	Recording started at 191.66 (15:56 AM) - 192.36 (08:32 AM)	4.428	191.66 (15:56 AM)	0.288	192.36 (08:32 AM)		
	192	192.36 (08:32 AM) - 193.36 (08:40 AM)	5.226	192.80 (19:12 PM)	8.977	192.79 (19:00 PM)	Clockwise	
	193	193.36 (08:40 AM) - 194.33 (08:00 AM)	3.465	193.57 (13:36 PM)	0.063	193.54 (12:58 PM)	Clockwise	
	194	194.33 (08:00 AM) - 195.33 (07:54 AM)	4.044	194.63 (15:10 PM)	0.096	194.58 (13:50 PM)	Clockwise	
	195	195.33 (07:54 AM) - 196.10 (02:30 AM)	3.803  4.391	195.66 (15:50 PM) 195.96 (23:08 PM)	0.109  0.147	195.59 (14:04 PM)  195.88 (23:10 PM)	Clockwise and Anticlockwise	10.653 195.76 (18.16 PM)
	196	196.10 (02:30 AM) - 197.34 (08:04 AM)	3.873	196.21 (05:02 AM)	0.08	196.22 (05:18 AM)	Anticlockwise	13.27 196.10 (02.30 AM) - 196.31 (07:30 AM).
	197	197.34 (08:04 AM) - 198.33 (08:00 AM)	2.73	197.68 (16:14 PM)	0.079	197.50 (11:54 PM)	Clockwise	
	198	198.33 (08:00 AM) - 199.34 (08:14 AM)	3.314	198.65 (15:42 PM)	0.14	198.54 (12:58 PM)	Clockwise	
	199	199.34 ( 08:14 AM) - 200.33 (07:48 AM)	3.477	199.63 (15:10	0.37	199.45 (10:45 AM)	Clockwise	

			AM)				
200	200.33 (07:48 AM) - 201.31 (07:24 AM)	3.842	200.67 (16:06 PM)	0.177	200.60 (14:28 PM)	Clockwise	
201	201.31 (07:24 AM) - 202.30 (07:08 AM)	4.152	201.58 (13:54 PM)	0.217	201.58 (13:52 PM)	Clockwise	0.402 201.73 (17:30 PM) - 201.74 (17:48 PM)
202	202.30 (07:08 AM) - 203.37 (08:50 AM)	5.133	202.63 (15:08 PM)	0.282	202.63 (15:10 PM)	Clockwise	1.608 202.16 (03:54 AM) - 202.23 (05:28 AM)
203	203.37 (08:50 AM) - 204.30 (07:12 AM)	5.21	203.75 (18.04 PM)	0.27	203.64 (15:28 PM)	Clockwise. Smaller loops of clockwise and anticlockwise	
204	204.30 (07:12 AM) - 205.30 (07:12 AM)	5.965	204.78 (18:42 PM)	0.309	204.75 (17:56 PM)	Clockwise	
205	205.30 (07:12 AM) - 206.36 (08:34 AM)	7.305	205.76 (18:14 PM)	0.519	205.64 (15:20 PM)	Clockwise	
206	206.36 (08:34 AM) - 207.33 (07:52 AM)	7.019	206.57 (13:40 PM)	0.671	206.60 (14:28 PM)	Anticlockwise	
207	207.33 (07:52 AM) - 208.34 (08:10 AM)	5.276	207.51 (12:18 PM)	2.963	207.69 (16:38 PM)	Anticlockwise	
208	208.34 (08:10 AM) - 209.38 (09:14 AM)	3.696	208.62 (14:56 PM)	0.237	208.63 (15:10 PM)	Anticlockwise	
209	209.38 (09:14 AM) - 210.33 (07:58 AM)	3.267	209.67 (16:10	0.095	209.74 (17:42 PM)	Anticlockwise and Clockwise	

				PM)				
210	210.33 (07:58 AM) - 211.31 (07:24 AM)	3.719	210.70 (16:52 PM)	0.222	210.60 (14:30 PM)	Clockwise		